STUDY OF BIOGEOCHEMICAL AND CLIMATOLOGICAL IMPACTS ON SPATIAL AND SEASONAL VARIABILITY OF AIR-SEA CO_2 FLUXES OVER THE INDIAN OCEAN

Thesis

submitted in partial fulfilment of the requirements of the degree of

Doctor of Philosophy

By

Lekshmi K
166104102

Under the supervision of

Dr. Rishikesh Bharti and Prof. Chandan Mahanta

Department of Civil Engineering
Indian Institute of Technology Guwahati
November 2022

Indian Institute of Technology Guwahati

DECLARATION

I, Lekshmi K, declare that this PhD thesis entitled "Study of biogeochemical and climatological impacts on spatial and seasonal variability of air-sea CO_2 fluxes over the Indian Ocean" is carried out by me under the guidance of my supervisors.

I certify that,

1. This thesis is a presentation of my own original research work

2. Any part of this thesis has not been submitted for any degree or diploma or any other qualification either in this institute or in any other university

3. Whenever I have referred to any published things or quotes from other resources, every effort has been clearly accredited by citing them in the text of the thesis work

4. Whenever contributions of others are involved, I have acknowledged to indicate this clearly

5. I confirm that the present thesis is free from plagiarism to the best of my knowledge and I take the whole responsibility if any complaint arises

6. I also affirm that my supervisors are not in a position to check for any possible instance of plagiarism within this submitted work

Signature

Date: 17-May-2023

Indian Institute of Technology Guwahati

CERTIFICATE

This is to certify that the thesis entitled "**Study of biogeochemical and climatological impacts on spatial and seasonal variability of air-sea CO_2 fluxes over the Indian Ocean**" submitted by Lekshmi K, in partial fulfilment of the requirements for the award of the degree of Doctor of Philosophy, to the Indian Institute of Technology Guwahati, Assam, India, is a record of the original bonafide research work carried out by her under our supervision and guidance at the Department of Civil Engineering, Indian Institute of Technology Guwahati, Assam, India. The thesis work, in our opinion, is worthy of consideration for the award of the degree of Doctor of Philosophy in Civil Engineering of the Institute. The work presented in this thesis has not been submitted in part or full to any other university or institute for the award of any degree/diploma.

Date: 17-May-2023

Place: Guwahati

RISHIKESH BHARTI

Assistant Professor, Earth System Science and Engineering

Department of Civil Engineering, IIT Guwahati

ACKNOWLEDGEMENTS

I take this opportunity to express my sincere thanks to a lot many people who supported and helped me to make this dissertation possible.

First and foremost, I express my sincere gratitude to my project supervisors Prof. Chandan Mahanta, Department of Civil Engineering, IIT Guwahati, and Dr. Rishikesh Bharti, Assistant Professor, Department of Civil Engineering, IIT Guwahati, for their valuable assistance and encouragement all through my Ph.D. tenure at IIT Guwahati.

I am extremely thankful to my doctoral committee members Prof. Subashisa Dutta, Prof. Kannan Pakshirajan, and Dr. Archana M Nair, for their guidance and valuable advice throughout this thesis work.

I would like to thank the Department of Civil Engineering, and the Indian Institute of Technology Guwahati for all the necessary facilities provided during this thesis work.

Thanking the Ministry of Education, Government of India, for providing financial assistance.

Last but not least, I thank all my friends who supported me during my life at IIT Guwahati.

Abstract

The role of oceans in regulating the global climate is significantly affected by the spatial and seasonal variations in the CO_2 gas exchange process at the marine-atmosphere interface. The concentrations of CO_2 gas in the atmosphere and ocean surface are the chief factor determining the flux direction and are regulated by the physical, chemical, and biological processes in the marine environment. These processes and their impacts vary regionally and seasonally, impacting the spatial and seasonal trends in the CO_2 fluxes. The Indian Ocean, with its contrasting flux trends in the western and eastern counterparts, plays a unique role in the CO_2 transfer process. While the Arabian Sea acts as a net annual CO_2 source, the Bay of Bengal serves as a net sink. Being an underexplored oceanic region, the exact reasons behind this contrasting behavior are yet to be understood.

The present study has tried to compare and analyze the spatial and seasonal variations in these fluxes in relation to varying trends in the sea surface temperature and primary production caused by the differential availability of nutrients in both sub-basins. The northern Indian Ocean flux values were observed to reach a maximum range of 5 – 93 mmol m^{-2} day^{-1} in the northern Arabian Sea and drop to a minimum of -47 – 1.5 mmol m^{-2} day^{-1} in the southern waters of BoB during monsoon season. The ocean productivity exhibited the maximum values in monsoon, reaching up to 2500 mgC m^{-2} day^{-1} in the northern Arabian Sea, and minimum values during the pre-monsoon season, falling to 120 mgC m^{-2} day^{-1} in the northern BoB waters. However, the minimum range was observed in the southern Arabian sea with values of 150–200 mgC m^{-2} day^{-1}. BoB productivity was observed to exhibit less spatial fluctuation. An attempt has been made to develop regional algorithms for estimating the sea water CO_2 partial pressures for both sub-basins using the in-situ observations. The Arabian sea pCO_2 algorithm produced a model accuracy of 10.7 µatm with a coefficient of determination of 0.77. The BoB algorithm provided an accuracy of 6 µatm and an R^2 value of 0.78 with multiple polynomial regression functions. In contrast, the prediction accuracy has improved with the random forest method, which provided an RMSE value of 0.05 µatm for the Arabian Sea and 0.06 µatm BoB, with an R^2 value of 0.98 for both basins.

Analysis of the nutrient dynamics over these basins showed higher concentrations of nitrate (44 µM), phosphate (3 µM), and silicate (65 µM) over BoB, whereas low values of nitrate (17 µM) and phosphate (1.7 µM) and silicate (30.5 µM) were observed in the Arabian Sea. The study also investigated the impacts of climatological phenomena, such as warm and cold events, on the flux distribution. The warm anomalies were attributed to reduced sea surface pCO_2 in the coastal and central Arabian sea, while cold events enhanced the coastal upwelling leading to increased surface pCO_2. A positive wind anomaly has caused a turbulent action leading to an increase in the pCO_2 in the southern Arabian Sea. Warm anomaly has resulted in an increase in surface pCO_2 in coastal, and both warm and cool events and positive wind anomaly enhanced the pCO_2 over the southern BoB waters.

Contents

Fig. No. **List of Figures**

Table No. **List of Tables**

Abbreviations

AS	Arabian Sea
BoB	Bay of Bengal
pCO_2	Partial pressure of carbon dioxide
SST	Sea Surface Temperature
SSS	Sea Surface Salinity
Chl-a	Chlorophyll-a
DIC	Dissolved Inorganic Carbon
mmol	milli mol
µatm	micro atmospheres
µM	micromolar
pH_2O	saturation vapour pressure of seawater
PP	Primary Productivity
P_T	Sea level pressure
TA	Total Alkalinity
Tg	Terra gram
SMAP	Soil Moisture Active Passive
ASHSW	Arabian Sea High Salinity Water
NEC	North Equatorial Current
VGPM	Vertically Generalised Production Model
MLR	Multiple Linear Regression
MPR	Multiple Polynomial Regression
RF	Random Forest
NOAA	National Oceanic and Atmospheric Administration
WOA	World Ocean Atlas
ECMRWF	European Center for Medium Range Weather Forecast
CMIP	Coupled Model Intercomparison Project

1

INTRODUCTION

1.1 Overview

Ocean-atmospheric circulations primarily govern Earth's climate. Oceans possess excellent heat capacity, almost 1000 times higher than the atmosphere, which gets stored in the ocean's upper layers. Ocean currents play vital roles in regional climate by transporting the stored heat and water masses, while large-scale thermohaline circulations significantly influence the global climate (Solomon et al., 2007). These ocean circulations, both at the surface and deep layers are regulated considerably by the variations in the atmospheric circulation; atmospheric effects mainly drive surface circulations while deep water movements are defined by sea water density. Triggered by the frictional force from surface wind dragging, the surface circulations are especially high-velocity horizontal flows. Trade winds and westerlies are responsible for such surface water movements, forming large anticyclonic cells, i.e., gyres. Wind action on the ocean surface results in the formation of the mixed layer; below this uniform temperature layer lies a narrow zone termed thermocline, characterized by rapid temperature change. Circulation patterns below the thermocline are attributed to variations in sea water temperature and salinity, hence named thermohaline circulations. Wind action also induces vertical movements, i.e., upwelling and downwelling processes; the former process is responsible for bringing the nutrients and gases trapped in the subsurface layers to the surface, enhancing marine primary production (Brian & Stephen, 1995; Chester, 2000).

The marine system acts as a sink or source for the various atmospheric gases through the gaseous exchange process at the marine-atmosphere interface. This gaseous interchange significantly regulates these atmospheric gases' biogeochemical cycles, thus playing crucial roles in the global environment. Carbon dioxide (CO_2) is such an important gas, being exchanged through the air-sea interface, and these CO_2 fluxes at the marine surface carry high relevance in the global carbon cycle (Chester, 2000). CO_2, even though it constitutes only a minor fraction (0.04%) of the volume of air, is the highest contributing greenhouse gas to global warming, thus acting as one of

the significant factors in the radiative climate forcing. CO_2 gas emissions contribute about 77% of the anthropogenic greenhouse gas emissions and 63% of the direct radiative forcing (Lutgens and Tarbuck, 2004; Velasco & Roth, 2010). About 50% of this added CO_2 concentration in the atmosphere is absorbed by the oceans, serving as the global CO_2 storage. CO_2 flux can be divided into two constituents; the exchange of natural CO_2 and the uptake of anthropogenic CO_2 emissions. CO_2 is released to the atmosphere from natural sources like biological respiration, organic decomposition, volcanic activities, and chemical weathering, as well as manmade sources like land-use change, cement production, and fossil fuel burning associated with manufacturing and industry, households and public buildings and transport (Fletcher et al., 2007; Velasco & Roth, 2010). The Intergovernmental Panel on Climate Change (IPCC) has reported an increase of the global average CO_2 concentrations by 40 % from 278 ppm since the industrial era (Ciais et al., 2013), which has reached around 417 ppm in 2022 as per the trends (https://gml.noaa.gov/ccgg/trends/) published by the National Oceanic and Atmospheric Administration (NOAA) Global Monitoring Laboratory based on the observations from the Mauna Loa Observatory, Hawaii. The atmospheric CO_2 concentrations are regulated by the marine carbon cycle through the continuous gaseous exchange at the sea surface.

1.1.1 Marine Carbon Cycle

Cycling of CO_2 gas between the atmosphere and marine systems occurs via various physico-chemical and biological processes. The CO_2 flow across the marine surface is a function of windspeed through the surface mixing action and also depends on the CO_2 concentration difference between the sea water and the air above. Atmospheric CO_2 enters the marine system by simple diffusion, which then gets converted into organic form by primary producers like algae and photosynthetic bacteria. Zooplankton, the secondary producers, consume the photosynthetically converted carbon, thus moving it through the food chain until it gets released back to water by oxidative reduction, respiration, and remineralization processes (Botkin and Keller, 2000; Chester, 2000). The marine calcifier organisms convert sea water carbon into calcium carbonate ($CaCO_3$), utilizing it as the shells and skeleton building materials. Such converted carbon eventually sinks and becomes a part of deep marine sediments, locked for millions of years (Botkin and Keller, 2000; Horst & Matthias, 2006).

1.1.2 CO_2 uptake and storage in the marine system

The dynamics of CO_2 (uptake and release) cause alterations in marine biogeochemistry, thus ultimately affecting the climate system (Falkowski et al., 2000; Solomon et al., 2007). The capacity of the oceans to capture and store CO_2 is controlled by

i.) The chemical characteristics of CO_2 in the sea water, i.e., the solubility pump, and the carbonate system reactions associated with it,

ii.) Transportation of CO_2 to deep oceanic layers from the surface, i.e., the biological pump, and

iii.) Circulation rate and patterns of the ocean water, i.e., the physical pump.

Solubility pump is a function of sea water gas solubility, the transfer process through which oceans uptake atmospheric CO_2. This involves CO_2 transfer into the mixed layer across the marine-atmospheric interface. The high-latitude cold waters possess increased CO_2 solubility, thus transporting the gas into deeper layers, whereas a decreasing effect on solubility is observed over the low-latitude warm waters. CO_2 in the mixed layer moves to the deeper ocean through the physical and biological pumps (Figure.1.1). Physical pump involves the downward mixing and downwelling processes associated with the formation of deep-water masses and the onset of thermohaline circulation; it is coupled with the solubility pump.

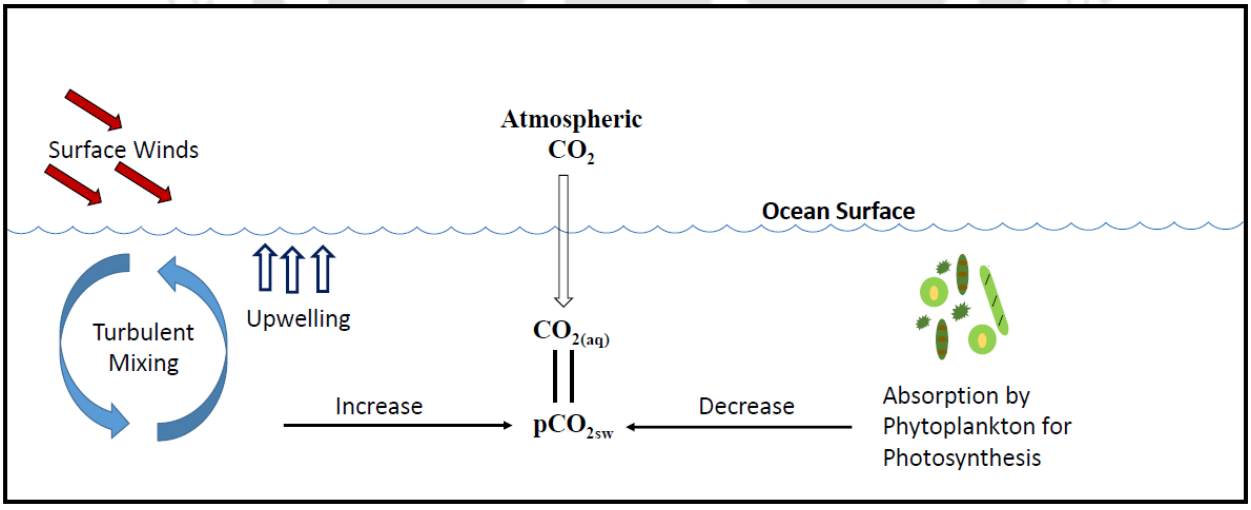

Figure 1.1: Physical and biological CO_2 pump regulating pCO_2 at the marine–atmosphere interface

The biological pump comprises the biogenic production of carbonate minerals and organic matter at the surface, and their transport into the deep ocean. This carbon transport in the euphotic

zone involves vertical gravitational settling of biogenic debris, manifesting a dissolved inorganic carbon gradient characterized by low surface values, gradually increasing towards the deeper layers. This process causes the lowering of surface CO_2, thus enhancing ocean CO_2 uptake. Pathways of the biological pump can be expressed in the following steps.

i.) The sinking of CO_2, which is further utilized in photosynthetic carbon fixation, can be expressed as equation 1.

$$C6CO2 + 12H2O \rightarrow C6H12O6 + 6O2 + 6H2O \quad (1.1)$$

ii.) Transport of particulate inorganic carbon to the deeper ocean from the surface can be expressed as equation 2.

$$Ca2 + + 2HCO3- \rightarrow CaCO3 + CO2 + H2O \quad (1.2)$$

iii.) The sinking of fecal pellets

iv.) Downward advection and diffusion processes of inorganic and organic carbon materials (Botkin and Keller, 2000; Chester, 2000; Zondervan et al., 2001).

The CO_2 uptake is regulated by the ocean circulations and ocean carbonate chemistry (Balino et al., 2000; Feely et al., 2001; Bernstein et al., 2007; Davila et al., 2007). An increase in the sea water concentration of CO_2 acidifies the water, thus altering the chemical equilibrium, resulting in a reduced buffering capacity of the marine carbonate system (Prentice et al., 2001; Bindoff et al., 2007; Zeebe, 2012). CO_2 dissolved in the ocean occurs mainly as three inorganic forms, namely free aqueous carbon dioxide (CO_2aq), bicarbonate ion (HCO_3^-), and carbonate ion (CO_3^{2-}) where, HCO_3^- represents majority of the ocean inorganic carbon. The chemistry of this process, as given by DOE (1994)6 and Zeebe (2012), is shown in equations 3 to 6. A minor percentage of the diffused CO_2 exists as carbonic acid, about 0.3% of the aqueous CO_2.

$$CO_2(g) \rightarrow CO_2(aq) \quad (1.3)$$

$$CO_2(aq) + H_2O\ (l) \leftrightarrow H_2CO_3(aq) \quad (1.4)$$

$$H_2CO_3 \leftrightarrow H^+ + HCO_3^- \quad (1.5)$$

$$HCO_3^- \leftrightarrow H^+ + CO_3^{2-} \quad (1.6)$$

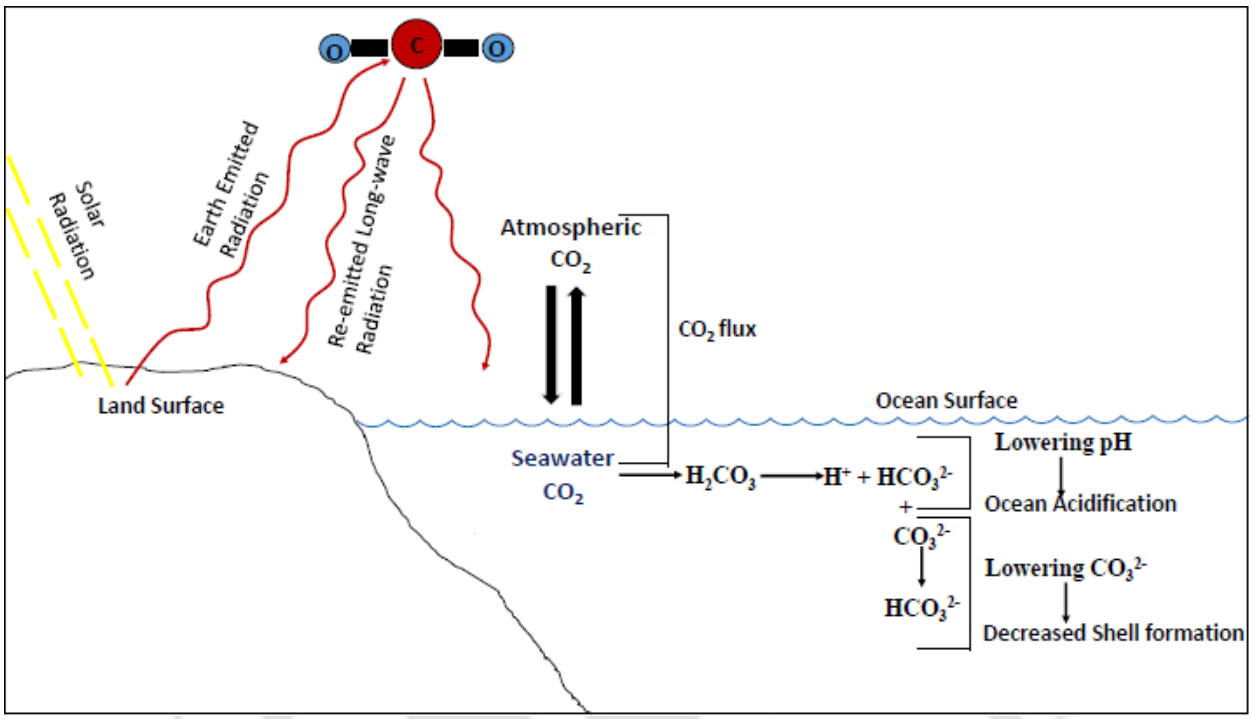

Figure 1.2: CO_2 gas exchange process within the earth systems

The sea water CO_2 partial pressure (pCO_2) is proportional to the concentration of the free CO_2 (aq) and the direction of the CO_2 fluxes is defined by the partial pressure differences of CO_2 between the sea surface and the atmosphere. Compared to the atmosphere, more significant pCO_2 fluctuations are visible on the sea surface. Hence the CO_2 flux direction is primarily controlled by the sea surface temperature (SST) and salinity (SSS) variations along with biological processes like respiration and photosynthesis. Besides having a similar effect on the pCO_2 distribution, these parameters over certain oceanic regions were found to have a compensating effect, establishing a balance between the ocean uptake and release of CO_2 (Feely et al., 2001). The maximum impact of ocean primary productivity on CO_2 gas transfer can be visible during bloom conditions where the enhanced photosynthetic activity leads to increased CO_2 uptake. The role of oceans in regulating the global climate is significantly affected by the spatial and seasonal variations in the CO_2 gas exchange process at the marine-atmosphere interface (Figure1.2). Analysis of the regional controls on the direction of these fluxes is important in understanding the capacity of various oceanic regions in balancing the global CO_2 concentrations (Feely et al., 2001; Zeebe, 2012).

1.2 Motivation

Studies have been carried out globally to understand the factors and mechanisms that govern the air-sea exchange of CO_2. The concentrations of CO_2 gas in the atmosphere and ocean surface are the

chief factor governing the flux direction (Feely et al., 2001; Zeebe, 2012). These concentrations are regulated by the physical, chemical, and biological processes in the marine environment. These processes and their impacts vary regionally and seasonally, impacting the spatial and seasonal trends in the CO_2 fluxes. Even though the global ocean acts as a net CO_2 sink, the regional fluctuations in the CO_2 exchange have potential repercussions on the global trends of CO_2 fluxes (Feely et al., 2001). The ocean-atmosphere interactions and their vital role in regulating global biogeochemical cycles significantly contribute to the global climate system. Such natural processes are continuously being interrupted by anthropogenic activities such as the emission of greenhouse gases like CO_2 and other lethal trace gases. Analysis of the transport, transformation, and recycling of the stored carbon in the ocean is essential in understanding the carbon cycling in the marine-atmospheric system and, thereby, its significance in the global climate (Buesseler et al., 2013).

The ongoing reduction of ocean pH following the uptake of atmospheric CO_2 is referred to as ocean acidification. The increase in oceanic CO_2 leads to a decrease in the carbonate ion and an increase in bicarbonate ion concentrations. Such reduction in the carbonate concentration results in the decrease of $CaCO_3$ stability, leading to the deficiency of $CaCO_3$ for marine calcifying organisms (Caldera & Wickett, 2003; Zeebe, 2012). Oceans serve as the primary reservoir for anthropogenic CO_2, holding about 93% of the carbon compared to the other reservoirs. Effective greenhouse gas emissions regulations require accurate global carbon cycle modeling to understand the ocean's role as the global CO_2 sink (Zeebe, 2012).

The CO_2 flux is primarily defined by the CO_2 gas transfer velocity, seawater solubility of the CO_2, and the difference in the CO_2 partial pressures at the sea surface and the air above termed as δpCO_2. Among these, pCO_2 is the thermochemical steering factor for the net air-sea CO_2 flux, determining the flux direction at the ocean-atmospheric interface. Compared to atmospheric pCO_2, spatial and seasonal fluctuations are more prominent in the seawater pCO_2, making it the principal factor in flux determination (Chester, 2000; Takahashi et al., 2002). Accuracy of the CO_2 flux estimation thus depends on the Spatio-temporal resolution of the measured pCO_2. Efforts have been made worldwide to obtain pCO_2 with better resolution using buoys and shipboard measurements. However, the spatial resolution of the present measurement network is far coarser (<250km grid), which emphasizes the requirement for improved extrapolation techniques (Ono et al., 2004). Subsequently, Landschutzer et al. (2016) generated observational-based global monthly gridded sea

surface pCO_2 from 1982 to 2015. Figure.1.3 represents the global seasonal pCO_2 map (Landschutzer et al., 2016). The maximum value observed in the equatorial Pacific Ocean in all the seasons ranges between 450 to 475 µatm, whereas the Arctic Ocean exhibits minimum values ranging from 250 to 275 µatm in summer. In addition, low pCO_2 values (275-300 µatm) were observed in the Southern Ocean in the spring and winter.

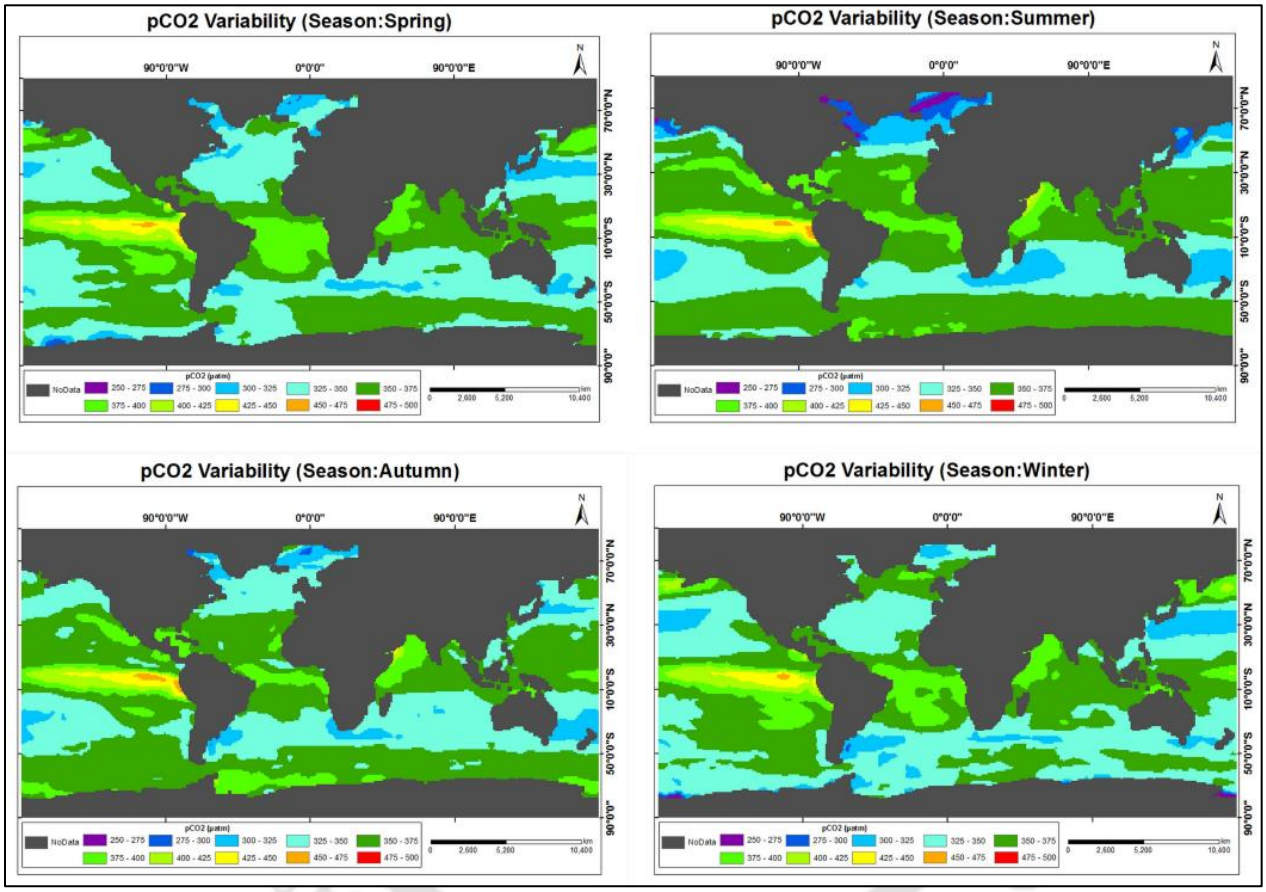

Figure 1.3: Seasonal variability of global pCO_2

Observations on the pCO_2 climatology of the global oceans indicate that the tropical oceanic region (14˚N-14˚S) acts as a CO_2 source, while 20˚-50˚ latitudes in both hemispheres act as a belt of CO_2 sink. CO_2 super saturation in the high latitude of the Southern Ocean and under saturation in the high latitude North Atlantic was also observed (Takahashi et al., 2009; Landschutzer, 2016). However, there is limited observational evidence on the variability of CO_2 exchange over the North Indian Ocean with adequate spatial and temporal coverage. The western and eastern regions show contrasting trends in terms of CO_2 fluxes. The Arabian Sea acts as a perennial CO_2 source, while the Bay of Bengal exhibits seasonal flux variability, acting as a net annual CO_2 sink. Most of the data

available are for the western part (Arabian Sea), whereas very few observations are made for the eastern Indian Ocean, i.e., the Bay of Bengal (BoB). BoB experiences strong thermohaline stratification compared to the Arabian Sea due to the heavy river runoff and the annual precipitation exceeding evaporation. This hinders the vertical mixing and affects the surface partial pressures of CO_2 (Kumar et al., 1996; Sarma et al., 1998). While the Arabian Sea is considered among the most productive oceanic regions, BoB has poor biological productivity. Monsoonal upwelling and winter convective mixing bring the subsurface waters rich in nutrients to the Arabian Sea, enhancing productivity. On the other hand, the large amounts of nutrients received by the BoB from riverine flux are lost into the deep ocean. The nutrient-limited coastal waters, the shallow euphotic zone caused by the heavy cloud cover, and the sediment-induced turbidity during the otherwise productive summer monsoon season contribute to the comparatively low productivity in BoB (Madhupratap et al., 1996; Sarma et al., 2012). Such contrasting phenomena in these basins should be addressed in detail to understand the contrasting trends of CO_2 in the western and eastern parts of the North Indian Ocean.

1.3 Study Area

The Indian Ocean, with its unique physiography as compared to other major oceanic basins, is enclosed by the Indian sub-continent in the north and by the African and Arabian Peninsula in the west, linked to the tropical Pacific Ocean in the east by the Indonesian Throughflow (ITF) and connected to the Southern Ocean in the south. The Northern Indian Ocean (Figure.1.4), divided into western (Arabian Sea) and eastern (Bay of Bengal) sub-basins, is considered in the present study (0-30˚ N and 30-100˚ E). It is dominated by a tropical monsoon climate, with semi-annually reversing winds. Contrasting to the dominant trade wind system in the other tropical basins, westerlies predominate along the equator in the Indian Ocean. This leads to an east-west flat equatorial thermocline, with the propagation of the annual SST cycle in the west-to-east direction, resulting in the absence of upwelling over the eastern tropical Indian Ocean (Sarma et al., 2013).

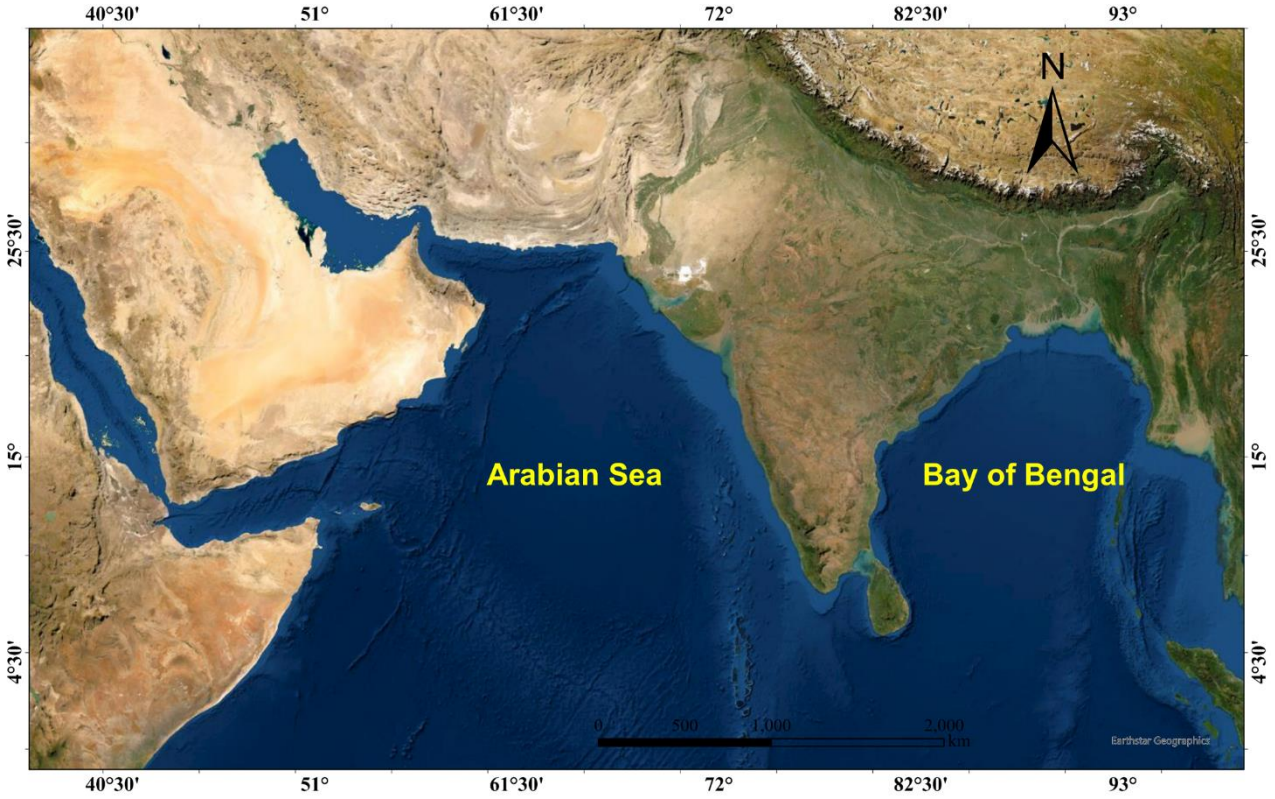

Figure 1.4: Study Area: Northern Indian Ocean

The Arabian Sea has an average depth of 2734 m and a surface area of 3,862,000 sq.km; four important branches are the Gulf of Oman to the northwest, the Gulf of Aden in the southwest, the Gulf of Kutch, and Cambay on the Indian coast. The major rivers flowing into this basin include Narmada, Netravathi, Sharavathi, Mahi, and Tapti and the important islands are Lakshadweep, Socotra, Amindivi, and Minicoy (Goetz, 1987). It is one of the highly productive oceanic basins, attributed to the wind-driven summer upwelling along the coasts of Arabia and Somalia and the southwest coast of India, as well as the winter cooling and convective mixing in the northern part of the basin. Salinity values ranging from an equatorial minimum value of 35 psu to a maximum of 36.6 psu in December to the north of 15° N were observed over the Arabian Sea. Temperature distribution over this sub-basin ranged from the lowest recorded value of 20°C in December to the peak value of 30°C during May (Tang et al., 2002; Prasannakumar & Narvekar, 2005).

Bay of Bengal (BoB) has a total surface area of 2,173,000 sq. km and an average depth of about 2600m (Goetz, 1987). It is characterized by heavy river discharge, coastal circulation, and cold-core eddies; the primary production and marine carbonate system of BoB are significantly

influenced by these physical forcings (Shanthi et al., 2016). The high influx of freshwater through precipitation, as well as river discharge, leads to the formation of a surface barrier layer, manifesting a thermohaline stratification that hinders the upward movement of nutrients to the euphotic zone, thus affecting the primary productivity, which renders the BoB waters low productive region irrespective of the heavy nutrient input in the monsoon season. Depleted surface pCO_2 levels characterize the resulting stratified low salinity zones due to the negative impact of SSS reduction on the CO_2 solubility since CO_2 solubility is a function of SSS and SST. These zones can be identified as atmospheric CO_2 sinks, and the fall in seawater pCO_2 goes far below the atmospheric pCO_2 levels, exceeding a pCO_2 gradient of 100 μatm during the northeast monsoon (Kumar et al., 1996). However, the southern BoB exhibits seasonal and inter-annual variability in annual CO_2 fluxes. The southwest coastal waters shifting from CO_2 sink to source was observed during the NE monsoon season (Shanthi et al., 2016).

2

LITERATURE REVIEW

2.1 Introduction

This chapter deals with the literature background on ocean carbonate chemistry, the significance of marine biogeochemistry on the CO_2 gas transfer at the air-sea interface, and the importance of ocean meteorology such as SST and windspeed on the CO_2 fluxes; that leads to identifying the research gaps and framing the objectives of this particular study.

2.2 Spatial and seasonal variability of air-sea CO_2 fluxes

Assessment of the spatial and temporal distribution of CO_2 fluxes is important in understanding the ocean's efficiency in controlling the excess quantities of CO_2 gas released into the atmosphere and balancing the atmospheric CO_2 concentrations. The capacity of the oceans to act as the anthropogenic CO_2 sink will be reduced eventually, upsetting the seawater carbonate speciation and the marine carbon cycle. The quantification and analysis of the CO_2 fluxes between the ocean and atmosphere will give a picture of the oceans' past and current trends in CO_2 gas regulation (Takahashi et al., 1993; Davila et al., 2007).

2.2.1 The Indian Ocean

The study on CO_2 emissions over the Arabian Sea conducted by Kortzinger et al (1997) showed a supersaturation of pCO_2 during the southwest (SW) monsoon leading to strong outflux to the atmosphere. Extreme supersaturation levels reaching up to 750 µatm were found along the Omani coast, and high pCO_2 values of around 525 µatm along with cold upwelled waters were observed about 300 NM (nautical miles) off the coast due to Ekman pumping. Variations in the flux densities were evident from the coastal region towards the open ocean, with values ranging from 43435 mmol m^{-2} y^{-1} on the coast to 730 mmol m^{-2} y^{-1} in the open ocean waters. The SW monsoon has a significant role in the annual CO_2 emissions to the atmosphere, with total emissions ranging from 0.672 to

1.73×10^{15} mmol C. The wind forcing, in combination with intense coastal upwelling during this season, makes the Arabian Sea a primary CO_2 source.

Analysis of the temporal variations in CO_2 partial pressures and CO_2 fluxes over the Arabian Sea was done by Goet et al (1998) using continuous pCO_2 measurements of seawater and atmosphere for the year 1995. Strong physical forcing due to the seasonal monsoons significantly regulates the Arabian Sea's partial pressures. Variations in pCO_2 were found to be very small in the offshore regions with values less than 40µatm were that of coastal areas crossed around 260 µatm. The monthly and annual fluxes were calculated using SST, wind speed, and the pCO_2 data. The mean monthly values ranged from 99.6 to 528 mmol m^{-2} y^{-1} for most of the year, while they showed significantly higher values during the SW monsoon, reaching up to 3753.6 mmol m^{-2} y^{-1} along the coast of Oman resulting from the strong upwelling. Arabian Sea was found to act as an annual CO_2 source to the atmosphere with annual emissions of 0.159×10^{15} mmol C yr^{-1}.

Sarma et al (1998) analyzed the seasonal and inter-annual variations in the central and eastern Arabian Sea's pCO_2 and total CO_2 (TCO_2). Coulometric methods determined that the total CO_2 and pCO_2 were computed from TCO_2 and pH. Seasonal changes in the TCO_2 were observed with variations in ocean circulation and primary production. TCO_2 values were high during the winter and low in the SW monsoon season. This was supposed to be attributed to the winter convective mixing bringing subsurface CO_2 to the upper ocean and accelerated primary production during the SW monsoon resulting from nutrient enrichment. Seawater pCO_2 was higher in all seasons compared to the atmosphere in the Arabian Sea except during the SW monsoon on the Indian coast. The analysis revealed that the Arabian Sea is a perennial CO_2 source in almost all seasons, with annual emissions of 1.02×10^{15} mmol C yr^{-1} to the atmosphere.

Data collected during the Indian and US JGOFS program and Indian Land-Ocean Interactions in the Coastal Zone process study programs were used to investigate the sea surface pCO_2 and air-sea CO_2 fluxes by Sarma (2003). Using multiple linear regression, the dissolved inorganic carbon content was derived from SST, salinity, and chlorophyll. Total alkalinity from salinity and surface pCO_2 from carbonate dissociation constants were computed. High variability was observed in the Arabian Sea's seasonal and spatial partial pressure distributions and CO_2 fluxes. A rise in the partial pressures can be observed on the west coast during the SW monsoon induced by the intense upwelling. The highest surface partial pressure values were observed during the SW

monsoon, with about 700 µatm in the upwelling region of the western coast and >480 µatm along the SW coast of India. In the open ocean, high partial pressures were found in the northern Arabian Sea with values >420 µatm. An increase in the sea surface temperatures by 2-3 ˚C was visible in the fall monsoon compared to the SW monsoon. This decreased surface pCO_2 levels to 360-380 µatm in the western coastal regions, particularly the Arabian coast, due to stratification and biological processes triggered by high nutrient availability and high chlorophyll content. A lowered partial pressure range of 370-380 µatm was noticed in the central Arabian Sea owing to increased SST and bacterial respiration. Lower pCO_2 values occurred along the southwest coast of India during the northeast (NE) monsoon resulting from the inflow of low saline waters from the Bay of Bengal. The decrease in the partial pressures caused a lowering of the coastal pCO_2 values to <360 µatm, while the central Arabian Sea showed a partial pressure range of 380-420 µatm. The spring inter-monsoon was characterized by increased coastal partial pressures from <360 µatm to about 370-380 µatm, resulting from the reversed surface circulation breaking off the influence of low saline water mass. Analysis of the CO_2 flux distribution showed more substantial emissions from the western coast, and the annual emissions from the Arabian Sea were about 2.04×10^{15} mmol C yr^{-1}, thereby acting as a CO_2 source.

The CO_2 emission study carried out in 27 estuaries along the Indian coast by Sarma et al (2012[a]) reported that the CO_2 emissions were 4-5 times higher in the monsoon season than dry period. The pCO_2 values ranged from 300 to 18492 µatm. The monsoonal fluxes were about 0.0363×10^{15} mmol C while the annual CO_2 emissions from the estuaries were 0.0436×10^{15} mmol C yr^{-1}. The high fluxes during the wet period are attributed to the high organic matter content in the estuaries due to the monsoonal river discharge and subsequently increased rates of microbial aerobic respiration. The occurrence of phytoplankton blooms drawing down the CO_2 levels and the increase in light penetration with the decreased suspended sediment concentration in summer account for the reduced summer fluxes.

Observations on the western continental shelf of the Bay of Bengal by Sarma et al (2012[b]) show that the sources and sinks of CO_2 in the shelf region depend on the river discharges and the distribution of the discharged water by the East India Coastal Current (EICC). The peninsular river discharge regulates the CO_2 partial pressures in the southwest (SW) coast and the northwest (NW) region by the Ganges river discharge. The partial pressures were lower than atmospheric levels in the NW region, whereas the SW coast exhibited supersaturation. The comparatively low salinity

caused the lower values in the NW region due to freshwater discharge and higher productivity than the SW coast. The CO_2 fluxes for the SW region were 2847 mmol m^{-2} y^{-1}, thus acting as a CO_2 source, and for the NW region were -3978.5 mmol m^{-2} y^{-1}, thereby acting as a sink. The mean fluxes for the entire western coast were about 73 mmol m^{-2} y^{-1} which suggests that the coast acts as a net annual source.

A study on the atmospheric CO_2 sinks in the southern Indian Ocean by Valsala et al (2012[a]) examined the seasonal, inter-annual and inter-decadal variability of the CO_2 fluxes. They reported that the south of the tropical-to-subtropical Indian Ocean region is a broad zone of subduction where the subducting water mass traps and carries the atmospheric trace gases from the atmosphere. The highest concentrations of anthropogenic CO_2 were found to be primarily concentrated at 150m depth between15˚ S to 50˚ S. The study area was divided into two distinct zones, namely north and south zones located at 15˚ S to 35˚ and 35˚ S to 50˚ S, respectively. In the north zone, the CO_2 flux was controlled by the solubility pump. In contrast, the CO_2 uptake was dominated by solubility and a biological pump in the south zone due to the high phytoplankton concentrations in the south. Analysis of the wind stress over this region indicated a coincidence of the locations of the largest concentrations of anthropogenic CO_2 with the subtropical zone of positive wind stress curl. Since a positive curl indicates the Ekman downwelling process in the southern hemisphere, the subsurface CO_2 trapping in the south of the Indian Ocean was reported to be induced by the atmospheric forcing due to positive wind stress. The study concludes that the deepening of subduction and consequent invasion of the CO_2 gas into the northern part of the Indian Ocean has resulted in the sinking of anthropogenic CO_2 in this region.

The CO_2 fluxes over the Indian Ocean from 1990 to 2009 were estimated by Sarma et al (2013) as part of the Regional Carbon Cycle Assessment and Process (RECCAP). The solubility pump regulated the fluxes in the northern Indian Ocean (18˚S to 30˚N), while both the biological and solubility pumps equally dominated the southern region (44˚S to 18˚S). The results suggested that the south of the Indian Ocean acts as a net annual CO_2 sink with flux values -9.77×10^{15} mmol C yr^{-1} and the northern counterpart serves as a net source with annual mean values 2.95×10^{15} mmol C yr^{-1}. The Indian Ocean is a net sink for atmospheric CO_2 with annual flux values -8.41×10^{15} mmol C yr^{-1}. The monsoonal wind action and upwelling processes in the northern Indian Ocean contribute to the CO_2 release, whereas the low saline waters in the southern region enhance the CO_2 uptake.

Seasonal and inter-annual variability study of the CO_2 flux by Valsala and Maksyutov (2013) simulated the CO_2 flux over the northern Indian Ocean by coupling the biogeochemical model with an ocean tracer transport model, which is based on 30-year reanalysis ocean data such as ocean currents, temperature, and salinity. Maximum variability was observed in the coastal Arabian Sea (AS) and Southern Peninsular India SP). The modeled CO_2 flux values showed an annual emission scenario of (2.72±0.909) $\times 10^{15}$ mmol C yr^{-1}. The CO_2 flux anomalies in AS and SP were then correlated with two significant climate anomalies, i.e., ENSO (El Niño-Southern Oscillation) and Indian Ocean Dipole/ Zonal Mode (IODZM). It was observed that a strong correlation of CO_2 flux in AS and SP with IODZM is accompanied by a weak correlation of the flux with ENSO and vice versa. The surface water pCO_2 was calculated from dissolved inorganic carbon (DIC), temperature, alkalinity, and salinity. Analysis of the effects of these components on the flux showed an increase in the temperature effect with a positive correlation between the flux and IODZM and vice versa in AS. In contrast, changes in DIC mainly control the CO_2 emission in SP. The DIC effect in SP was found to weaken during a negative correlation between CO_2 emission and ENSO.

Time-series estimation of chemical processes in the upper 100m water column was carried out in the Visakhapatnam region on the western coast of the Bay of Bengal by PreethiLatha et al (2015). Measurements were made for temperature, salinity, DIC, TA, and nutrients to derive the seawater pCO_2 and the atmospheric pCO_2 was measured directly using the pCO_2 sensor. The seawater pCO_2 values showed an increasing trend with a depth ranging from 450 µatm at the surface to 1300 µatm at 100m depth. The CO_2 fluxes were estimated empirically from the CO_2 solubility, gas transfer velocity, and partial pressure difference between air and seawater. The calculated fluxes suggest that the region acts as a net CO_2 source to the atmosphere with average values of 0.186 mmol C m^{-2} y^{-1}. The strong wind mixing of the sea surface water was a significant contributing factor to the fluxes in this region.

Valsala and Murtugudde (2015) have attempted to analyze the intra-seasonal and mesoscale variations occurring in the CO_2 gas transfer during boreal summer (June-September) over the western Arabian Sea. The oceanic circulation triggered by the fluctuations in the atmospheric circulation in this season induces intense upwelling, eddy formation, increased salinity levels, and consequently elevated levels of nutrients and carbon content in the surface waters of the Somali coast. The study used a biogeochemical model called the Ocean Tracer Transport Model (OTTM) based on a reanalysis of ocean data and surface fluxes. The sea surface pCO_2 was observed to

undergo consistent intra-seasonal variability in this region driven by the changes in sea surface temperature and dissolved inorganic carbon content. The analysis showed a correlation of 0.86 between pCO_2 variability and temperature, which decreased with the increased upwelling and Ekman pumping. This pCO_2 variability during the boreal summer accounts for 40% of this season's mean monthly CO2 flux variability. The seasonal co-variability of the outflux of CO_2 gas with decreased SST can be explained by the increase in DIC resulting from the intense upwelling. The study also establishes the significance of ocean dynamics in the pCO_2 and CO_2 flux intra-seasonal variability by analyzing the response of SST, DIC, alkalinity, pCO_2, and biological pumps towards the dynamic processes in the ocean system.

The CO_2 flux pattern study between seawater and air over the southern Bay of Bengal by Shanthi et al (2016) reported high seasonal variations in the physicochemical and biological parameters. The summer season was characterized by intense light penetration due to low cloud cover, reduced nutrient concentration due to the absence of river discharge and vertical mixing, consequent decrease in biological production, lowering surface pCO_2 and negative CO_2 fluxes. The summer trends in the physical, chemical and biological factors reversed during the monsoon season. Strong wind action and enhanced upwelling contributed to the high pCO_2 values and sea-to-air fluxes. The annual CO_2 flux variability ranges from -1752 mmol C m^{-2} y^{-1} to 4088 mmol C m^{-2} y^{-1} with an annual mean of 73 mmol C m^{-2} y^{-1}.

CO_2 partial pressure and flux measurements were made in the Hooghly estuary by Padhy et al (2016) using in-situ measurements and satellite data. SST and Chl-a were used to derive the seawater partial pressure, revealing supersaturation levels. The high riverine fluxes account for the high DIC levels in this region, contributing to enhanced pCO_2 levels. The winter pCO_2 levels range from 340-375 µatm, and summer values were found to be about 450 µatm. The comparatively lower values in winter are attributed to the lowering of salinity by the river discharge and weak wind action. The average annual CO_2 fluxes were about 4.5×10^4 mmol C m^{-2} $year^{-1}$, proving the region as a CO_2 source.

2.2.2 The Pacific Ocean

Midorikawa et al (2002) analyzed the CO_2 partial pressure distribution and dissolved inorganic carbon and nutrients concentrations in the western subarctic North Pacific region. The fluxes derived during winter to summer were about 5840 mmol m^{-2} y^{-1}, and during summer to autumn were -1460

mmol m^{-2} y^{-1}. The high fluxes during winter and summer are due to the high DIC in the mixed layer and the deep vertical mixing. The decreased CO_2 partial pressures due to the increased biological consumption and the comparatively low wind speed during the summer season have resulted in the reversal of fluxes from summer to autumn.

Carbon dioxide fugacity measurements of surface water were carried out by Feely et al (2004) in the equatorial Pacific Ocean, which showed a CO_2 supersaturation of seawater with average values of 473 µatm. The higher partial pressure values were attributed to the enhanced upwelling in the region, which resulted in about 20-40 µatm higher than normal values, with the highest values obtained in the southern equatorial Pacific, where the upwelling was intense. The drawdown of CO_2 by the ocean's primary productivity was counterbalanced by the upwelling and surface warming, thus maintaining the sea-to-air fluxes. A relationship between the CO_2 gas transfer and wind speed was developed along with estimates of air-sea partial pressure differences to derive CO_2 fluxes. The average CO_2 fluxes were 3.7×10^3 mmol m^{-2} yr^{-1}. The variability in fluxes was contributed mainly by the partial pressure changes in this region, where the influence of wind field and gas transfer variability was less.

Inter-annual and decadal flux variability over the equatorial Pacific Ocean was studied by Feely et al (2006) using ship measurements of SST and CO_2 fugacity collected during the period November 1981 to June 2004, which included five El Nino and four La Nina events. An increase in the sea surface CO_2 was observed at a similar rate to that of atmospheric CO_2, indicating an active exchange of air-sea CO_2 in the equatorial waters. A significant inter-annual ENSO variability was observed for the entire region from analyzing seawater fugacity in combination with SST and wind data. At the same time, the seasonal changes were noted as weaker in the eastern Pacific. A noticeable increase in the fCO_2sw (CO_2 fugacity of seawater) was observed over the entire study period and a slight intensification of the CO_2 out flux after the 1997-1998 warm-to-cold regime shift resulting from the Pacific Decadal Oscillation (PDO).

Ship measurements of SST, salinity, sea surface and atmospheric CO_2 from the northwest and northeast Pacific were analyzed by Takamura et al (2010) to investigate the inter-annual and seasonal variability in the CO_2 fluxes from 1999-2006. In the western and eastern North Pacific, the fluxes showed the minimum values during late summer (August/September) and reached the maximum during late winter (January/February). The summer flux values over the western region

ranged from -73 to 219 mmol m^{-2} y^{-1}, whereas the flux maximum during the winter exhibited a value range of 2993 to 4161 mmol m^{-2} y^{-1}. The eastern region has the minimum flux range within -1058.5 to -657 mmol m^{-2} y^{-1} during summer and a maximum range of 1898 to 2482 mmol m^{-2} y^{-1} in the winter season. The fluxes from air to seawater were found to increase over the study period, where the western North Pacific showed a comparatively higher rate of 69±18.25 mmol m^{-2} y^{-1}, indicating a much stronger CO_2 sink than the eastern region with a flux rate of 32.85±10.95 mmol m^{-2} y^{-1}.

Climatic impacts on the CO_2 flux variability in the northern Pacific Ocean were investigated by Valsala et al (2012[b]) for the period 1980 to 2004. CO_2 flux data was analyzed for Spatio-temporal variability over the study area, followed by a comparative analysis of interannual variability with the seasonal changes. Spatial flux variability induced by Pacific Decadal Oscillation, generated by the SST anomalies in the North Pacific, was analyzed using correlation analysis between monthly CO_2 fluxes and PDO index anomalies. The study revealed minimal spatial variability of fluxes about PDO, which was attributed to the weak inter-annual flux anomalies in the North Pacific. Flux anomalies were noticed in the Subtropical Gyre where PDO accompanied SST cooling has resulted in CO_2 absorption and eventual generation of the sink, thus establishing an active flux response to climate variability. It was observed that thermocline shifts associated with PDO were reflected in subsurface DIC levels.

Valsala et al (2014) studied the seawater pCO_2 and CO_2 fluxes over the equatorial Pacific for the seasonal, inter-annual, and multi-decadal variability from 1961–2005. They used the biogeochemical model based on the reanalysis of ocean products to study the seasonal cycle and spatio-temporal characteristics of the pCO_2 and CO_2 fluxes during the ENSO period, both individual and combined effects of the wind and ocean dynamics on the variability of pCO_2 and CO_2 fluxes, the impact of the canonical and modoki ENSOs on the fluxed and also the carbon dynamics variability and its association with Pacific Decadal Oscillations. The analysis revealed a dominance of ENSO on the interannual flux variability. A reduction in CO_2 emission was observed in the central to eastern equatorial Pacific during the El Niño period. The effect of canonical El Niño was found mainly between 160˚ W and 110˚ W. At the same time, the El Niño-Modoki dominated over the western (160˚ E - 160˚ W) and far eastern (110˚ W - 90˚ W) equatorial Pacific. A correlation of the pCO_2 was observed with the canonical El Niño to the east of 140˚ W, and with the El Niño-Modoki to the west of 140˚ W. A nonlinear relationship between the pCO_2 and CO_2 fluxes was introduced in some parts of the equatorial Pacific by the individual as well as combined influence of the ENSO

induced wind and ocean dynamics. Abrupt shifts were observed in the equatorial Pacific CO_2 sinks during the 45-year study period. The multi-decadal variability brought about an increased uptake of the atmospheric CO_2 from 1961 to 1982, followed by a reduction until 2000 and again a strengthening of the sinking process. The study concluded that the PDO and El Niño-Modoki are the major controlling factors of the pCO_2 and CO_2 flux multi-decadal variability, while the canonical El Niño events dominate the inter-annual variability.

Time series data of high-resolution CO_2 flux were calculated by Sutton et al (2017) over the Pacific Ocean from moored observations of sea surface pCO_2 and wind speed measures. These moorings are located in four specific locations of north and south subtropical oligotrophic region, subtropical and subarctic North Pacific regions. Atmospheric and seawater pCO_2, SST, and salinity were measured from four locations using moored autonomous pCO_2 system setup in open ocean buoys located at subtropical North and South Pacific and subarctic North Pacific regions. Total alkalinity was calculated using SST and salinity, which was further used along with the seawater pCO_2 to calculate dissolved inorganic carbon. The CO_2 flux was calculated using gas transfer velocity, CO_2 solubility, and pCO_2 difference between seawater and atmosphere. The analysis showed an eventual shift of this oceanic region from an annual sink to a source of CO_2, which was attributed to elevated levels of sea surface pCO_2 resulting from the thermal anomalies in the North Pacific region. The subtropical North Pacific location proved the strongest sink with -647.7 mmol C m^{-2} yr^{-1} and the southern subtropical oligotrophic region was the only source with 106.8 mmol Cm^{-2} yr^{-1}.

2.2.3 The Atlantic Ocean

Inter-annual CO_2 flux variability over the northern North Atlantic Sea for the period 1981-2001 during the winter season were analyzed by Olsen et al (2003). The data analysis was carried out from October to March to calculate the fluxes using seawater CO_2 fugacity, CO_2 mole fraction, gridded datasets of SST, sea level pressure, and wind speed. A net annual air-to-sea CO_2 flux of 1.818×10^{15} mmol was obtained for the winter season for the study period with an inter-annual variability of ±0.7%. This variability was attributed mainly to the variations in wind speed and atmospheric CO_2 fugacity. The air-sea CO_2 flux was also sensitive to the variations in North Atlantic Oscillation (NAO), and an increased CO_2 influx to the ocean with a high NAO index was observed.

A study on the inter-annual variability in the CO_2 sinks in North Atlantic subtropical gyre over a two-decadal period was carried out by Bates (2007). Oceanic CO_2 was monitored continuously from 1983-2005, which showed an increasing annual trend in the DIC and pCO_2 with an increase in atmospheric CO_2 concentrations, followed by a subsequent decrease in seawater pH, carbonate concentration, and $CaCO_3$ saturation states. An imbalance in the seasonal CO_2 sink and source rates was also observed, attributed to the comparatively higher CO_2 uptake in winter than the summer outflux, proving this region is a CO_2 sink. The net air-sea CO_2 flux was estimated to be between -815 to -1295 mmol C m^{-2} yr^{-1}. The occurrence of Hurricane events enhanced the fluxes during the summer season. The fluxes also correlated with the North Atlantic Oscillation (NAO) variability in the summer and fall seasons. However, poor correlations were found in the case of the winter fluxes with NAO or Arctic Oscillation (AO), whereas they showed higher values during El-Niño years. The study period also observed an increase of 5-17% in the net annual CO_2 flux rate.

Oliveiraa et al (2019) studied the CO_2 fluxes over the southern Atlantic Ocean coastal and open ocean waters during the austral winter period of 2015. They analyzed the eddy covariance measured in-situ CO_2 fluxes for the 13^{th} and 14^{th} of July of 2015 in three sub-regions of the study area, namely the Brazilian southeast coastal region (BCR), the region influenced by the Brazil Current (BC) and the open ocean (OPO). The analysis showed a contrasting flux trend over the three selected study regions. The BC and BCR regions were found to act as carbon sinks, as demonstrated by the measured negative flux values. It was noticed that an intensified mixing process at the ocean-atmosphere interface in the BC region induced by the intense winds in this oceanic part favoured the CO_2 absorption by the ocean waters, which again strengthened by the temperature difference between the sea surface and atmosphere at the marine atmospheric boundary layer. The presence of coastal upwelling was the consequence of the CO_2 sinking in the BCR region. Here the low values of SST and SSS were observed to increase the CO_2 solubility of surface waters, resulting in enhanced primary productivity. In contrast to BC and BCR, the OPO region lacks the CO_2 sink due to the decreased sea level pressure and weakened wind speeds triggering vertical movements in the MABL over this area leading to a decrease in atmospheric CO_2. As a result, the OPO region acts as a CO_2 source in the atmosphere. The study region exhibited a mean sinking behaviour in the flux trends during the sampling period caused by the combined impact of large-scale atmospheric processes, and the local atmospheric modulations developed from the SST variations. The authors conclude

with a statement suggesting the inclusion of further in-situ data with a better spatial and temporal resolution for an enhanced understanding of the carbon budget over the southwest Atlantic region.

Orselli et al (2019) tried to understand the significance of the Agulhas eddies in the air-sea CO_2 fluxes over the south Atlantic Ocean using in-situ measurements from six eddies and their surrounding waters carried out as a part of FORSA (Following Ocean Rings in the South Atlantic) cruise during the period 27th June to 15th July 2015. The study area was divided into eastern and western basins, with the Mid-Atlantic Ridge as the boundary. The sea surface and atmospheric CO_2 partial pressures were calculated from the measured parameters like temperature, salinity, and CO_2 mole fraction for seawater and overlying air. The surface temperature, salinity, and seawater CO_2 partial pressure values were comparatively less in the eastern basin, while low values of atmospheric partial pressures were obtained in the western basin. Eastern basin fluxes were regulated by physical forcing mechanisms driven by the Agulhas eddies, whereas biological dominance can be considered in the case of flux trends in the western basin. The difference in the ocean and atmospheric partial pressure calculated was -39.1 µatm, proving the oceanic region a sink for atmospheric CO_2 with a mean flux value of -1372.4 mmol m^{-2} y^{-1}. Temperature domination in the CO_2 absorption was observed during the study period, and the contribution of Agulhas eddy in this CO_2 uptake was found to be -262×10^5 mmol C y^{-1}.

2.2.4. Other Oceanic Regions

The study on seasonal variations in CO_2 and nutrients in the high latitude oceanic regions by Takahashi et al (1993) analyzed the CO_2 and nutrient concentration and pCO_2 data to define their seasonal relationship and compare the inter-ocean variations of these parameters. The springtime phytoplankton blooms in the North Atlantic Ocean were found to reduce the surface pCO_2, nutrient, and CO_2 concentrations, which lasted only until the exhaustion of the available nutrients. Such processes were limited only to the high latitude waters north of 40˚N. In the North Pacific, the seasonal CO2 and nutrient concentrations variations were occurring gradually. In contrast, nutrient consumption was partially observed in the subarctic North Pacific and the Southern Ocean regions. The concentrations of CO_2 and nutrients and the surface pCO_2 showed higher values during winter in the subpolar, and polar waters of the South Atlantic, North Pacific, and North and South Atlantic Oceans compared to the summer season. The high latitude areas of the North Atlantic, North Pacific, and the Weddell Sea acted as sources of CO_2 to the atmosphere in winter and sinks in summer. This

seasonality in the fluxes was attributed to the intense winter upwelling and increased summertime photosynthesis. However, in the case of tropical waters, the CO_2 uptake from the atmosphere was found to occur during winter, while out fluxes were observed in summer. Here, the temperature was the critical element regulating the seasonal pCO_2 fluctuations due to the weakening of biological factors. The combined effect of subtropical cooling and strong photosynthetic consumption of CO_2 in subpolar waters resulted in the generation of an intense sink in the subtropical convergence region.

Estimation of global CO_2 fluxes by Takahashi et al (1997) involved the measurement of partial pressure differences between air and ocean surface for around 250,000 global observations. The global monthly pCO_2 differences distribution was constructed from the lateral advection-diffusion transport equation, and the net CO_2 flux was calculated from the partial pressure and CO_2 gas transfer coefficients. An annual net uptake of 13.6-30.45$\times10^{15}$ mmol C yr^{-1} by the oceans was estimated, and the analysis revealed the temperate and polar regions as CO_2 sinks while equatorial regions as sources. The Atlantic Ocean was the most intense sink, accounting for about 60% of the global CO_2 uptake. The Pacific equatorial belt was a strong CO_2 source balanced by the temperate sinks. Thus, the Pacific Ocean was observed to act neutral in terms of fluxes. The contribution from the Indian and Southern Oceans combined for the CO_2 uptake was 20%.

Climatological monthly pCO_2 data, seasonal effects of biological factors, and temperature were used by Takahashi et al (2002) to calculate the global air-sea CO_2 fluxes, where the monthly and annual fluxes were estimated using mean monthly wind speed data. The net annual uptake estimates were obtained as 50×10^{15} mmol C yr^{-1} and the regions between 40˚ and 60˚ latitudes were found to be the significant CO_2 sinks in both hemispheres consequent to the mixing of nutrient-rich sub-polar cold waters with the poleward flowing warm waters along with the biological CO_2 uptake, subsequently resulting in decreased pCO_2 in subpolar waters. The high wind speed over the low surface pCO_2 waters also enhanced the oceanic CO_2 uptake. Thermal and biological effects were observed to control the pCO_2 seasonality for specific areas, whereas the pCO_2 seasonal maximum was regulated by thermal and physical forcing such as upwelling. The biological component dominated the eastern equatorial Pacific, equatorial and subpolar waters, the north-western Arabian Sea, the Antarctic, and the sub-Arctic North Pacific coastal waters, while the temperature component was found to influence the subtropical gyre areas.

Air-sea CO_2 fluxes over the northern South China Sea were derived by Zhai et al (2005) during spring, summer, and autumn seasons. Data collection for temperature, pCO_2, and salinity was done during the ship measurements conducted for the summer of 2000, spring in 2001, and fall season of 2002. The surface water partial pressures in the offshore region of about >100 km from the coast were in the range of 360-450 µatm and were higher than that of the atmosphere in all three seasons. The sea-to-air difference in the partial pressures was observed to be about 0-50 µatm in the spring, 0-90 µatm in the autumn, and 50-100 µatm in the summer. The average flux values from the ocean to the atmosphere were 2555 mmol m^{-2} y^{-1} for summer and 365-1095 mmol m^{-2} y^{-1} during spring and fall seasons. The observations convey that the seasonal variations in the sea surface partial pressures are influenced primarily by temperature changes, and the region was found to act as a net CO_2 source.

The study by McNeil et al (2007) in the Southern Ocean empirically derived the seawater CO_2 partial pressures from SST, sea surface salinity, DIC, and total alkalinity (TA) and computed the CO_2 fluxes for winter and summer seasons. The CO_2 partial pressures were higher up to 40 µatm in winter than in summer in the Antarctic Zone due to the winter upwelling. In the Sub Antarctic Zone, the winter cooling decreases the pCO_2 values by up to 70 µatm. The changes in winter to summer DIC showed significant variations in the pCO_2. The high DIC values in the winter due to the upwelling enhanced the pCO_2 by up to 150 µatm in the Antarctic Zone, while in the Sub-Arctic Zone, temperature-induced seasonal partial pressure changes dominated the DIC variations. The estimation of CO_2 fluxes showed that the Southern Ocean acts as a weak to moderate global sink with average flux values -9.09×10^{15} mmol C y^{-1}.

The Southern Ocean is reported to act as a significant atmospheric CO_2 sink based on observational and modeled data sets. However, the study conducted by Gray et al (2018) based on flux measurements using biogeochemical profiling floats as a part of the Southern Ocean Carbon and Climate Observations and Modeling (SOCCOM) project during 2014-2017 reported a strong CO_2 source region around Antarctica resulted from upwelling of deep carbon-rich waters. The lack of ship-based observations in this high-latitude region can be the principal reason behind the delay in identifying this CO_2 source region. Data sets of various parameters like temperature, salinity, pH, NO_3, and dissolved oxygen from 35 profiling floats were analyzed. The study area was divided into five zones based on SST, salinity, and nutrient content, namely Subtropical Zone (STZ), Sub Antarctic Zone (SAZ), Polar Frontal Zone (PFZ), Antarctic Southern Zone (ASZ) and Seasonal Ice

Zone (SIZ) from north to south. The seasonal average of CO_2 fluxes was calculated for each zone. The results were found to agree with the temperature, and DIC drove regulations in the summer CO_2 uptake by biological processes and winter release. The analysis showed that, despite the outgassing in the STZ and SAZ, these regions acted as sinks with flux values -7.95×10^{15} and -2.27×10^{15} mmol C y^{-1} respectively. While PFZ and SIZ were found to act as weak sources with negligible outgassing (0.227×10^{15} mmol C y^{-1}), the ASZ represents a substantial CO_2 source, outgassing 8.18×10^{15} mmol C y^{-1}.

Mongwe et al (2018) examined the significance of temperature and dissolved inorganic carbon in driving the seasonal cycle of CO_2 flux in the Southern Ocean. As per recent studies, the seasonality in the CO_2 fluxes over this oceanic region is not well simulated by the Coupled Model Inter-comparison Project version 5 (CMIP5), as evident from a comparison with observational data. This study explains the CMIP5 model's bias related to seasonal variations in SST and DIC. SST-related biases were grouped as group-SST, the most commonly observed bias exhibiting an exaggerated rate of seasonal temperature variations during warming and cooling peaks in the spring and autumn seasons. Group-DIC bias shows the exaggerated primary production scenarios, indicating a DIC-dominated flux variation. The study selected 10 CMIP5 models for the analysis, based on the availability of required parameters like pCO_2, CO_2 fluxes, SST, vertical temperature fields, surface DIC, annual DIC, Mixed Layer Depth (MLD), surface oxygen, chlorophyll and net primary production (NPP). The analysis showed a low model sensitivity for the inter-basin CO_2 flux differences. The study reports that this is most likely due to the less sensitivity of the carbon cycle in these models compared to the observational data towards the inter-basin difference in the driver parameters of the fluxes. This results in a zonal uniformity in the seasonal flux biases. Moreover, since the flux direction is dependent on the air-sea partial pressure difference and the sea surface partial pressures are regulated by the SST and DIC concentrations, the model's ability to simulate the flux seasonality is dependent on the sensitivity of the model toward the regulation of fluxes by variations in SST and DIC. As the CMIP5 models lack a proper representation of inter-basin contrasts in the CO_2 fluxes and phytoplankton biomass compared to observational and remote sensing data, the study concludes with remarks explaining the necessity of further investigations with the following generation models such as CMIP6, giving a proper representation of carbon process parameterization and dynamics of the water column physics.

2.3 Interrelationship Between the Spatio-Temporal Distribution of Ocean Primary Productivity and CO_2 Fluxes

The air-sea CO_2 fluxes are regulated primarily by the fluctuations in the sea water CO_2 partial pressures. The major controlling factors of sea water partial pressure are variations in sea water temperature and biological consumption of CO_2. An increase in the SST decreases the CO_2 gas solubility, thus enhancing the gas release, while a decrease in SST increases the CO_2 dissolution in water. However, warming the waters will induce surface stratification and reduce vertical mixing. The marine biological productivity consumes the surface CO_2, thus reducing the partial pressures. The biologically trapped CO_2 in the subsurface layers will be released back in to surface during upwelling triggered by a reduction in the SST. Therefore, a combination of the SST and productivity will decide the flux direction between the water and air (Metzl et al, 2006; Sharada et al, 2008)

Analysis of seasonal variations of CO_2 fluxes was carried out in the high-latitude oceans by Takahashi et al (1993). The high-latitude regions of the North Pacific, North Atlantic, and Weddel Sea are characterized by surface stratification and high phytoplankton blooms in summer. The stratification prevents surface mixing, and the increased productivity draws down the surface CO_2, which makes these regions sink of CO_2. During winter, the intense upwelling in these waters' releases CO_2 gas into the atmosphere, acting as a source. The subtropical waters have low levels of nutrients and productivity. Thus, the flux regulation is primarily controlled by temperature variations. These waters act as a CO_2 source in summer due to the enhanced gas emission rates with an increase in temperature and become sinks in winter.

The variations in the summer and winter CO_2 fluxes over the Sothern Ocean were studied by Metzl et al (2006). The partial pressures during summer were very low compared to the atmosphere. The summer fluxes range from -2 to -4 mmol m^{-2} day^{-1} in the seasonal ice zone. The CO_2 exchange in winter is limited in this region by the surface ice cover. In the permanent open ocean zone, the summer fluxes ranged from -1.1 to -1.7 mmol m^{-2} day^{-1}. The partial pressures increased from summer towards winter by up to 10-30 µatm. The winter partial pressures were higher than the atmospheric values and the fluxes ranged from 2.5 to 11.6 mmol m^{-2} day^{-1}. The high photosynthetic consumption of DIC during summer lowers the water CO_2 levels, resulting in the absorption of atmospheric CO_2. During winter, the Chlorophyll concentrations are low, and the light limitation

reduces the photosynthetic activity. The deep mixing elevates the surface DIC levels and partial pressures.

The role of the primary productivity in seasonal variation of sea-air CO_2 fluxes in the Arabian Sea and Bay of Bengal was analysed by Sharada et al (2008). The northwestern Arabian Sea's intense upwelling triggers high monsoon productivity, which consumes the DIC through carbon fixation and lowers the surface CO_2 levels. The biological impact on the CO_2 fluxes is comparatively less in the Bay of Bengal since upwelling and surface mixing are weak in this region. The domination of the regeneration process over carbon fixation in the Bay of Bengal increases CO_2 levels.

The seasonal pCO_2 cycle and its impacts on biological production for the northeastern Atlantic Ocean by Kortzinger et al (2008). The study revealed that the surface waters were undersaturated by up to 40 µatm concerning the atmospheric values, making the region a perennial CO_2 sink with flux values -3.2 mol m^{-2} $year^{-1}$. The pCO_2 cycle experiences a summer minimum and winter maximum, where the biological forcing dominates in summer. Summer stratification, along with biological CO_2 consumption, causes a reduction in pCO_2 values. The winter ventilation by deep mixing brings the CO_2 from subsurface respiration, attaining the winter pCO_2 maximum. A rapid change of deep winter mixing to summer stratification is exhibited by the oceanic region, significantly affecting biological production and resulting in the accumulated biomass in the deep ocean.

Wang and Moore (2012) studied the variability of CO_2 fluxes and primary productivity in the Southern Ocean. The study reported a decreasing trend in sinking particulate organic carbon and primary productivity and a consequent decrease in atmospheric carbon uptake by the ocean. The productivity was controlled by the light limitation in the mixed layer. The sea ice cover also restricted the photosynthetically available radiation and the sea-air CO_2 exchange, affecting productivity and fluxes. The annual primary production decreased by 0.4 PgC $year^{-1}$. The CO_2 fluxes from the atmosphere to the ocean exhibited a weakening trend by about 0.05 PgC $year^{-1}$.

2.4 Development of a Regional Model for Basin-Scale pCO_2sw

The seawater partial pressures are primarily regulated by thermal variations and biologically induced CO_2 concentration changes in the water, while other important factors acting in combination with these are salinity, nutrient concentrations, and mixed layer depth. These parameters' significance in

controlling the partial pressures depends on the biogeochemistry of the oceanic regions (Takahashi et al., 2002; Padhy et al., 2016).

2.4.1 Remote Sensing Approach in partial pressure estimation

The key parameters governing the upper ocean biophysical processes are sea surface temperature and marine chlorophyll (Chl-a) concentration. Their precise measurements can be done on global and regional scales for world oceans using satellite remote sensors. Therefore, attempts have been made worldwide to derive various biophysical parameters potentially affecting the CO_2 partial pressures from Sea Surface Temperature (SST) and Chl-a. For example, seawater pCO_2 was estimated by equation 2.1 (Dickson and Goet, 1994) using total alkalinity and dissolved inorganic carbon.

$$pCO_2w = g \times (2 \times DIC - TA) + h \quad (2.1)$$

Total alkalinity (TA) was estimated by equation 2.2 as a function of SST by Millero et al (1998).

$$TA = e \times SST + f \quad (2.2)$$

Nutrient concentration was calculated as given in equation 2.3 from SST and Chl-a, by Goes et al (2000).

$$N = \alpha \times SST + \beta \times SST^2 + \gamma \times Chl\text{-}a + \delta \times Chl\text{-}a^2 + \varepsilon \quad (2.3)$$

Lee et al (2000) derived dissolved inorganic carbon using SST and nutrient concentration given as equation 2.4.

$$DIC = a \times SST + b \times SST^2 + c \times N + d \quad (2.4)$$

Where a, b, c d, e, f, g, α, β, γ, δ and ε are estimated constant parameters from the least square method.

These equations were combined to develop semi-empirical quadratic relation given in equation 2.5 by Ono et al (2004) for deriving sea surface pCO_2 as a function of sea surface temperature and chlorophyll concentration.

$$pCO_{2sw} = A \times SST + B \times SST^2 + C \times Chl - a + D \times Chl - a^2 + E \quad (2.5)$$

A, B, C, D, and E are the least square constants. Monthly averaged satellite data for SST and Chl-a from OCTS (Ocean Colour and Temperature Sensor) onboard the ADEOS (Advanced Earth

Observation Satellite) platform to develop monthly pCO_2 maps for subarctic and subtropical oceanic regions.

Other studies that incorporated satellite data for the pCO_2 determination include application of statistical regression techniques on SST data from NOAA AVHRR (Advanced Very-High-Resolution Radiometer) and Chl-a from SeaWiFS (Sea-Viewing Wide Field-of-View Sensor) by Sarma et al (2006) for the North Pacific Ocean, deriving partial pressure for northern South China Sea by Zhu et al (2009) using SST and Chl-a retrieved from AVHRR and SeaWiFS respectively, mapping pCO_2 over Huanghai and Bohai Sea by Zui et al (2012) from Aqua MODIS (Moderate Resolution Imaging Spectroradiometer) SST and SeaWiFS Chl-a, using SST from AMSR-E (Advanced Microwave Scanning Radiometer- Earth Observing System) on board Aqua and Chl-a from SeaWiFS and MODIS on board Terra and Aqua by Liu & Xie (2014) for calculation of partial pressure for global oceans, use of SST and Chl-a from MODIS for Hooghly estuary by Padhy et al (2016) and the study by Jang et al (2017) where Chl-a, colored dissolved organic matter (CDOM) and band reflectance from Geostationary Ocean Color Imager (GOCI) on board COMS (Communication, Ocean and Meteorological Satellite) satellite were used over East Sea**.**

2.4.2 pCO_2 Estimation Techniques

Stephens et al (1995) developed sea surface pCO_2 maps for the North Pacific by deriving statistical relationships between the ship-measured pCO_2 and SST and applying them to the entire region using satellite-derived SST with a root mean square error of ±17µatm. The derived relation was given as equation 2.6.

$$\ln[pCO_2(10^{\circ}C)] = A + B \times SST + C \times SST^2 + D \times longitude \quad (2.6)$$

Seasonal and inter-annual relationships between the CO_2 fugacity and SST from ship measurements were developed by Cosca et al (2003) for the central and eastern equatorial Pacific Ocean for El-Niño cool and warm event and non-El-Niño cool and warm event periods. The RMS values were ±20.3 µatm and ±16.6 µatm for El-Niño warm and cool seasons, respectively; ±28.8 µatm and ±30.2 µatm for non-El-Niño warm and cool seasons, respectively. The linear statistical algorithm obtained can be represented as equation 2.7.

$$fCO_2 = A + B \times SST \quad (2.7)$$

The seawater CO_2 partial pressures in the North Pacific Ocean were derived from ship measurements of Chl-a and SST by Ono et al (2004), and pCO_2 maps for the region were developed using satellite-derived Chl-a and SST. The RMS value for the satellite-derived pCO_2 was ±21 µatm. Incorporating Chl-a along with SST in the pCO2 derivation reduced the RMS error compared to the previous study by Stephens et al (1995) that developed the pCO_2 maps from the SST data in this region. The algorithm designed for sea surface pCO_2 is given in equation 2.5.

The distribution of sea surface pCO_2 in the North Pacific Ocean was mapped by Sarma et al (2006) from satellite-derived Chl-a, SST, and sea surface salinity by applying multiple regression equations developed from in-situ data. The RMS error obtained for the satellite-derived pCO_2 was 17-23 µatm. The algorithms were developed for spring and summer periods, and the general form of the algorithm is given in equation 2.8.

$$pCO_2 = A - B \times SST + C \times SSS - D \times Chl - a \quad (2.8)$$

Zhu et al (2009) estimated the sea surface CO_2 partial pressure and CO_2 fluxes in the northern South China Sea using statistical relationships derived from in-situ measurements of SST and Chl-a, and pCO_2 maps were developed from the satellite-derived SST and chlorophyll. Two algorithms were developed using regression analysis for deriving sea surface pCO_2, the first one with in situ SST data and the other with in situ SST and chlorophyll measurements. The satellite-derived pCO_2 was compared with the in-situ values, which showed a root-mean-square error of 4.6 µatm for the two-parameter algorithm, while it was found to be 25.1 µatm for the SST-based relation. The relationship of pCO_2 and SST can be given as equation 2.9.

$$pCO_2 = A \times SST^2 - B \times SST + C \quad (2.9)$$

Equation 2.10 shows the pCO_2 relationship with SST and Chl-a

$$pCO_2 = A \times SST^2 + B \times Chl - a^2 - C \times SST - D \times Chl - a + E \quad (2.10)$$

Shipboard measurements of pCO_2sw, SST, and salinity were used to develop the partial pressure algorithm for seawater from SST, salinity, and time component by Takamura et al (2010) over the eastern and western North Pacific Ocean. The time parameter was introduced to address the temporal variations. The equation describing the relation can be expressed as equation 2.11.

$$pCO_{2sw} = a0 + a1 \times SST + a2 \times SSS + a3 \times t \quad (2.11)$$

where t is the elapsed time in months, the sea surface salinity exhibited the maximum significance among the parameters on the variability of partial pressure. The root-mean-square error obtained for the eastern North Pacific Ocean was ±11.3 µatm. For the western region, different temperature conditions were considered for the statistical analysis, where the error received was ±13.4 µatm for <17.5˚C and ±12.1 µatm for ≥17.5˚C.

Zui et al (2012) investigated the seasonal variability of seawater pCO_2 in the Huanghai and Bohai Sea about SST and Chl-a using ship measurements. The study proposed an empirical relation between the pCO_2, SST, and Chl-a to develop pCO_2 maps using the satellite data. The satellite-derived pCO_2 value showed an RMS error of 13.45 µatm. The algorithm was developed for three different SST ranges given as SST<12˚C, 12˚C≤SST≥23˚C, and SST> 23˚C. The basic form of the algorithm can be written as equation 2.12

$$pCO_2 = A \times SST + B \times SST^2 - C \times Chl - a + D \times Chl - a^2 + E(T) \quad (2.12)$$

Carbon dioxide fugacity in the East Sea was derived from in-situ measurements of dissolved organic matter, SST, salinity, mixed layer depth (MLD), Chl-a, and band reflectance by Jang et al (2017). The fCO_2 was derived using multivariate non-linear regression (MNR), where SST showed maximum correlation with pCO_2 distribution, and the major contributing factors for fCO_2 variations were SST, salinity, and MLD. The MNR algorithm can be given as equation 2.13.

$$\mathrm{fCO2} = \sum_{i=1}^{n} k_i x_i + \sum_{l=1}^{n-1} \sum_{m=l+1}^{n} k_{lm} x_l x_m + \sum_{j=1}^{n} k_j x_j^2 \quad (2.13)$$

where 'n' is the number of input parameters, x_i is each input parameter, and k is the coefficient associated with each term. The RMSE obtained for validation of the algorithm was 10.59 µatm.

Seawater pCO_2, SST, and SSS time series data for the Bay of Bengal open ocean waters were used to derive multiple linear regression models by Dixit et al (2018). The empirical relation obtained was applied on satellite SST and SSS to develop the pCO_2 map for the case 1 waters of the Bay of Bengal (BoB) (Equation 2.14).

$$pCO_2 = 11.81\mathrm{SST} + 11.71\mathrm{SSS} - 337.1 \quad (2.14)$$

where SST is the sea surface temperature, SSS is the sea surface salinity, and the RMSE for validating the derived pCO_2 was 9.22µatm.

2.5 Impacts of Nutrient Distribution, Surface Temperature, and Wind Anomalies on CO_2 Fluxes

2.5.1 Nutrient Dynamics

The variations in nutrient availability are regulated by the fresh water and sediment fluxes by river discharge. The nutrient distribution of the Bay of Bengal exhibits significant seasonal fluctuations due to the heavy monsoonal discharge of fresh water by the Ganga-Brahmaputra river system. The sediment fluxes contributed by the river influx dominate the nutrient availability and primary productivity in BoB. The composition of the particle fluxes plays a significant role in the carbonate chemistry of surface waters. The elemental composition of the suspended particles in the water can help understand the marine biogeochemical cycles and their interlinkages. The ratio of the organic to carbonate particles affects the surface CO_2 levels. A high ratio indicates increased biological activity on the surface, thus increased absorption of atmospheric CO_2 into the water (Ittekot et al, 1991; Martiny et al, 2014).

The study on the fresh water discharge induced particle fluxes in the Bay of Bengal by Ittekkot et al (1991) reported the maximum discharge during the southwest monsoon. The monsoon discharge exhibited two peaks; the first peak was in early June due to melt water influx, and the riverine sediment flux caused the second. The southwest monsoon fluxes represent about 40-50% of the total annual fluxes, while fluxes were considerably low during the northeast and inter-monsoon periods. North to south increase in the carbonate fluxes and decrease in organic carbon and particulate matter observed. The flux patterns were regulated by seasonal changes in river input which ultimately influences the marine biogenic production and consequent variations in the CO_2 fluxes.

Global distribution of the nutrients nitrate, phosphate, and silicate by Levitus et al. (1993) with depth has reported high nutrient concentrations in the high latitude surface waters along with the presence of upwelling phenomena, whereas the nutrients get depleted towards the mid-latitudes due to the development of subtropical anticyclonic gyres. Nutrient content in the water column was observed to be increasing with depth. Nitrate is the most limiting nutrient in the surface waters since it is depleted by most phytoplankton in the photic zone. The eastern tropical pacific and high-latitude oceanic regions were the exceptions. Surface concentration patterns showed maximum nitrate south of the Sub-Antarctic Convergence zone. Phosphate, unlike nitrate, is present in most global surface

waters owing to its faster regeneration rate; the highest concentrations are in the Antarctic (> 2 $\mu molL^{-1}$). Its abundance can also be detected in the sub-polar gyres of the Pacific and Peru's upwelling regions. The depleted phosphate levels were found in the mid-latitude regions of the North, South Pacific, and North Atlantic. The regeneration processes of silicate nutrients are different from that of nitrate and phosphate, and its depletion is prominent where blooms of siliceous plankton are present. This nutrient is found limiting over the southern region of 45° N Pacific and the northern region of 45° S Atlantic and Indian Ocean surface waters. Silicate can be detected in abundance in the Weddell Sea. Considering the deeper layers, the distribution of the nutrient concentrations is defined by the biochemical processes; reaching depths more than 1000m, high concentrations were found in the Northern Indian and North Pacific Oceans, while the Atlantic Ocean showed relatively low nutrients.

Ramaswami and Nair (1994) studied the particle fluxes in the Arabian Sea and Bay of Bengal to analyze the monsoon impacts on the marine biogeochemical cycles. The maximum fluxes were observed during both oceanic regions' southwest and northeast monsoon seasons, but the particle transport mechanism was different. The primary mechanisms involved in particle transport in the Arabian Sea are wind-induced coastal upwelling and aeolian dust transport during the monsoon season. The upwelled coastal fluxes are transported offshore by intense wind action. The aeolian carrier is the primary source of iron and other nutrients in the photic zone. In the Bay of Bengal, the prime source of particle flux is the river discharge by the Ganga-Brahmaputra river system. Organic carbon and inorganic nutrient concentrations were increased during the monsoon river discharge, contributing to the Bay of Bengal's marine productivity.

A lithogenic flux study in the Bay of Bengal by Ramaswami et al (1997) reported substantial seasonal variations in the trends. About 43-49% of the fluxes occur during the southwest monsoon when the fresh water influx is maximum. The East India Coastal Current and the rainfall variability controls the seasonal variations. The transport of the slow-settling lithogenic particles into the sea floor was enhanced by the aggregation with the heavy biogenic particles in BoB, resulting in increased lithogenic deep fluxes. The lithogenic particle removal to the deep ocean is active around the year with significant seasonal variations. The maximum scavenging occurred during the southwest monsoon due to the simultaneously increased productivity and suspended sediment load.

The effects of fresh water discharge and physical forcing on the seasonal variations of biomass and primary productivity of Bay of Bengal was studied by Gomes et al (2000). Bay of Bengal is characterised by the heavy fresh water influx by river discharge in monsoon, resulting in the salinity stratification and consequent hindering of vertical nutrient transport. The stratification was eroded by the physical processes like coastal currents and wind action, enhancing the phytoplankton concentrations. But the productivity was found to be comparatively less during the south west monsoon due to the light limitation induced by the heavy cloud cover in this region. The north east monsoon season was found to have an enhanced productivity due to the reduction in the cloud cover and the increased biomass and high nutrient availability from the south west monsoon season.

Martiny et al (2014) investigated the global oceanic distribution of concentrations and ratios of particulate organic phosphorus (POP), nitrogen (PON) and carbon (POC). The analysis used the time series cruise data for 40 years including about 6940 measurements of POP, 46728 measurements of PON and 46937 measurements of POC. The obtained ratios included 5573 C:P, 5948 N:P and 45476 C:N. The global ratios of C:N:P observed were 163:22:6.6.

2.5.2 Effects of SST and Wind Speed Anomalies on CO_2 Fluxes

El Niño is a basin-wide warming phenomenon caused by the displacement of the warm pool in the western Pacific Ocean towards east due to prolonged westerly winds. This leads to the breakdown of the normal west to east SST gradient from warm to cold which imbalances the quasi equilibrium of the ocean-atmosphere system and results in abnormal global temperature variations. Unusual variations in the SST trends have considerable impacts on the sea-air CO_2 fluxes (Feely et al, 1999; Sheu et al, 2010).

The role of El Niño in the CO_2 outgassing of the equatorial Pacific Ocean was studied by Feely et al (1999) during the 1991-1994 El Niño period. The study involved seasonal and inter-annual analysis of the sea-air CO_2 fluxes and compared the results with the non-El Nino fluxes of 1996. The comparison results showed that the El Niño fluxes were about 30-80 % of that in the non-El Niño period. The inter-annual effects of El Niño were higher during the spring season due to the prevalence of the warm El-Niño phase, which showed an increase in the flux values from 1.2 mol m^{-2} $year^{-1}$ in the 1992 El Niño period to 3.1 mol m^{-2} $year^{-1}$ in the 1996 non-El Niño period. Such trends in fluxes were caused by the weakening effect of warm phase on the upwelling of the CO_2

rich subsurface waters. The autumn fluxes in 1994 and 1996 showed high values, which were the result of intense upwelling triggered by strong winds in these periods. The net CO_2 fluxes from sea to air during the 1991-1994 period were considerably lower as compared to the fluxes in the 1996 non-El Niño period.

The study on the impact of wind speed and SST anomalies on the CO_2 fluxes over the equatorial Pacific Ocean by Feely et al (2004) reported a significant effect of ENSO on the CO_2 partial pressures. A reversal and weakening of the easterly trade winds during the 1997-1998 El-Niño event triggered a movement of the warm waters of the western Pacific towards the east causing unusual warming of the sea surface in the eastern Pacific. This resulted in the suppression of the upwelling in the eastern Pacific leading to a decrease in the CO_2 fluxes. The La Nina event followed this in late 1998 resulting in strong trade winds and upwelling with enhanced sea-to-air CO_2 fluxes. The difference in the CO_2 fluxes was about a factor of 6 between the El Niño and La Nina events in this region.

Sea surface pCO_2 variations in the equatorial Pacific Ocean during five El Niño and four La-Nina events from 1981-2004 were studied by Feely et al (2006). The pCO_2 values in the western Pacific were lower during the El Niño periods as compared to the non-El Niño periods due to the lateral transport of warm low CO_2 waters due to the strengthening of westerly winds. In contrast, there was an increase in the partial pressures in the eastern and central Pacific during the El-Niño period. During the El Niño periods, an increase in the influx of cold CO_2 rich waters was observed in the central Pacific by increased upwelling of deep waters and lateral transport of subtropical waters due to the increased wind speed, contributing to the increased pCO_2 levels.

Bates (2007) analysed the air-to-sea CO_2 flux variability in the North Atlantic Ocean during the El-Niño and La Nina events for two decades. The wind speed variability strongly influenced the interannual CO_2 distribution during the summer and fall seasons, which strongly correlated with the North Atlantic Oscillation. The winter fluxes were elevated by about 11-40% during the El Niño period compared to La Nina. The supersaturation levels in the stratified waters cause an efflux of CO_2 during summer. In contrast, the deep vertical mixing causes the dissolution of atmospheric CO_2 into the waters during the fall and winter seasons.

The influence of El Niño on the CO_2 fluxes over the northern South China Sea was studied by Sheu et al (2010), and reported a negative impact on the CO_2 release from the ocean to the

atmosphere in this region. The analysis showed that the fluxes were considerably reduced (85%) during the El Niño events compared to La Nina events. The reduced or no vertical mixing, along with the lateral transport of warm waters, has resulted in weakened fluxes. This reduction in fluxes during the El Niño events in the South China Sea contributes to an annual net reduction of about 0.032 Gt of carbon from sea to air.

2.6 Aim and Objectives of the Thesis:

Based on the research gaps observed from the studies carried out on the carbonate chemistry of northern Indian Ocean sub-basins and its impact on the CO_2 gas exchange process with the overlying atmosphere, the aim of the study has been outlined as "studying the significance of ocean biogeochemistry and climatology on spatial and seasonal variability of air-sea CO_2 fluxes in North Indian Ocean". To achieve this, the following research objectives have been identified:

1) To study the spatial and seasonal variability of air-sea CO_2 fluxes over the Indian Ocean,
2) To study the inter-relation between the spatio-temporal distribution of ocean primary productivity and CO_2 fluxes,
3) To develop a regional model for basin-scale pCO_2sw estimation from in situ measurements,
4) To study the impacts of nutrient distribution, surface temperature, and wind anomalies on CO_2 fluxes.

3

Spatial and seasonal variability in sea water pCO_2 and CO_2 Fluxes

3.1 Introduction

Oceans' primary role in balancing the anthropogenic CO_2 emissions to the atmosphere is better understood through spatial and seasonal analyses of the CO_2 flux distribution. The capacity of ocean in regulating these excess atmospheric concentrations will reduce eventually, due to disturbances in the marine carbon cycle and sea water carbonate speciation. Quantifying the past trends and analyzing the patterns to predict the future scenarios would help in better assessment of the key role played by the global oceans in maintaining the atmospheric CO_2 concentrations (Takahashi et al., 1993; Takahashi et al., 2002; Davila et al., 2007).

3.1.1 Carbon dioxide partial pressures as indicators of CO_2 fluxes

The CO_2 flux is primarily defined by the CO_2 gas transfer velocity, sea water solubility of the CO_2, and the difference in the CO_2 partial pressures at the sea surface and the air above termed as δpCO_2. Among these, pCO_2 is the thermochemical steering factor for the net air-sea CO_2 flux, determining the flux direction at the ocean-atmospheric interface. Compared to atmospheric pCO_2, spatial and seasonal fluctuations are more prominent in the sea water pCO_2, making it the principal factor in flux determination (Chester, 2000; Takahashi et.al. 2002). The accuracy of the CO_2 flux estimation thus depends on the spatio-temporal resolution of the measured pCO_2. Efforts have been made worldwide to obtain pCO_2 with better resolution using buoys and shipboard measurements. However, the spatial resolution of the present measurement network is far coarser (<250km grid), which emphasizes the requirement for improved extrapolation techniques (Ono et.al. 2004).

3.2 Methodology

Data sets and steps followed to calculate the CO_2 flux between the sea surface, and the air above is summarised in Table.3.1 and the methodology flow diagram (Figure. 3.1), respectively.

Table. 3.1 Data sources for CO_2 flux estimation

PARAMETER	SOURCE	SPATIAL RESOLUTION
SST	MODIS-AQUA	4km
Chl-a	MODIS-AQUA	4km
CO_2 mole fraction	AQUA-AIRS	2.5°×2°
Wind speed	AMSRE	0.25°×0.25°
Sea level pressure	MERRA	2/3°×1/2°
Salinity	World Ocean Atlas & Aquarius SMAP	1°×1° 0.25°×0.25°

The carbon dioxide flux is calculated using the formula from Santhi et al. (2016).

$$F = K_{wa} * Ko * (pCO_{2SW} - pCO_{2Air}) \quad (3.1)$$

F is the net ocean-atmosphere carbon dioxide flux in mmol/m^2/day

K_{wa} is the CO_2 gas transfer velocity in m/s; it is derived from sea surface temperature and wind speed (Wanninkhof, 1992)

$$K_{wa} = 0.31\ U^2\left(\frac{660}{Sc}\right)^{1/2} \quad (3.2)$$

K_{wa} normalised to a Schmidt number of 660 for sea water at 20°C. U is the wind speed in m/s at 10m above the surface. Sc is the Schmidt number derived from sea surface temperature where t is the temperature in degrees Celsius.

$$Sc = A - Bt + Ct^2 - Dt^3 \quad (3.3)$$

A= 2073.1 B= 125.62 C= 3.6276 D= 0.043219

Ko is CO_2 solubility in mol/l/atm in sea water derived as a function of sea surface temperature and salinity (Weiss, 1974), where T is the temperature in Kelvin and S is salinity in practical salinity units (psu).

$$\ln Ko = A1 + A2\left(\frac{100}{T}\right) + A3\ln\left(\frac{T}{100}\right) + S\left[B1 + B2\left(\frac{T}{100}\right) + B3\left(\frac{T}{100}\right)^2\right] \quad (3.4)$$

A1= -58.0931 A2= 90.5069 A3= 22.2940
B1= 0.027766 B2= -0.025888 B3= 0.0050578

The partial pressure of sea water (pCO_{2sw}) is derived as a function of satellite-obtained SST and Chl-a (Zhu et al., 2009) for the Arabian Sea as given in equation 3.5, and derived from SST and SSS (Dixit et al., 2019) for BoB, as given by equation 3.6.

$$pCO_{2sw} = 6.31T^2 + 61.9Chl\text{-}a^2 - 365.85T - 94.41Chl\text{-}a + 5715.94 \quad (3.5)$$

$$pCO_{2sw} = 19.8\ SST + 2.172\ SSS - 283.1 \quad (3.6)$$

where Chl-a is sea water chlorophyll concentration in mg/m^3, T is sea surface temperature in degrees Celsius, and pCO_{2Air} is the partial pressure of CO_2 in the air derived from equation 3.7. The Aquarius (1°×1°) and SMAP (0.25°×0.25°) salinity data sets were resampled to match the spatial resolution of MODIS SST and Chl-a data (4km), using the Nearest Neighbour method due to its computational simplicity as well as the preservation capability of the original pixel values (Jensen, 1996).

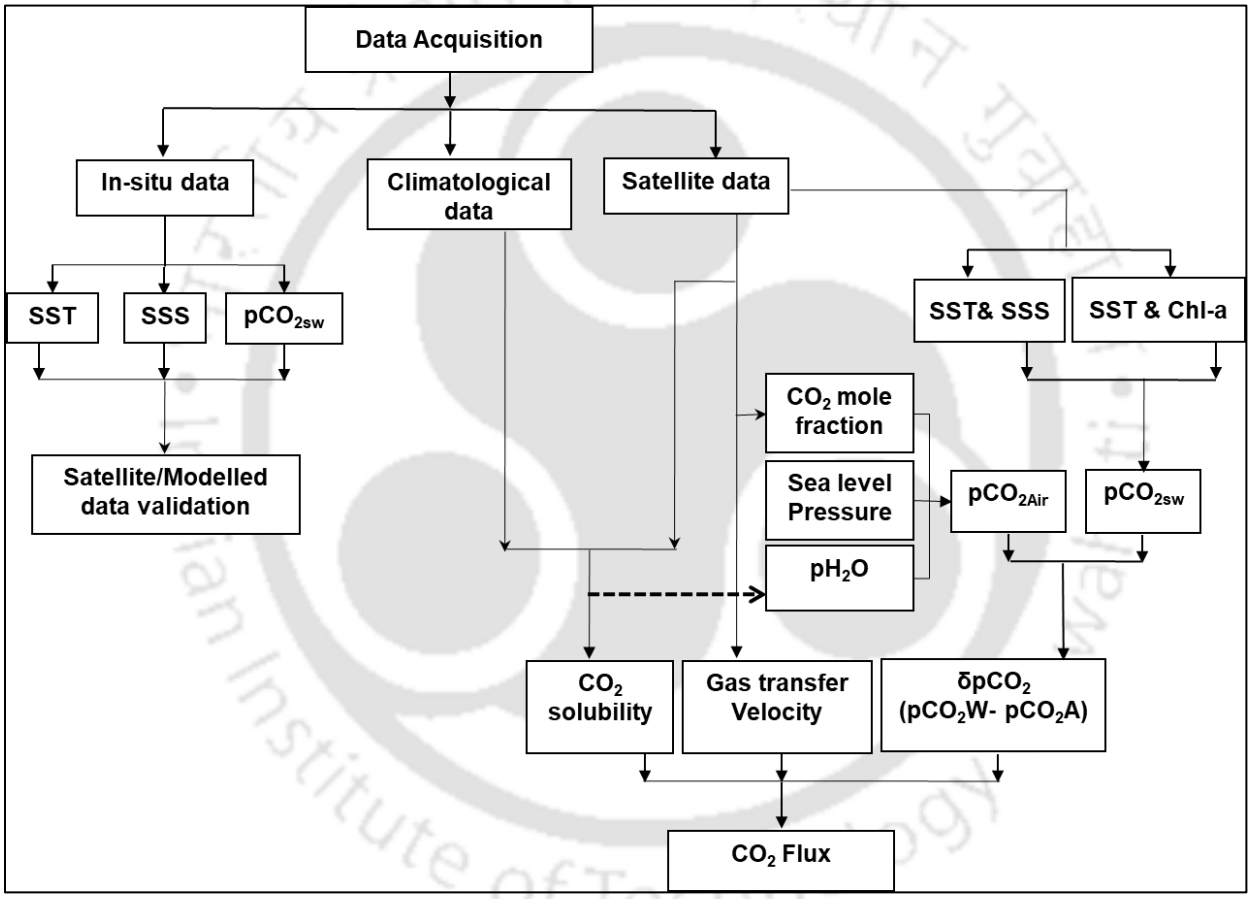

Figure. 3.1 Methodology flow diagram for CO_2 flux calculation

The partial pressure of air (pCO_{2Air}) is derived as given by equation 3.7.

$$pCO_{2Air} = xCO_{2Air}(P_T - PH_2O) \quad \text{(Dickson and Goet, 1994, Dickson et al., 2007)} \quad (3.7)$$

where xCO_2 is CO_2 mole fraction in ppm, P_T is sea level pressure in the atmosphere, and PH_2O is the saturation vapor pressure of sea water in the atmosphere as calculated by equation 3.8 (Weiss and Price, 1980)

$$PH_2O = \exp\left(24.4543 - 67.4509\left(\frac{100}{T}\right) - 4.8489 \times \ln\left(\frac{T}{100}\right) - 0.000544 \times S\right) \quad (3.8)$$

where T is sea surface temperature in Kelvin and S is salinity in psu.

3.3 Results

3.3.1 Spatiotemporal analysis of sea surface pCO_2

3.3.1.1 Estimation of carbon dioxide partial pressures of sea water

The sea water partial pressures are primarily regulated by thermal variations and biologically induced CO_2 concentration changes in the water. Other important factors combined with these are sea surface salinity, nutrient concentrations, and mixed layer depth. These parameters' significance in controlling the partial pressures depends on the biogeochemistry of the oceanic regions (Takahashi et.al., 2002; Padhy et.al., 2016).

3.3.1.2 Remote Sensing approach in partial pressure estimation

The key parameters governing the upper ocean biophysical processes are sea surface temperature and marine chlorophyll concentration. Their precise measurements can be done on a global and regional scale for world oceans using satellite remote sensors. An attempt has been made to derive the CO_2 partial pressures over the northern Indian Ocean using satellite-derived monthly SST, SSS, and Chl-a data sets. Statistical relationship derived from in-situ measurements of SST, Chl-a, and sea water pCO_2 by Zhu et al. (2009) is used to calculate pCO_2 over the Arabian Sea using monthly SST and Chl-a data from MODIS-Aqua. The MLR algorithm, developed by Dixit et al. (2019) from the in situ observations of SST and SSS obtained from the shipboard measurements over BoB waters and $MAPCO_2$ mooring located at 90˚E;15˚N in BoB is used to calculate pCO_2 over the BoB from monthly SST (MODIS-Aqua) and SSS (Aquarius and soil moisture active passive (SMAP)) data sets.

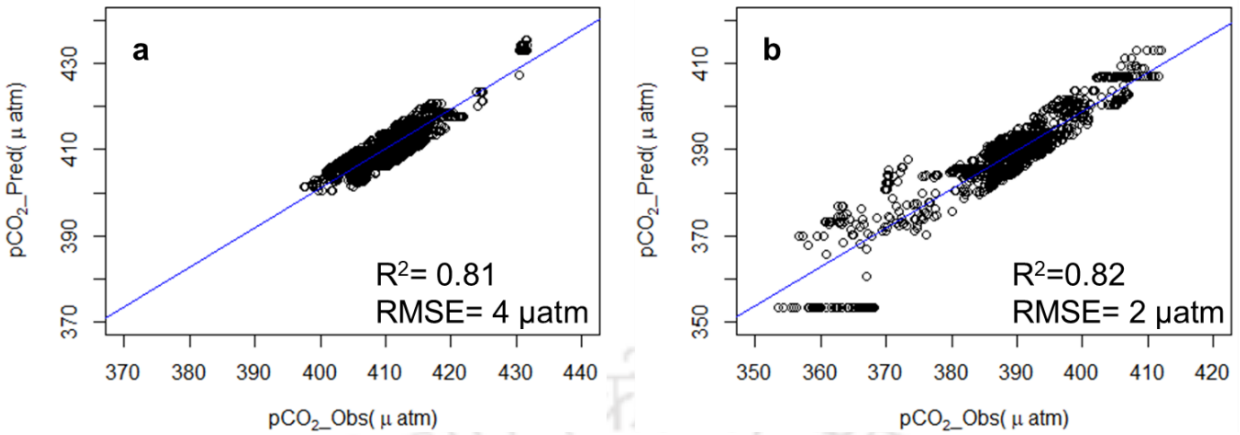

Figure. 3.2 Validation of satellite-derived sea water pCO_2 for Arabian Sea (a) and BoB (b)

Both the algorithms were validated using in situ data obtained from the Surface Ocean CO_2 Atlas (SOCAT) 2022 version and given in Fig.(a) and (b). the fCO_2 values in the SOCAT data were converted to pCO_2 using the equation (3.9) given by Takahashi et al. (2019).

$$pCO_2\ (\mu atm) = fCO_2\ (\mu atm) \times [1.00436 - 4.669 \text{ x } 10\text{-}5 \text{ x SST } (°C)] \quad (3.9)$$

A total of well distributed (both in space and time) 2700 data points over the Arabian Sea and 1600 data points over BoB basin were plotted against the corresponding model output. The SST-Chl-a algorithm applied over the Arabian Sea has provided a coefficient of determination value of 0.81, and a root mean square error (RMSE) value of 4 µatm. In contrast, the SST-SSS algorithm used for BoB was found to give slightly better results with a coefficient of determination value of 0.82 and RMSE value of 2 µatm.

The seasonal pCO_2 calculated for both basins were analysed for the spatial and seasonal variations from the coastal towards the open ocean waters as described in the section 3.3.1.3.The significance of the physico-chemical and biological influence on the spatio-temporal pCO_2 distribution in both basins was also analyzed, as given in the sections 3.3.1.4 to 3.3.1.6. The basins are divided in to 1°×1° grids and the values for pCO_2, SST, SSS and Chl-a were extracted for each grid, which were then averaged for each latitude from the equator towards the bay area. The latitudinal pCO_2 variations over both basins for all the seasons (Figure 3.3 and 3.4), along with the influence of the regional forcings on the pCO_2 distribution (Figure 3.5(i) to 3.10(ii)) were analyzed.

3.3.1.3 Latitudinal pCO_2 distribution over the Indian Ocean

Latitudinal variation in seasonal pCO_2 distribution of sea water over the Arabian Sea (Figure.3.3) showed maximum pCO_2 values towards the higher latitudes in winter and monsoon seasons. In contrast, the low latitudes exhibited comparatively higher values pre- and post-monsoon. Pre-monsoon pCO_2 values reached up to a maximum of 425 µatm over the low latitudes while gradually decreasing towards the central Arabian Sea, dropping till 401 µatm; equator to poleward change in the surface circulation pattern could be attributed to this reversal where the movement of low pCO_2 water mass is resulting in the reduced values towards the central latitudes, while the elevated SST levels enhance the surface pCO_2 levels in the southern waters. A further increase up to 410 µatm can be observed towards the extreme north, which may be due to the bacterial regeneration of organic matter (Sarma, 2003).

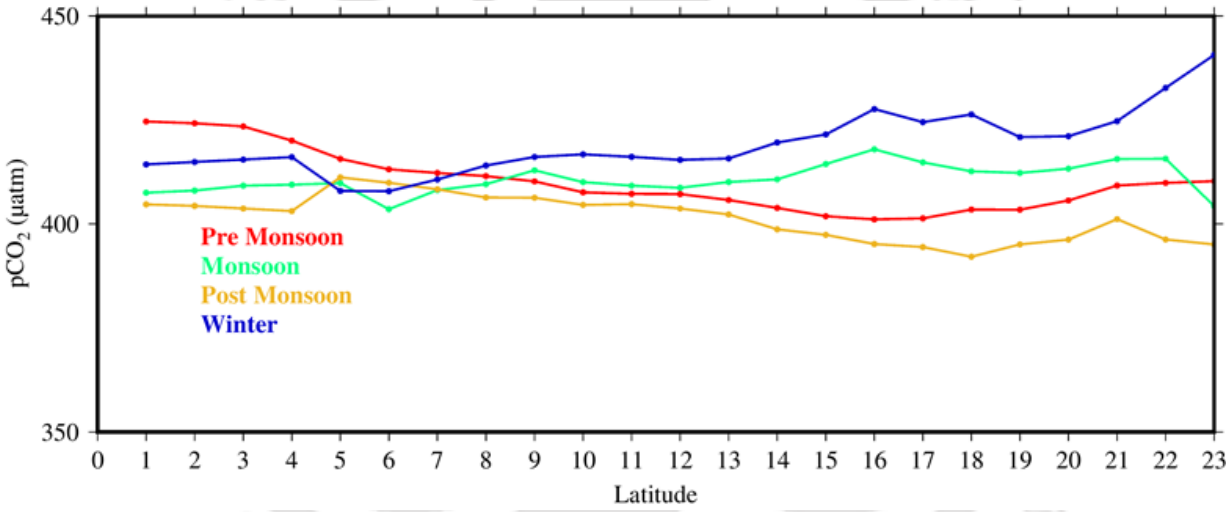

Figure.3.3 Latitudinal variation of sea water pCO_2 over the Arabian Sea

During monsoon season, the central to northern latitudes are observed to have high pCO_2 values reaching a maximum of 410-418 µatm over the upper-central latitudes, owing to the coastal upwelling and Findlater Jet induced open ocean upwelling (Madhupratap et al, 1996; Sarma, 2000; Sarma, 2003). The values reduced towards the southern latitudes, ranging from 404-409 µatm due to the absence of upwelling. A sudden drop around the upper-southern latitudes might result from the influence of low saline water mass (Sarma, 1998).

Post-monsoon season showed a comparatively low pCO_2 range, with a minimum value of 392 µatm in the upper-central latitude, reaching up to a maximum of 411 µatm towards the low latitudes. This might be caused by the biological consumption of available surface CO_2 in the

western Arabian Sea, following the enhanced primary productivity resulting from the monsoonal upwelling (Sarma, 2003). A slight increase in pCO_2 over the lower-central latitudes could have been due to an increase in solar radiation enhancing the SST, leading to reduced CO_2 solubility. Also, the elevated rates of bacterial decomposition of organic matter produced during monsoon could contribute to this increase (Ramaiah et al., 1996; Sarma et al., 2000; Sarma, 2003).

In winter, average latitudinal pCO_2 values reached 440.6 µatm towards the extreme north, while the minimum values dropped to about 408 µatm in the southern Arabian Sea. The elevated value range over the upper-central to northern latitudes can be caused by the winter convective mixing in the northern and western coastal regions, the absence of which could have dropped the values towards the southern waters (Sarma, 2000). A gradual drop in values over the lower-central to southern Arabian Sea can be visible, which might be attributed to the influence of low saline water influx from BoB with less dissolved inorganic carbon (DIC) content (Shetye and Shenoi, 1988; Kumar et al., 1996; Sarma, 2003).

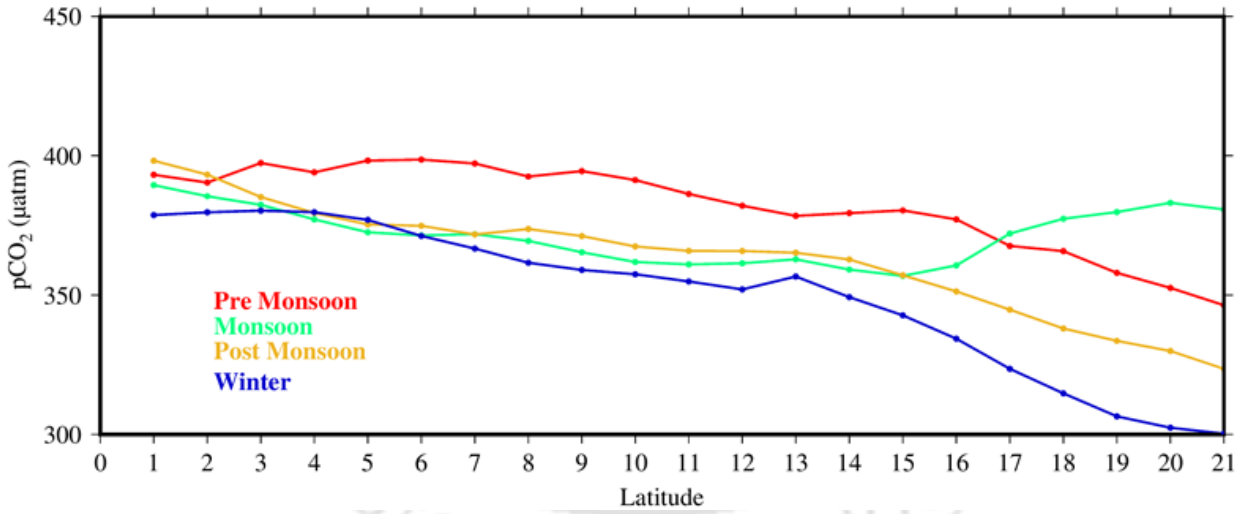

Figure.3.4 Latitudinal variation of sea water pCO_2 over BoB

Spatial variation of the averaged latitudinal sea surface pCO_2 over the BoB basin (Figure.3.4) showed a gradually increasing trend toward the low latitudes in pre-monsoon, post-monsoon, and winter seasons. In contrast, the trend was disturbed in monsoon over the upper-central latitudes, following a significant increase in the northern BoB waters. pCO_2 values reached the maximum during pre-monsoon season over the central and southern BoB ranging from 380-398 µatm, whereas towards the north from 17° N, the values gradually decreased to 346 µatm. This can be primarily

attributed to the sharp salinity gradient observed over the northern BoB from 17° N resulting from the seasonal coastal circulation reversing following a northward transport of high salinity waters by the western boundary current (Shetye et al., 1993; Kumar et al., 1996).

During monsoon, latitudinal averaged pCO_2 values peak over the southern latitudes, reaching a maximum of 389 μatm, gradually reducing to 357 μatm over the upper-central latitudes; further, they increase towards the northern waters, increasing up to 383 μatm. The north-south gradient of pCO_2 values can be attributed to the fresh water influx from river input and precipitation, lowering the salinity values in the north, while the southwest monsoon currents bring saltier water mass with high pCO_2 levels to the southern latitudes from the Arabian Sea (Murty et al., 1992; Vinayachandran et al., 1999; Vinayachandran et al., 2002). Also, sudden change in the pCO_2 values in the upper-central latitudes with an increase towards the northern region might be due to the upwelling by local wind action (Shetye et al., 1991; Murty et al., 1992; Gopalakrishna et al., 2002). Post-monsoon pCO_2 values showed a north-south gradient, with maximum values (398 μatm) observed over the southernmost latitudes, dropping to about 323.5 μatm in the extreme north, owing to the influence of the monsoonal fresh water influx induced stratification towards the high latitudes (Kumar et al., 1996).

Winter values also followed the north-south pCO_2 gradient, with only a slightly increased over the central waters. During winter, the circulation is reversed, with no movement of the high saline waters towards the north; this season is characterized by only the southern transport of low saline waters, spreading over the entire north and central bay, manifesting a visible onshore-offshore gradient (Shetye et al., 1993; Kumar et al., 1996). The values over the southern latitudes reached up to 380 μatm, while the lowest winter values were found in the northernmost latitude, reducing to an all-season minimum value of 300 μatm. The Ekman transport of the freshwater mass, leading to open ocean upwelling, could be the reason behind the sudden change in the gradient over the central latitudes, accompanied by an increase in pCO_2 values (Vinayachandran and Mathew, 2003; Vinayachandran et al., 2005).

3.3.1.4 Significance of chlorophyll variability over sea water pCO_2 distribution

Chlorophyll and sea water pCO_2 over the Arabian Sea showed a negative correlation during pre (Figure.3.5(i). a) and post-monsoon (Figure.3.5(ii). c) seasons and a positive correlation during monsoon (Figure.3.5(i). b) and winter (Figure.3.5(ii). d); the correlation of pCO_2 with the seasonal

chlorophyll distribution is observed to be not much significant except during winter (R= 0.78) (Figure.3.5(ii). d). Latitudinal average of Chl-a values showed high concentrations towards the high latitudes (19 ° N to 23° N) ranging from 0.3 $mg.m^{-3}$ (Figure.3.5(i). a) during pre-monsoon to about 1 $mg.m^{-3}$ (Figure.3.5(ii). d) during winter, whereas, the open ocean values were about 0.1 $mg.m^{-3}$, exhibiting lowest seasonal variation. The onshore and offshore chlorophyll blooms in winter and the monsoonal upwelling of nutrient-rich waters on the Oman coast are attributed to the presence of high Chl-a in the northern latitudes (Barber et al., 2001; Chauhan et al., 2001; Dey and Singh, 2003). While the high Chl-a concentration can lead to enhanced absorption of surface CO_2, the monsoonal upwelling and winter convective mixing can also be responsible for the increased CO_2 outflux from the subsurface, thus attributing to the high surface pCO_2 levels (Takahashi et al., 1997; Sarma et al, 2000; Sarma et al., 1998; Takahashi et al., 2002; Takahashi et al., 2009).

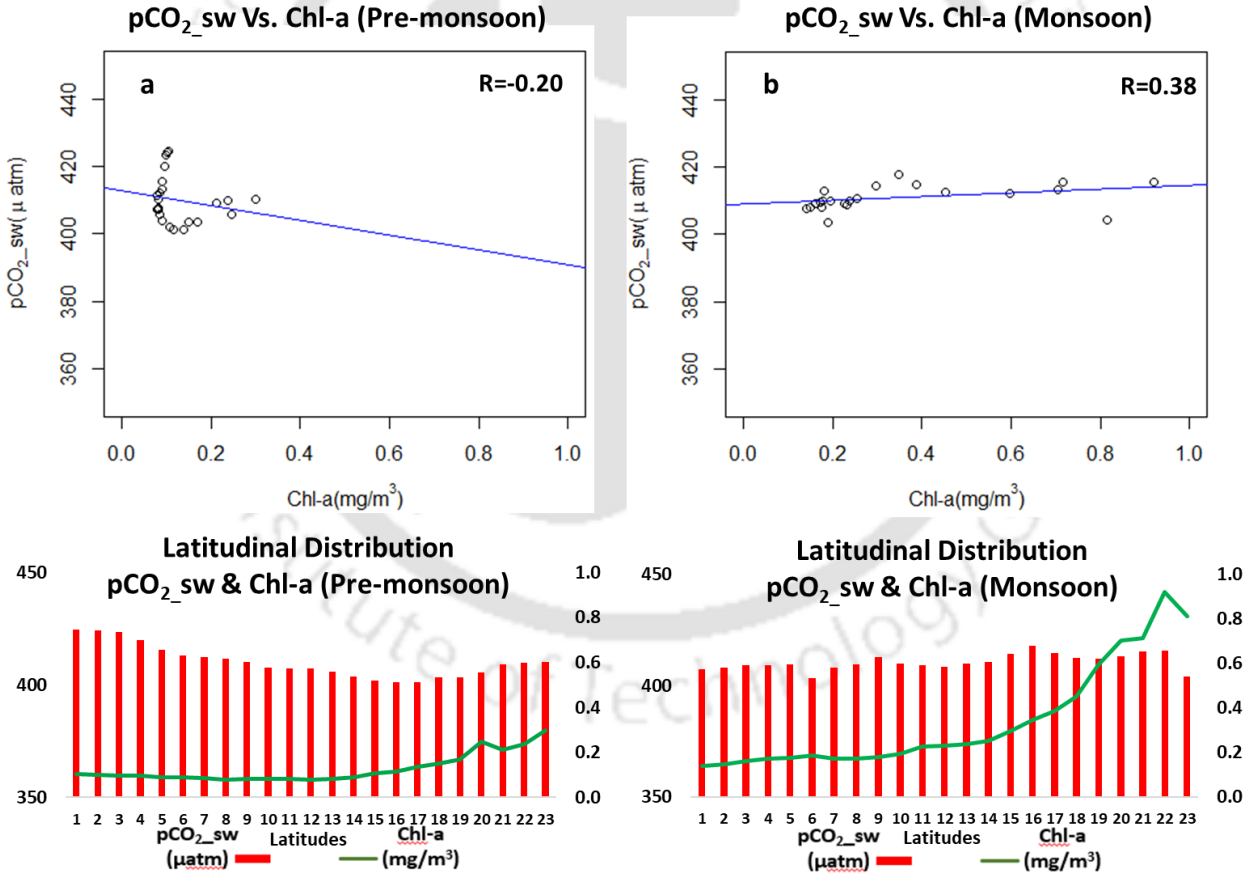

Figure.3.5(i) Significance of chlorophyll variations in pCO_2sw distribution over the Arabian Sea for pre-monsoon (a), monsoon (b) season

In BoB, Chl-a was found to have a negative correlation with the surface water partial pressures in all seasons except in monsoon (R= 0.40) (Figure. 3.6 (i). b). Higher Chl-a values up to 0.8 mg.m-3 are obtained during winter (Figure. 3.6 (ii). d) towards the northern latitudes due to Ekman Pumping driven upwelling (Vinayachandran and Mathew, 2003; Vinayachandran et al., 2005), while a reduction in the values is found in the post-monsoon (Figure.3.6(ii). c), with maximum values up to 0.2 mg.m-3 due to the influence of monsoonal river influx (Madhupratap et al, 2003; Sarangi, 2011).

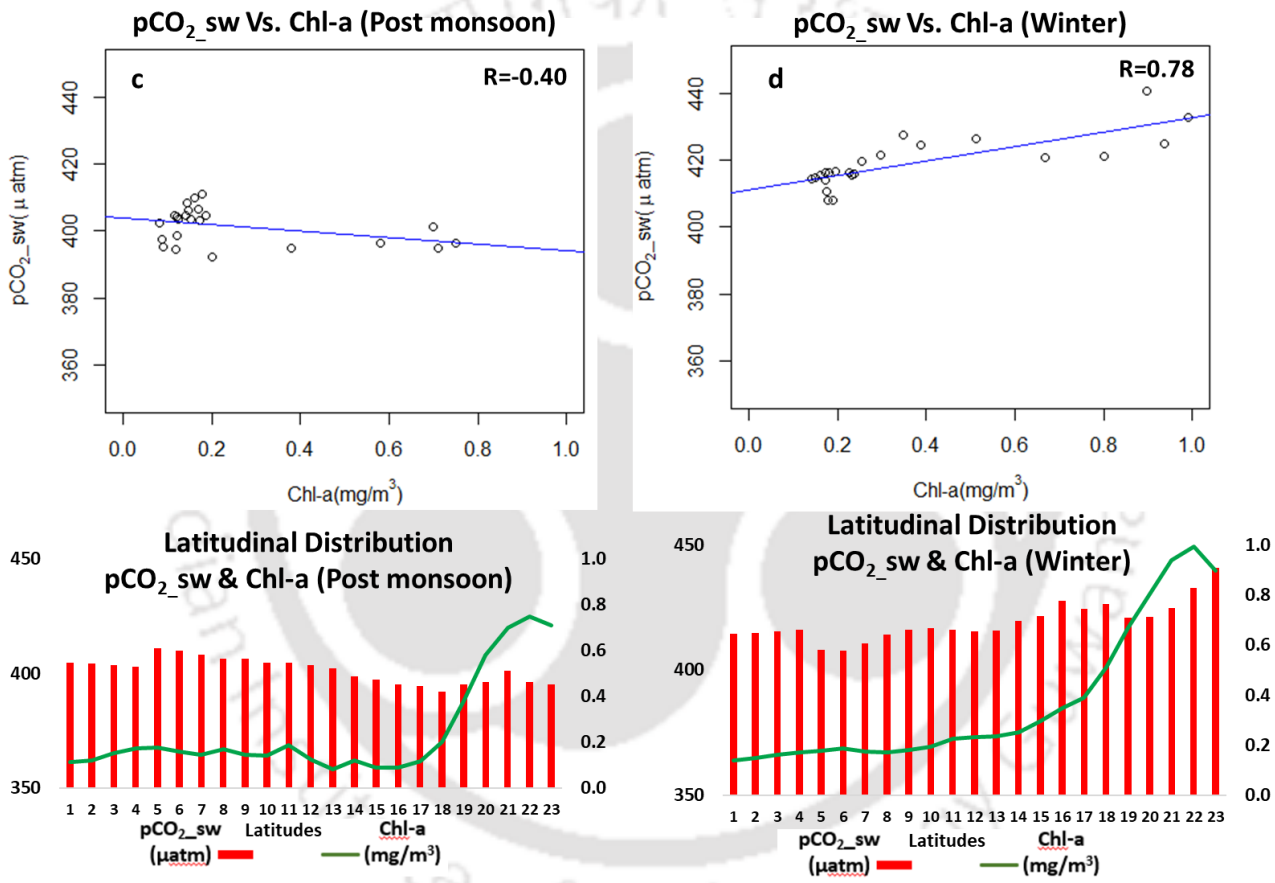

Figure.3.5(ii) Significance of chlorophyll variations in pCO_2sw distribution over the Arabian Sea for post-monsoon (c) and winter (d) season

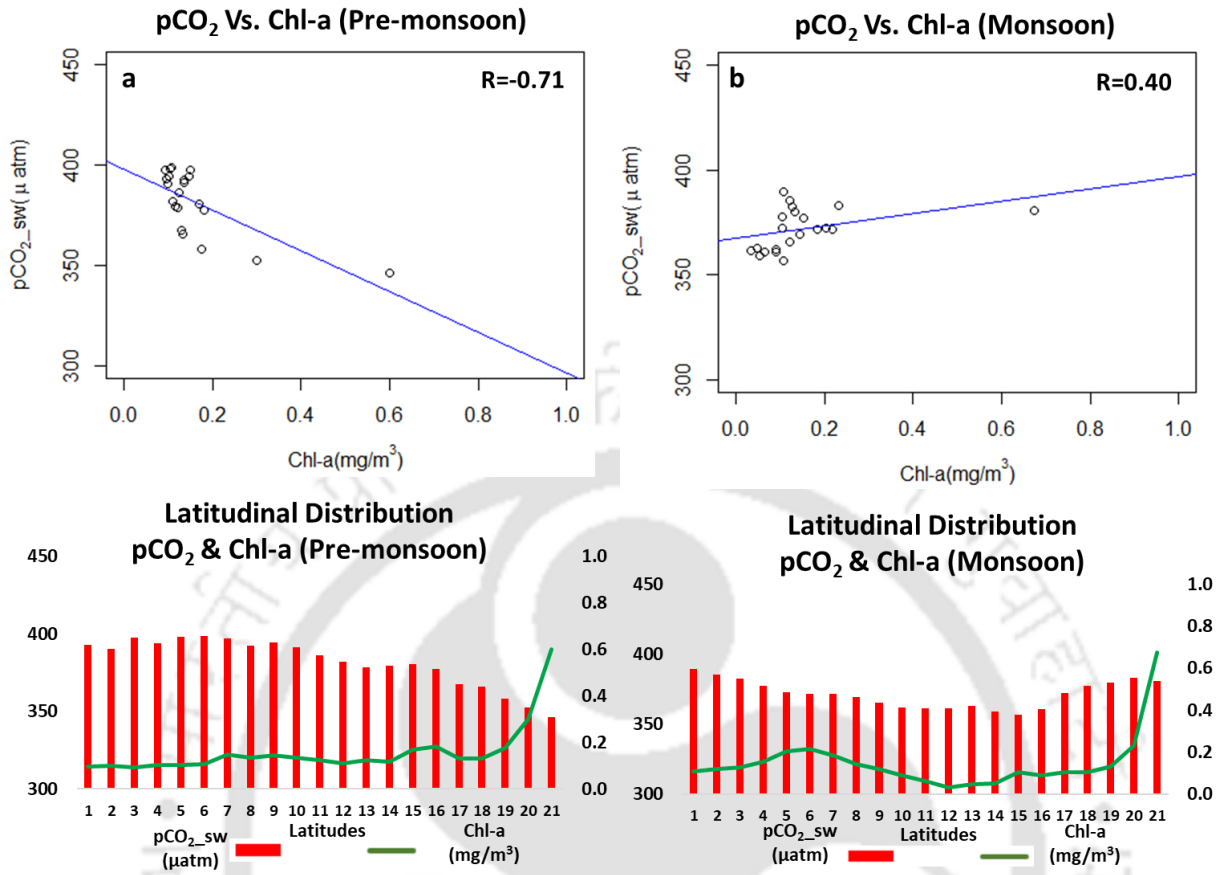

Figure.3.6(i) Significance of chlorophyll variations in pCO_2sw distribution over BoB for pre-monsoon (a) and monsoon (b) season

The high sediment input, along with the river discharge in the coastal waters, attenuates the light penetration, resulting in a shallow euphotic zone, thus limiting the primary productivity (Madhupratap et al, 1996; Kumar et al., 2002). Pre (Figure.3.6 (i). a) and post-monsoon (Figure.3.6(ii). c) showed a significant negative correlation with correlation coefficient values of -0.71 and -0.88, respectively. This is attributed to the high values of pCO_2 towards the low latitudes with reduced Chl-a concentration (Sardessai et al., 2010). Over the high latitudes, the pre and post-monsoon pCO_2 values exhibited a lowering trend with a significant reduction up to 20 µatm due to photosynthetic drawdown of surface CO_2, owing to the relatively high Chl-a concentration (Kumar et al., 2002; Roy et al., 2017). Monsoon and winter showed a moderate positive (R= 0.40) (Figure.3.6(i). b) and negative (R= -0.57) (Figure.3.6(ii). d) correlation, respectively. During monsoon season, the high nutrient influx from rivers can trigger the development of chlorophyll blooms, while an increasing trend in the pCO_2 values also found towards the north, which can be

due to coastal upwelling (Shetye et al., 1996; Vinayachandran et al., 2002, Dey and Singh, 2003; Thushara et al., 2016; Amol et al., 2020).

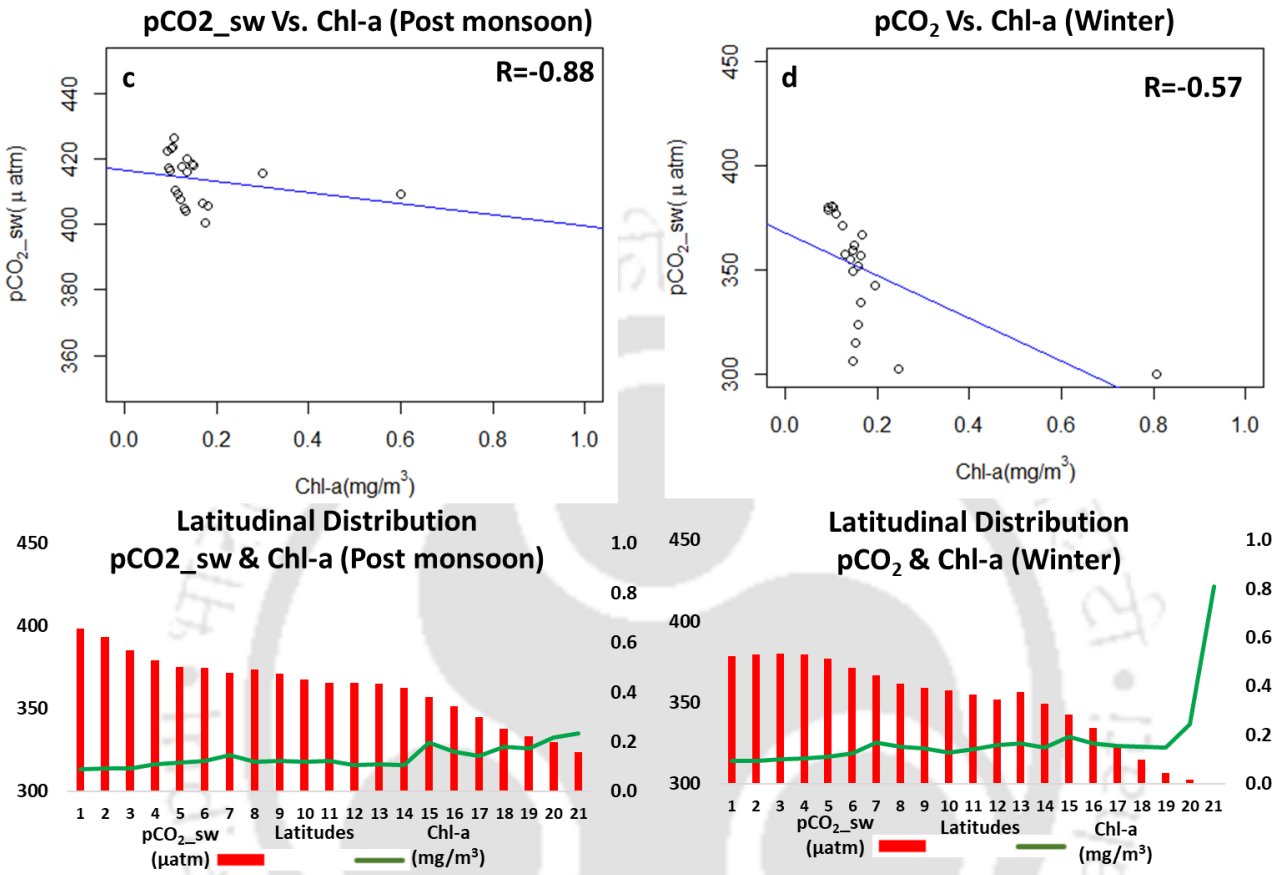

Figure.3.6(ii) Significance of chlorophyll variations in pCO_2sw distribution over BoB for post-monsoon (c) and winter (d) season

3.3.1.5 Significance of SST variability over sea water pCO_2 distribution

Medium to low correlation between the latitudinal distribution of SST and pCO_2 over the Arabian Sea was obtained during pre (R= 0.60) (Figure.3.7(i). a), post (R= 0.37) (Figure.3.7(ii). c) and monsoon (R= -0.43) (Figure.3.7(i). b) seasons, while a significant negative correlation was found during the winter (R= -0.87) (Figure.3.7(ii). d) season. An increasing trend was observed in SST distribution over the low latitudes.

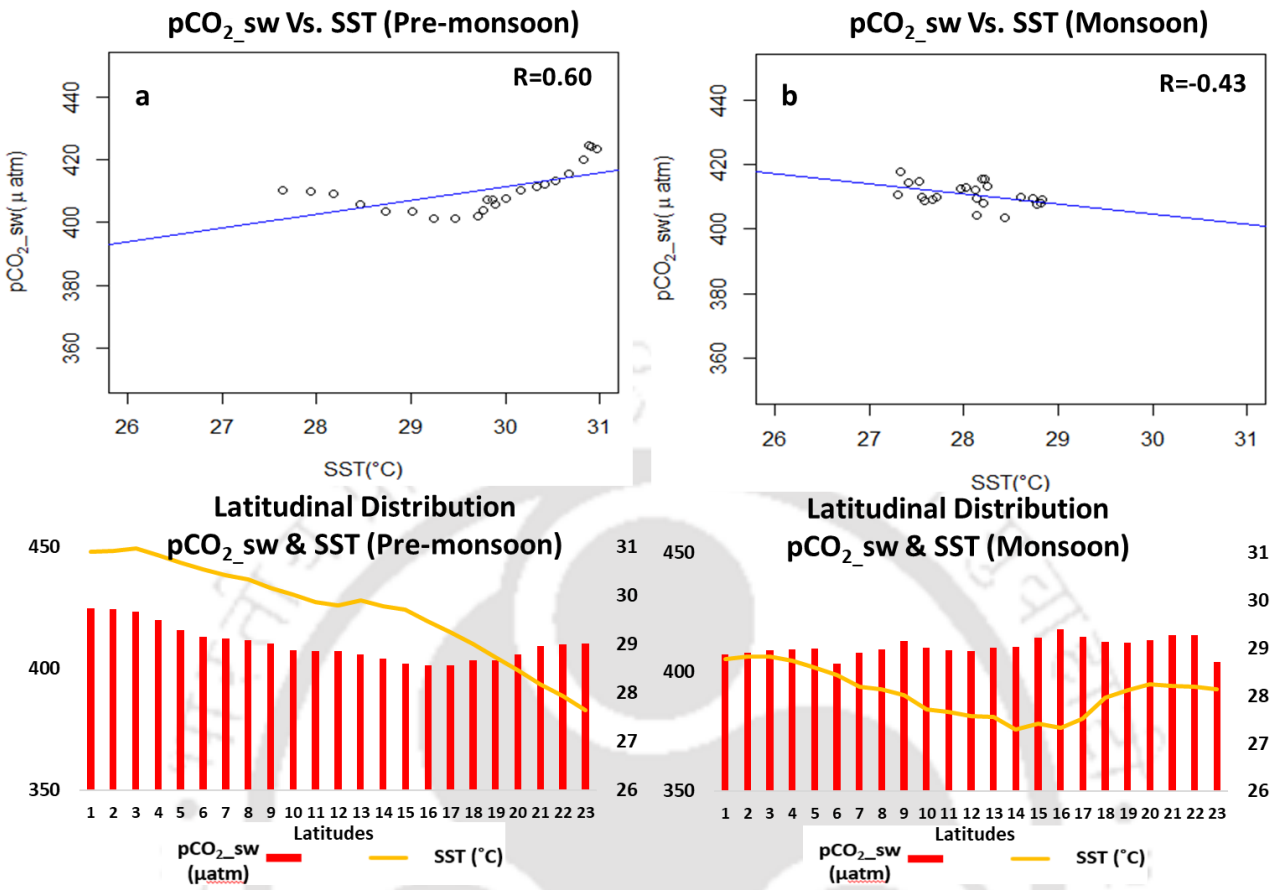

Figure. 3.7 (i) Significance of SST variations in pCO_2sw distribution over the Arabian Sea for pre-monsoon (a) and monsoon (b) season

In the monsoon (Figure.3.7 (i). b) and post-monsoon (Figure.3.7 (ii). c) seasons, the SST showed a dip over the mid-latitudes around 8 ° N to 17° N, followed by a rise towards the northern high latitudes, whereas, pre-monsoon (Figure.3.7(i). a) and winter (Figure.3.7(ii). d) SST exhibited a gradual decrease from the south towards north. SST values ranged from a minimum of 26 ˚C over the northern latitudes reaching up to 29 ˚C over the low latitudes during winter (Figure.3.7(ii). d), to a maximum of 28 ˚C in the north to 40 ˚C over the southern low latitude waters during pre-monsoon (Figure.3.7(i). a) season (Rao and Goswami, 1988). pCO_2 followed a similar trend as SST in the pre-monsoon season over the low and mid-latitudes, i.e., 1° N to 15° N (Figure.3.7(i). a), where an increase in surface temperature resulted in a reduced CO_2 solubility, contributing to the positive correlation between SST and pCO_2 during this season (Marra and Barber, 2005).

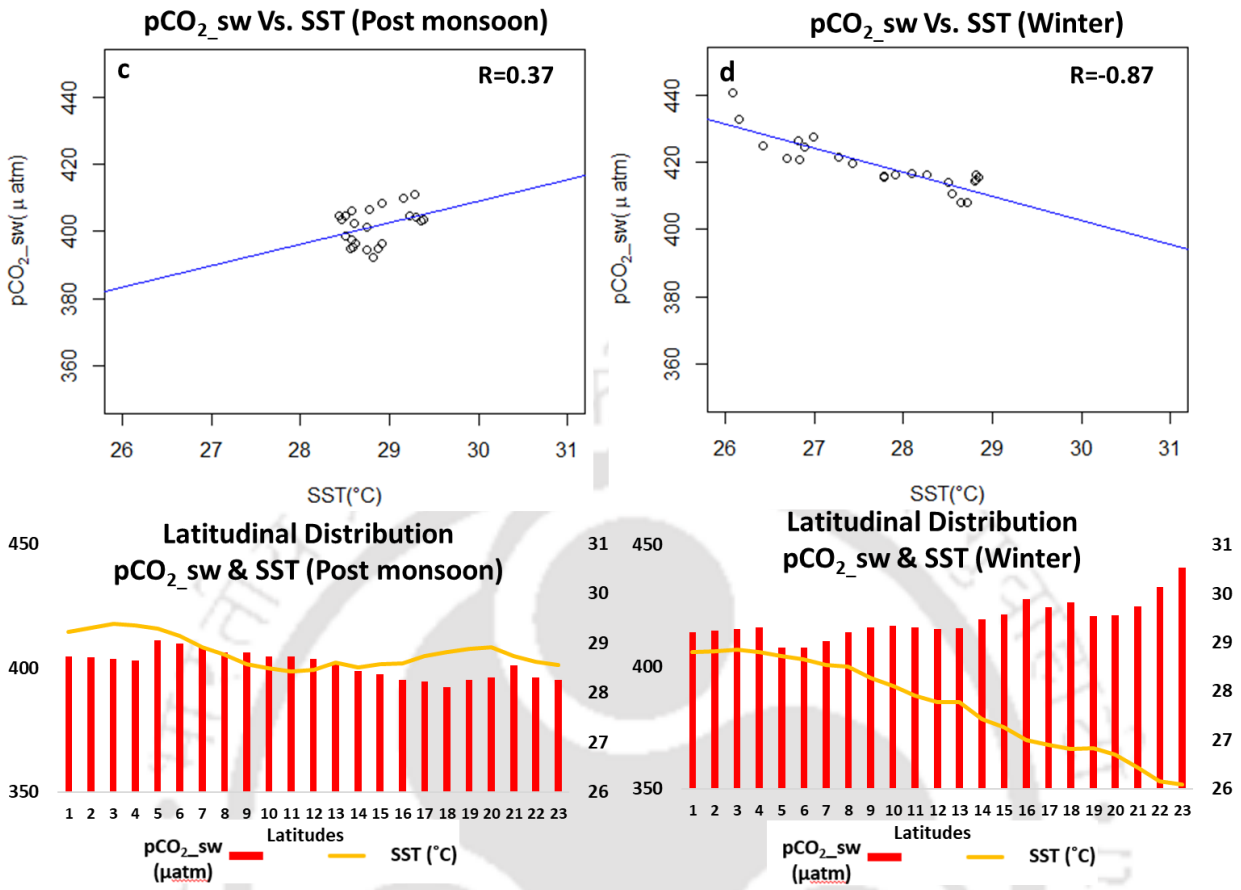

Figure.3.7(ii) Significance of SST variations in pCO_2sw distribution over the Arabian Sea for post-monsoon (c) and winter (d) season

During the monsoon season, the upwelling along the Somali coast brings cold subsurface water rich in CO_2, which spreads over the western Arabian Sea, lowering SST and increasing sea water pCO_2 over the mid-latitudes (Shukla, 1975). Similarly, winter convective mixing also causes the surfacing of cold waters, which reduces the SST while enhancing the surface CO_2 concentration ((Madhupratap et al., 1996; Sarma et al., 2000; Sarma, 2003).

The distribution of sea surface pCO_2 in BoB is observed to be significantly correlated with the spatial variations in SST during all the seasons, with R-value ranges from 0.98 for monsoon (Figure.3.8(i). b) and post-monsoon (Figure.3.8(ii). c) season to 0.99 for pre-monsoon (Figure.3.8(i). a) and winter(Figure.3.8(ii). d).

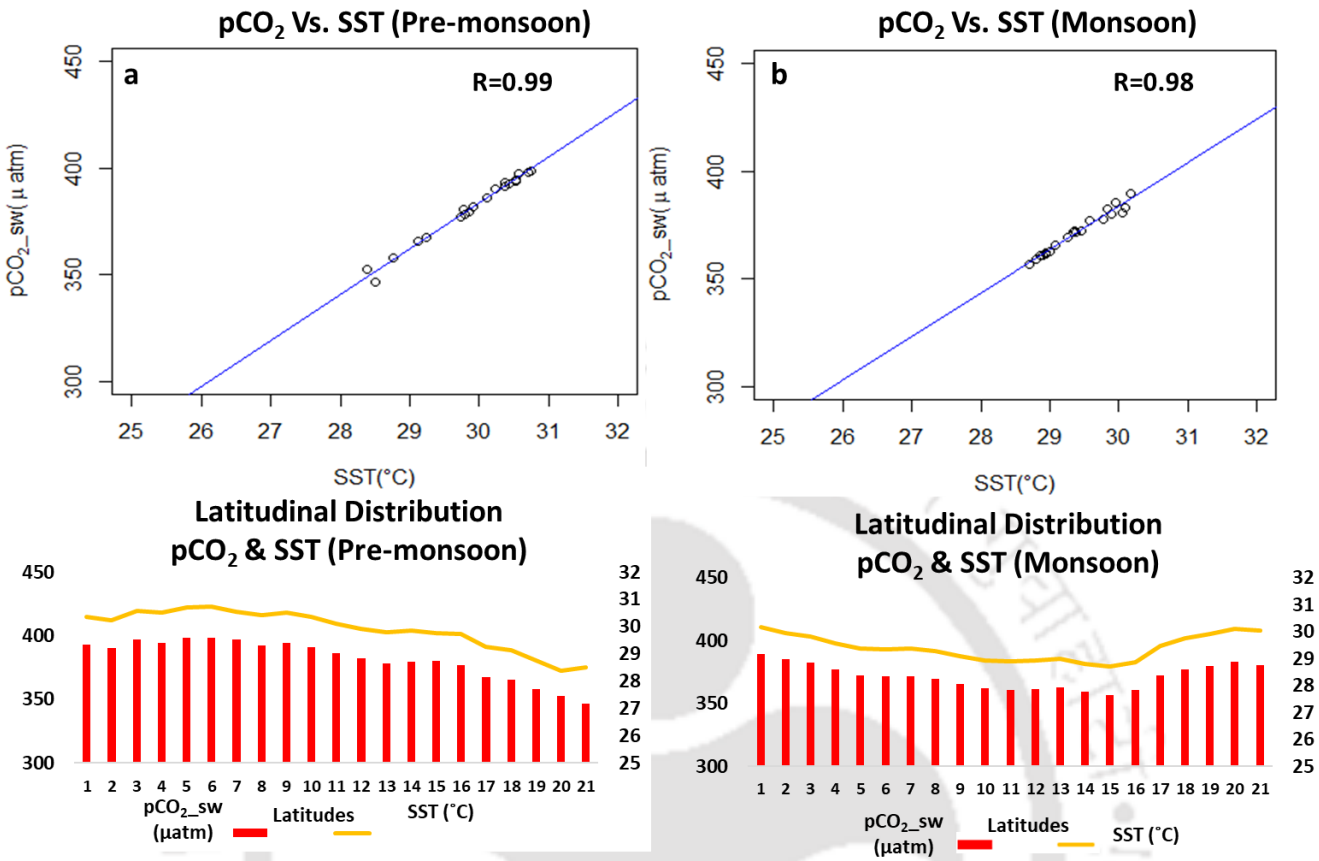

Figure.3.8(i) Significance of SST variations in pCO_2sw distribution over BoB for pre-monsoon (a) and monsoon (b) season

Winter SST (Figure.3.8(ii). d) showed the lowest values ranging from 25.8 ˚C along the coast, reaching up to 29.7 ˚C towards the open ocean. The maximum values are obtained for pre-monsoon season, in the range of 28.4 ˚C in the coastal, to about 30.8 ˚C in the open ocean waters (Figure.3.8(i). a); very small seasonal variation can be observed in the SST distribution. A gradual reduction in the SST values is evident towards the high latitude waters, except during monsoon (Figure.3.8(i). b), with pCO_2 showing a similar trend due to the influence of river discharge (Kumar et al. 1996). Monsoonal SST and pCO_2 values tend to increase from 16° N to 21° N, attributed to the development of a warm coastal front, leading to a northward thermal gradient and the cyclonic winds enhancing surface pCO_2 (Samanta et al., 2018).

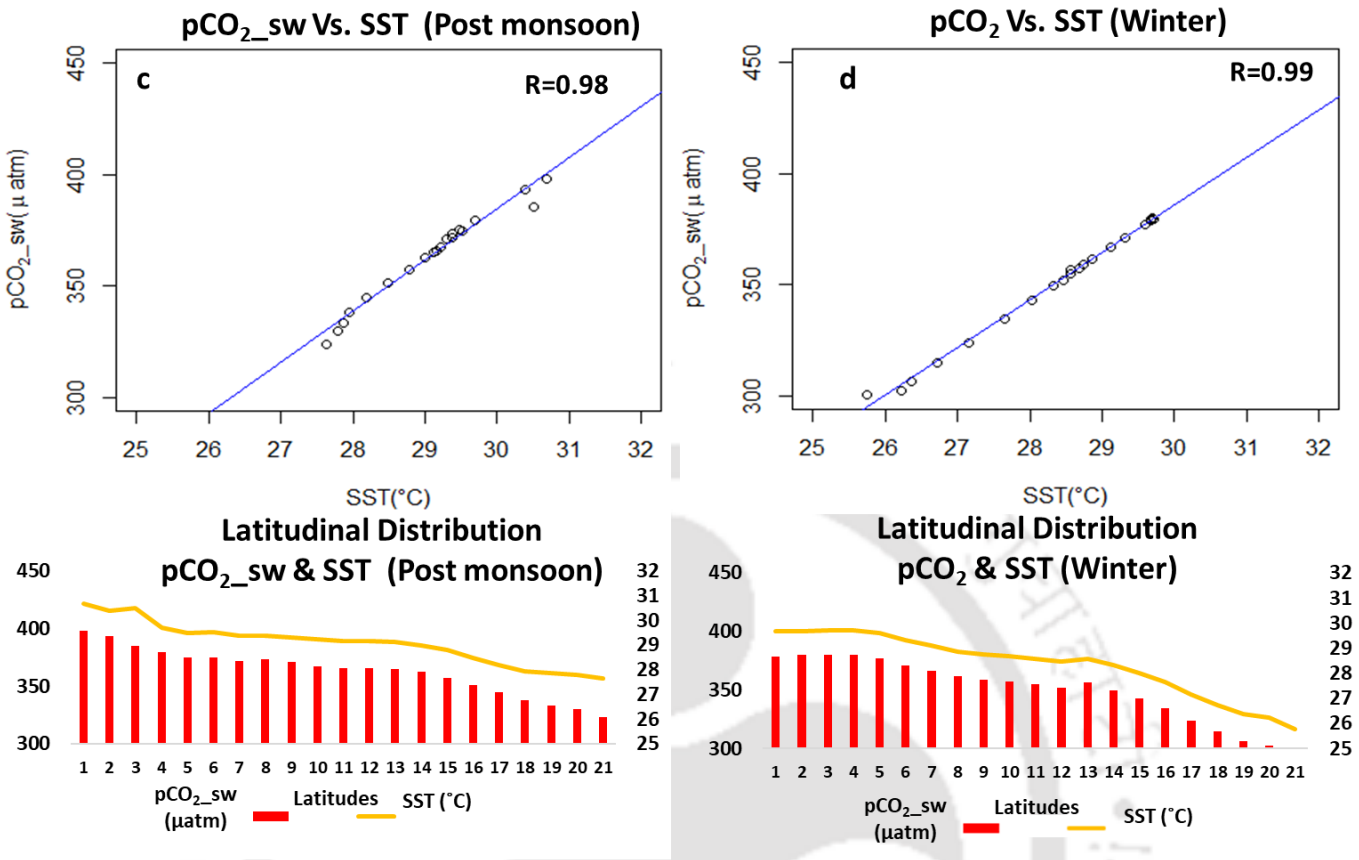

Figure.3.8(ii) Significance of SST variations in pCO_2sw distribution over BoB for post-monsoon (c) and winter (d) season

3.3.1.6 Significance of SSS variability over sea water pCO_2 distribution

Similar to the Chl-a- pCO_2 distribution, the SSS-pCO_2 correlation was also found to be negative during the pre (Figure.3.9 (i). a) and post-monsoon (Figure.3.9 (ii). c) in the Arabian Sea, while they were positively correlated during monsoon (Figure.3.9 (i). b) and winter (Figure.3.9 (ii).d). The latitudinal SSS distribution was also observed to be strongly correlated with that of pCO_2 (R= 0.80) in winter (Figure.3.9 (ii). d). At the same time, a moderate correlation can be seen during the other three seasons, with the coefficient of determination values ranging from 0.49 in monsoon (Figure.3.9(i). b) to -0.67 in pre-monsoon (Figure.3.9 (i). a).

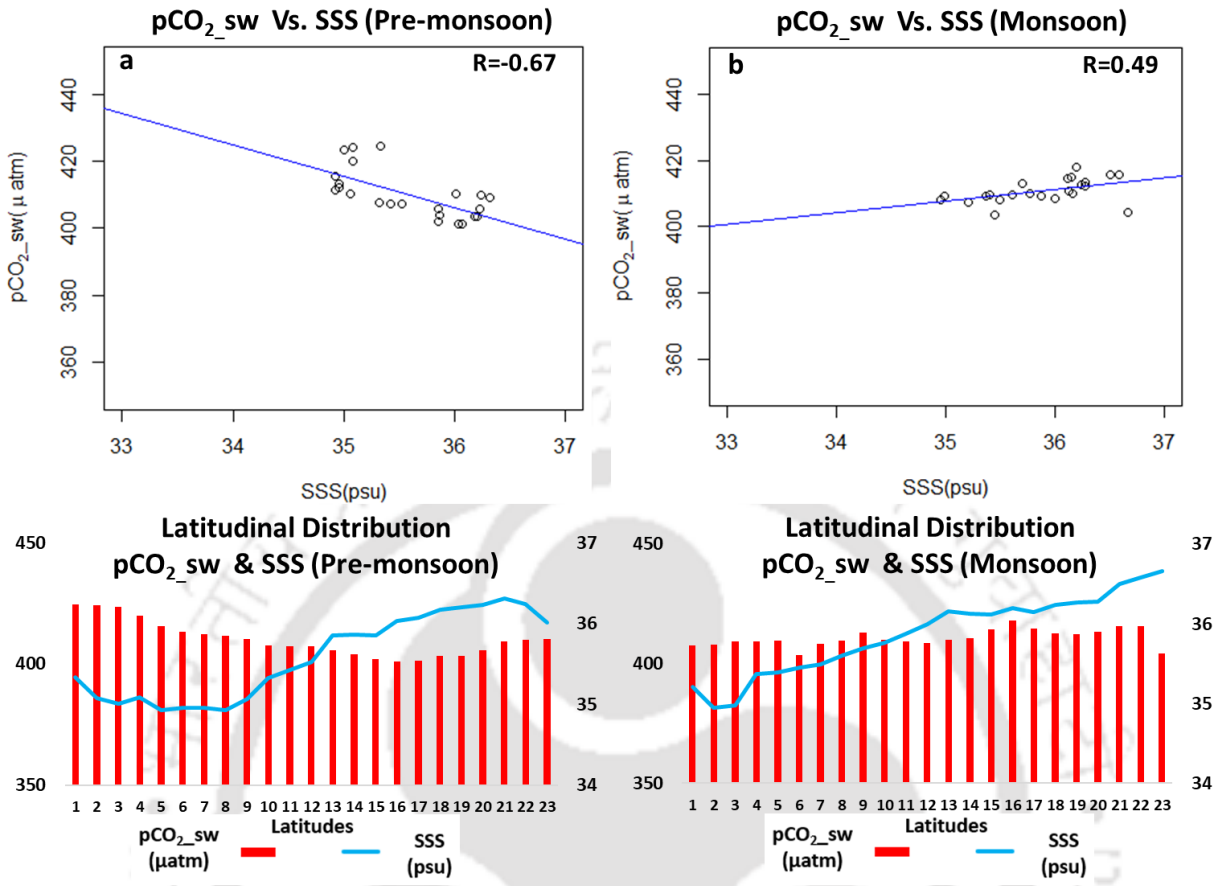

Figure.3.9(i) Significance of SSS variations in pCO_2sw distribution over the Arabian Sea for pre-monsoon (a) and monsoon (b) season

Low latitudes (1° N to 10° N) showed noticeable seasonal SSS variation, ranging from 35 psu during pre-monsoon (Figure.3.9 (i). a), increasing up to a maximum of 36 psu in the winter (Figure.3.9(ii). d). However, in the high latitude waters (13° N to 23° N), SSS distribution variability is not evident; the salinity values are around the 36-36.7 psu range. The high SSS values found in the north can be attributed to the influx of high salinity water masses from the Red Sea and the Persian Gulf and the existence of Arabian Sea High Salinity Water (ASHSW) mass. During winter, the ASHSW mass is restricted to north of 13° N, and the high saline waters from the Red Sea propagate southward along the Somali coast; the high saline water mass in the northern Arabian Sea spreads towards the south during the monsoon season, increasing the SSS values over the mid-latitudes, while the Red Sea water mass moves in the east direction during summer, lowering the SSS values over the southern latitudes during pre-monsoon season. The influence of the North Equatorial Current (NEC) and the BoB low-salinity water intrusion can be the reason behind the comparatively low SSS values in the lower latitude waters (Kumar and Prasad, 1999; Prasad and

Ikeda, 2002; Behera et al., 2019). While the high saline water mass enhances the winter SSS values, the convective mixing attributes to the increased surface pCO_2 this season, resulting in the high correlation.

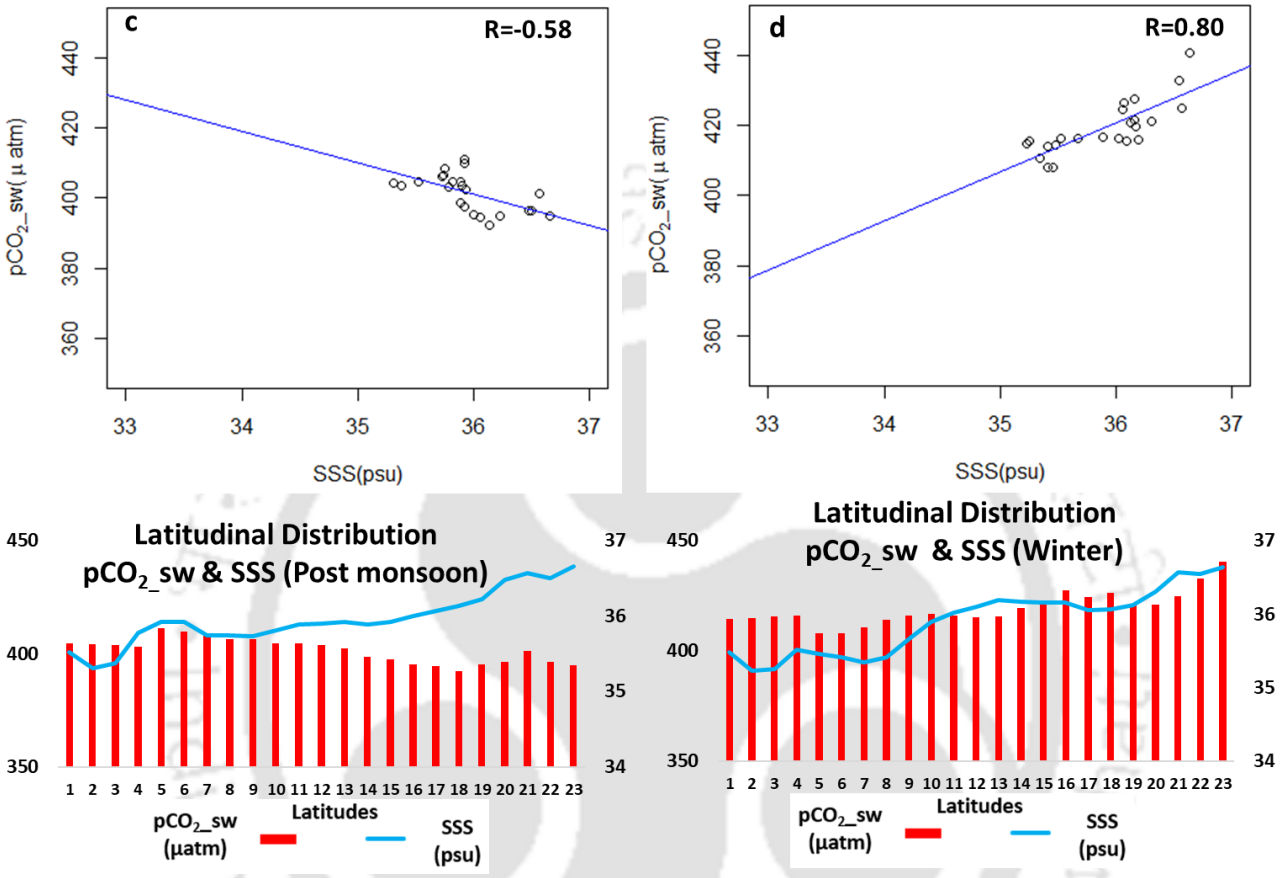

Figure.3.9 (ii) Significance of SSS variations in pCO_2sw distribution over the Arabian Sea for post-monsoon (c) and winter (d) season

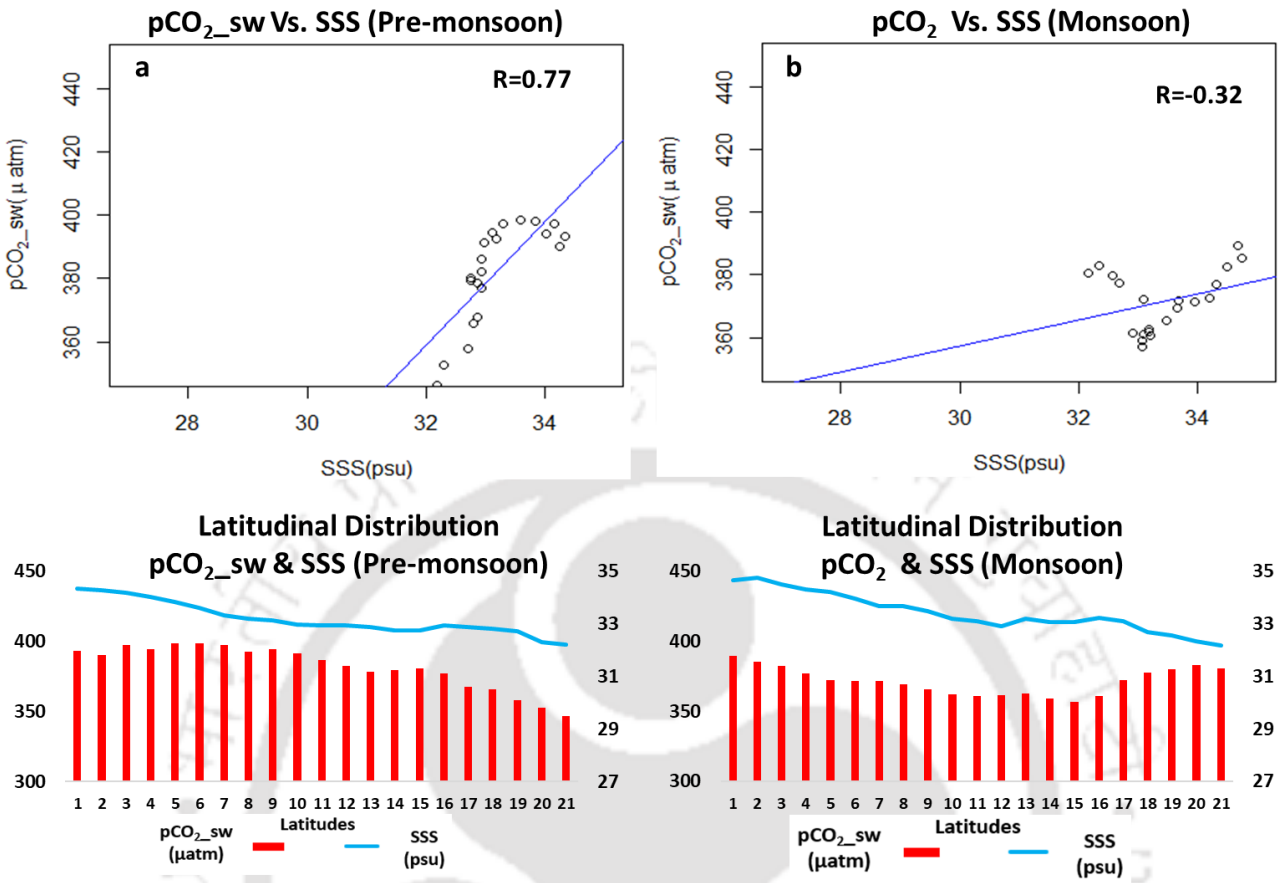

Figure.3.10 (i) Significance of SSS variations in pCO_2sw distribution over BoB for pre-monsoon (a) and monsoon (b) season

Latitudinal salinity variation also showed the same trend as SST over the pCO_2 distribution in BoB except in the monsoon season (Figure.3.10(i) &(ii)). The freshwater influx reduced salinity values towards the high latitudes (Gopalakrishna et al., 2002; Vinayachandran et al., 2002; Madhupratap et al., 2003), with a significant decrease of up to 27 psu during post-monsoon. Further, with the weakening of the south-westerlies, the advection of the river influx towards the southern BoB along the east coast would bring the freshwater towards the equator, which reduces the pCO_2 values over the basin (Han & McCreary Jr, 2001; Shankar et al., 2002; Babu et al., 2003; Sarma et al., 2012). Analysis showed a moderate correlation (R = 0.77) between SSS and sea water pCO_2 during pre-monsoon (Figure.3.10(i). a). In contrast, a better correlation was obtained for the post-monsoon (R = 0.94) (Figure.3.10 (ii). c) and winter (R = 0.99) (Figure.3.10 (ii). d) season. This may result from the thermal stratification zones where surface turbulence due to wind action is absent, leading to reduced surface partial pressures (Sardessai et al., 2010). Salinity is a significant factor in determining the mixed layer depth, thus reducing salinity and resulting in surface stratification

(Vinayachandran et al., 2002). Stratified waters tend to have low partial pressures since the release of subsurface CO_2 to the surface is disturbed. Monsoon pCO_2 values peaked towards the coast from 16 ° N to 21° N (Figure.3.10 (ii). b) due to the cyclonic activity enhancing the surface pCO_2 (Samanta et al., 2018).

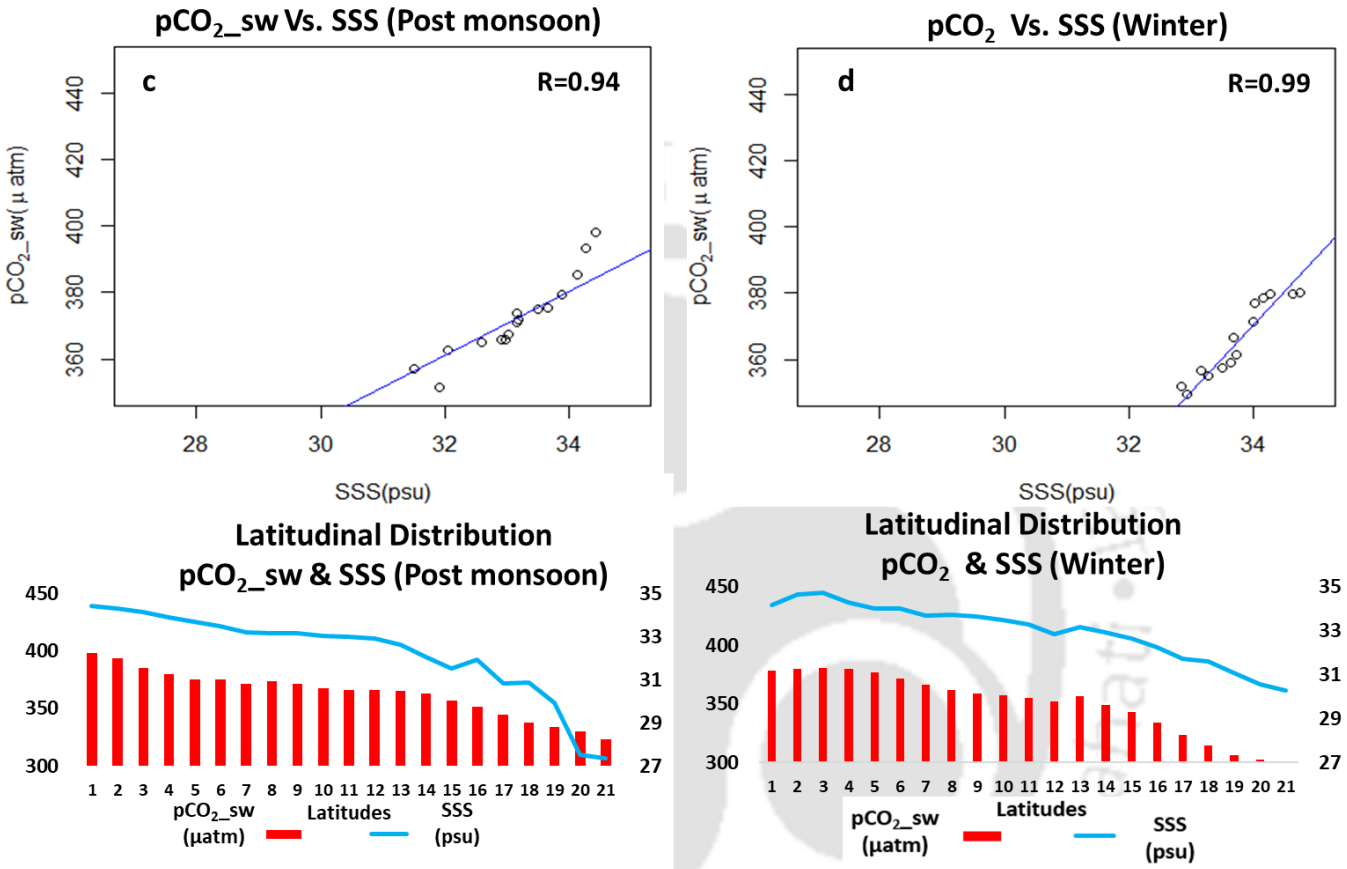

Figure.3.10 (ii) Significance of SSS variations in pCO_2sw distribution over BoB post-monsoon (c) and winter (d) season

3.3.2 Spatial and Seasonal distribution of CO_2 fluxes Over Indian Ocean

CO_2 fluxes were calculated and analysed to understand the seasonal and spatial distribution over the Arabian Sea and the Bay of Bengal. Seasonally, the fluxes were analysed for pre-monsoon, monsoon, post-monsoon, and winter. Spatial variation was studied for northern and southern regions of each sub-basins, where most coastal zones dominate the northern part, and open ocean waters occupy the south.

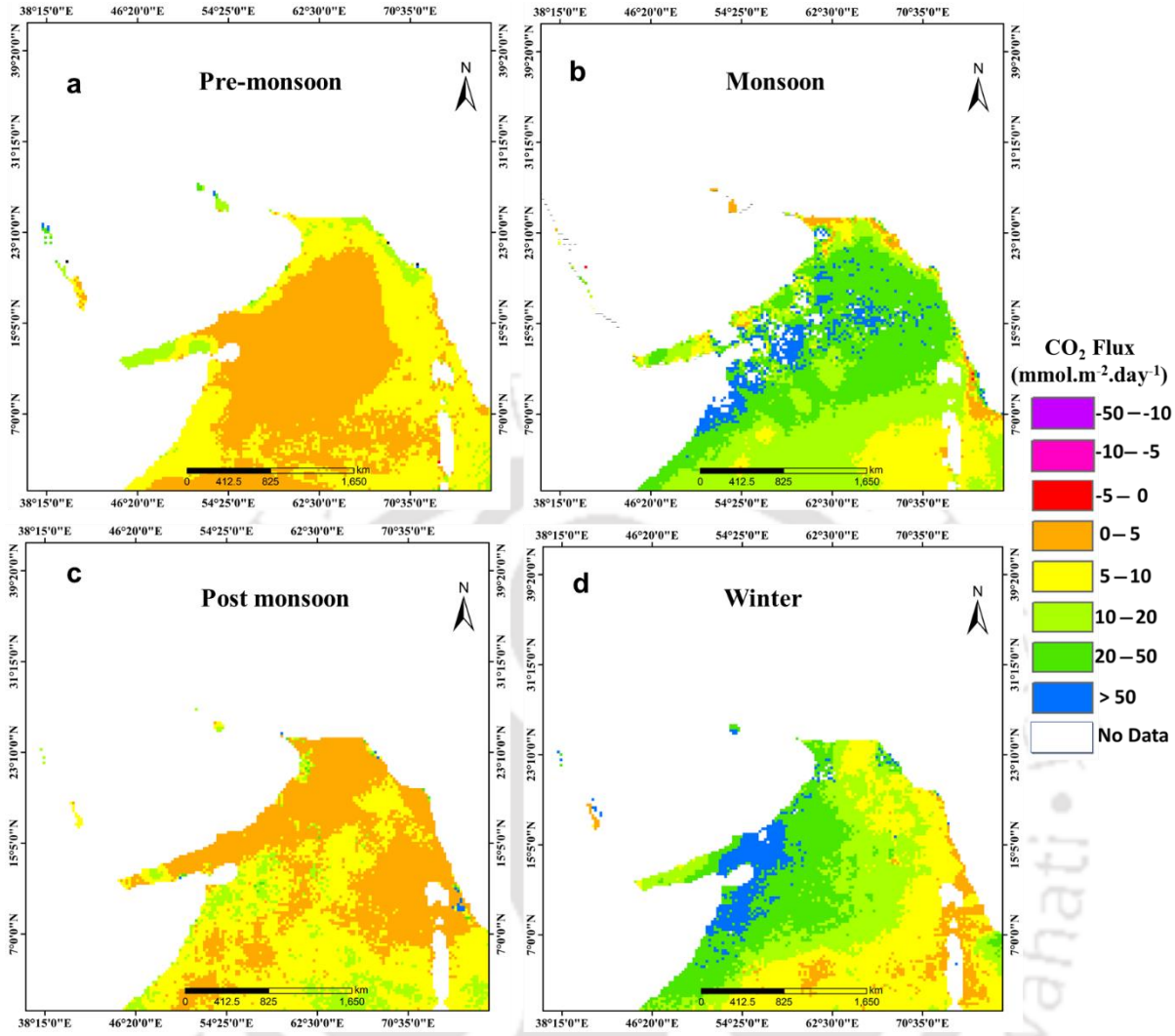

Figure.3.11 Spatio-temporal variation of CO_2 Fluxes over the Arabian Sea

Both sub-basins showed the highest flux values in the monsoon season. In the Arabian Sea, monsoon emissions were observed over a wide range of 5–93 mmol m^{-2} day^{-1} in the north and 3 – 25 mmol m^{-2} day^{-1} in the south (Figure.3.11-b), while BoB fluxes ranged from -20–70 mmol m^{-2} day^{-1} in the north to -47–1.5 mmol m^{-2} day^{-1} in the southern waters (Figure.3.12-b). Winter fluxes over the Arabian Sea were high on the north-western coast, with an average value range of 15–85 mmol m^{-2} day^{-1} (Figure.3.11-d), whereas the values over the south-east region showed the lowest emission range of 3–9 mmol m^{-2} day^{-1}.

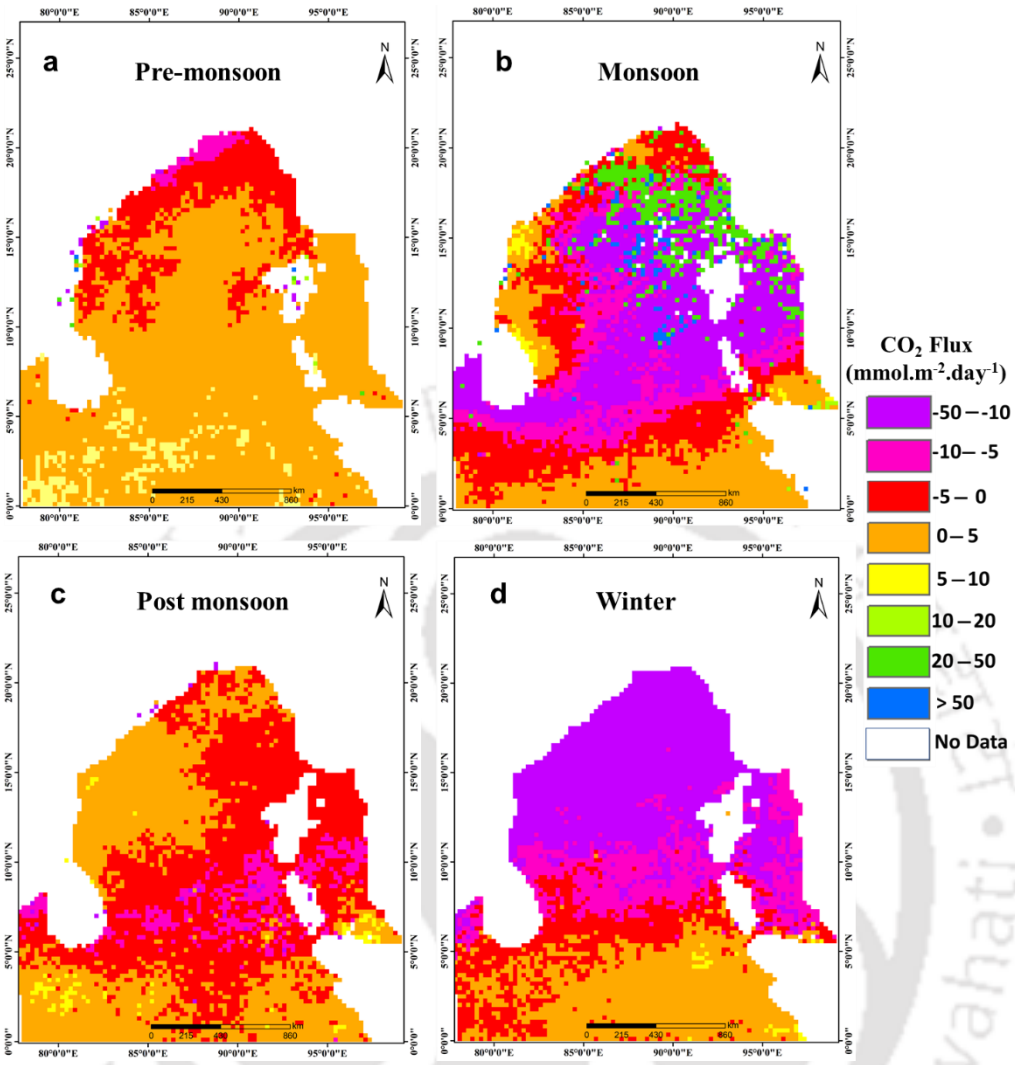

Figure.3.12 Spatio-temporal variation of CO_2 Fluxes over BoB

The increased emission of CO_2 in the monsoon season can be due to the upwelling of subsurface waters rich in CO_2, resulting in CO_2 oversaturation in the sea surface. The Findlater jet is one of the factors for upwelling in the monsoon enhancing the surface pCO_2 values (Madhupratap et al, 1996; Takahashi et al., 1997; Sarma et al., 1998; Sarma et al., 2000). In the winter season, the convective mixing brings subsurface waters enriched with CO_2, thus increasing the fluxes (Madhupratap et al., 1996; Sarma, 2003).

The lowest flux values were observed during the pre-monsoon season in the Arabian Sea, while winter fluxes showed the minimum seasonal values in BoB. Central and western Arabian Sea waters were found to have an average pre-monsoon flux value of 2–8 mmol m^{-2} day^{-1}, while towards the northeast and southwest coast, the values increased up to 13 mmol m^{-2} day^{-1} (Figure.3.11-a). The

absence of the low-salinity waters has increased the eastern flux values while, the equator to poleward change in surface circulation pattern, transporting low pCO_2 waters towards north has attributed to the lowering of fluxes over the northern central Arabian Sea and the adjoining western region (Sarma, 2003). In the pre-monsoon season, the central and east BoB waters exhibited a flux range of 0.5–5 mmol m^{-2} day^{-1} (Figure.3.12-a); flux values were found to decrease towards the north and north-west coastal regions (-0.1 to -7.5 mmol m^{-2} day^{-1}), while the pre-monsoon peak emissions were obtained over the southern open ocean waters, with a maximum flux value of 8 mmol m^{-2} day^{-1}. A reduction in the freshwater influx during pre-monsoon might have resulted in the central values while bacterial respiration could cause the increased outflux towards the southern waters (Sarma et al., 2000; Sarma, 2003)

Winter and post-monsoon fluxes in BoB showed the basin acts as a seasonal CO_2 sink, with the flux values ranging from 2 mmol m^{-2} day^{-1} to -4 mmol m^{-2} day^{-1} in the north, dropping to -11 mmol m^{-2} day^{-1} over the open ocean waters of central BoB during post-monsoon (Figure.3.12-c). Winter values over the northern BoB were found to be in the air-to-sea direction, where the influx ranged from -6 to -30 mmol m^{-2} day^{-1}; the maximum winter values were concentrated towards the southeast BoB, reaching up to a maximum of 3 mmol m^{-2} day^{-1} (Figure.3.12-d).

Post-monsoon fluxes also showed a decreasing trend in the Arabian Sea, especially in the northeast and northwest regions (Figure.3.11-c). The average value range showed 1–3.5 mmol m^{-2} day^{-1} which is less compared to that of the pre-monsoon values; the change in the direction of winds from south-westerly to north easterly post the south-west monsoon (Beal et al., 2013) brings the high CO_2 waters southward which establishes the south-north gradient whereas the relatively high pre-monsoon values are attributed to the increased levels of bacterial respiration enhancing the surface CO_2 in this season (Sarma et al., 1998; Sarma et al, 2000; Sarma, 2003). The east and north-west coastal regions showed the lowest fluxes ranging from 2 – 12 mmol m^{-2} day^{-1}, while relatively high values, reaching up to 15 mmol m^{-2} day^{-1} obtained in the southern open waters of the Arabian Sea.

Table 3.2. Spatial & Seasonal Distribution of CO_2 Fluxes

Seasons	CO_2Fluxes (mmol m^{-2} day^{-1})			
	AS-N	AS-S	BoB-N	BoB-S
Pre-monsoon	2 – 13	3 – 8	-13 – 2	0.7 – 8
Monsoon	5 – 93	3 – 25	-20 – 70	-47 – 1.5
Post-monsoon	2 – 12	2 – 15	-20 – 6	-10 – -7.5
Winter	15 – 85	3 – 9	-30 – -6	-11 – 6.5

The reduced emissions during pre and post-monsoon seasons in the Arabian Sea can be due to the absence of upwelling and convective mixing because surface layers' stratification hinders vertical transport. Also, CO_2 fixation during photosynthesis can reduce surface CO_2 (Madhupratap et al., 1996; Sarma et al., 2000; Takahashi et al., 2002). The spatial and seasonal distribution of fluxes is summarised in Table 3.2.

3.4 Summary and conclusions

The distribution of CO_2 fluxes in the Arabian Sea and BoB was estimated using satellite-derived and climatological parameters and analysed for spatial and seasonal variation. The sea surface partial pressures are an essential indicator of the CO_2 flux direction between the sea surface and the above atmosphere. The sea water pCO_2 over the Arabian Sea was calculated using the empirical algorithm derived from the SST and Chl-a, since the significant factors influencing the pCO_2 in this basin are the variations in sea water temperature and biological processes. In BoB the sea surface pCO_2 is primarily governed by the thermohaline stratification induced by the river fluxes and monsoonal freshwater input. Hence the SST-SSS relation was used in the sea water pCO_2 calculation.

The latitudinal distribution of the modelled sea surface partial pressures was analysed in relation to SST, SSS, and Chl-a variations to understand the physico-chemical and biological influence. The analysis revealed a reduction in the surface CO_2 levels by the photosynthetic activities during the inter-monsoon period, while the monsoonal upwelling and winter convective mixing increased the surface pCO_2 values in the Arabian Sea. In BoB, strong biological influence can be visible except in the monsoon season, where the pCO_2 distribution and biological activities are influenced by factors such as river and precipitation influx, sediment input, eddy formation, open ocean upwelling due to Ekman transport, and cyclonic activities.

Arabian Sea showed a maximum correlation between SST and pCO_2 distribution during pre-monsoon and winter seasons since the increase in the temperature in pre-monsoon would reduce the

CO_2 solubility, thus increasing the surface pCO_2 while the lowering of winter temperatures will cause the surface convective mixing, bringing subsurface CO_2 to the surface. In BoB, a high correlation was observed during all the seasons; pCO_2 and SST followed a similar spatial distribution trend. Increased temperatures in the pre and post-monsoon season over the open ocean waters of BoB increase the surface pCO_2. In contrast, the open ocean upwelling enhances the surface pCO_2 during monsoons and winter.

The occurrence of high salinity water mass in the north and central Arabian Sea is attributed to the north-south surface salinity gradient. While southern waters showed a reduction in salinity due to the influence of the BoB low saline waters, the increased temperatures elevate the surface pCO_2. Thus, no substantial effect of salinity on the surface pCO_2 distribution is observed in the Arabian Sea. The onset of the Arabian Sea High Salinity Water Mass and the winter convective mixing towards the north latitudes explains the strong correlation between SSS and pCO_2 during winter. A moderate to high correlation was observed between SSS and pCO_2 over BoB; similar to the SST-pCO_2 distribution, SSS and pCO_2 followed similar spatial trends. Monsoonal eddies and cyclonic activities could be the reason behind the disturbing correlation in monsoon season. The freshwater influx during the monsoon season reduces the salinities in the north, establishing a surface stratification, which eventually affects the post-monsoon and winter pCO_2 distribution, while the absence of such stratification and the increased temperatures result in a positive correlation between the SSS and pCO_2 in pre-monsoon.

The spatial and seasonal variation of CO_2 flux showed high sea-to-air fluxes over the Arabian Sea during monsoon followed by the winter season; BoB emissions were also increased during the monsoon while the basin acts as an intense sink in winter. The monsoonal upwelling and winter convective mixing enhance the surface CO_2 levels, leading to an oversaturation. The highest flux values were obtained in the northwestern region where the upwelling along the Somali coast and the influence of the Findlater Jet escalated the outflux. The low pre- and post-monsoon fluxes could result from thermal stratification and photosynthetic consumption. On the other hand, the comparatively high fluxes in the pre-monsoon over the open ocean waters of BoB could be due to the bacterial respiration and organic matter decomposition of the winter productivity. In winter and post-monsoon, the surface pCO_2 in BoB fall below the atmospheric pCO_2 owing to the surface stratification, leading to negative fluxes, especially over the northern latitudes.

4

Significance of ocean primary productivity and sea surface temperature distribution on spatial and seasonal variability of air-sea CO_2 fluxes

4.1 Introduction

The air-sea CO_2 fluxes are regulated primarily by the fluctuations in the sea water CO_2 partial pressures. The major controlling factors of sea water partial pressure are variations in sea water temperature and biological consumption of CO_2. An increase in the SST decreases the CO_2 gas solubility, thus enhancing the gas release, while a decrease in SST increases the CO_2 dissolution in water. However, the warming of the waters will induce surface stratification and reduce vertical mixing. The marine biological productivity consumes the surface CO_2, thus reducing the partial pressures. The biologically trapped CO_2 in the subsurface layers will be released back in to surface during upwelling triggered by a reduction in the SST. Therefore, a combination of the SST and productivity will decide the flux direction between the water and air (Metzl et al, 2006; Sharada et al, 2008)

4.2 Data and Methods

The spatial and seasonal distribution of ocean primary productivity was analyzed using the satellite-derived (MODIS-Aqua) Net Primary Productivity data calculated using the chlorophyll-based Vertically Generalised Production Model (VGPM). The VGPM model is used to derive the net primary productivity from the satellite-derived Chl-a, SST, and sea surface daily photosynthetically active radiation(PAR) and can be expressed as equation 4.1 (Behrenfeld and Falkowski, 1997).

$$PP_{eu} = 0.66125 * P^{B}_{opt} \frac{E0}{E0+4.1} * C_{SAT} * Z_{eu} * D_{IRR} \quad (4.1)$$

PP_{eu} is the daily carbon fixation in $mgCm^{-2}d^{-1}$ integrated to euphotic depth Z_{eu} in meter; euphotic depth is derived as a function of chlorophyll as given in equation 4.2-4.3.

$$Z_{eu} = \begin{cases} 568.2(C_{TOT})^{-0.746}, \text{ if } C_{TOT} < 102 \\ 200.0(C_{TOT})^{-0.293}, \text{ if } C_{TOT} > 102 \end{cases} \quad (4.2)$$

$$C_{TOT} = \begin{cases} 38.0(C_{SAT})^{0.425}, \text{ if CSAT } <1.0 \\ 40.2(C_{SAT})^{0.507}, \text{ if CSAT } \geq 1.0 \end{cases} \quad (4.3)$$

C_{SAT} is satellite-derived surface chlorophyll concentration (mg chl m^{-3})

P^B_{opt} is the optimal daily carbon fixation rate within a water column [mgC(mg Chl)$^{-1}h^{-1}$] derived as a function of sea surface temperature; it is either considered as the following criteria,

$$P^B_{opt} = \begin{cases} 1.13 & \text{if } T < -1.0 \\ 4.00 & \text{if } T > 28.5 \end{cases}$$

or if -1.0> T >28.5, it is derived as equation 4.4.

$$P^B_{opt} = 1.2956 + 2.749*10^{-1}*T + 6.17*10^{-2}*T^2 - 2.05*10^{-2}*T^3 + 2.462*10^{-3}*T^4 - 1.348*10^{-4}*T^5 + 3.4132*10^{-6}*T^6 - 3.27*10^{-8}*T^7 \quad (4.4)$$

T is sea surface temperature in degree Celsius, E_0 is sea surface daily PAR (mol quanta m^{-2} d^{-1}), D_{IRR} is the daily photoperiod calculated in decimal hours for the middle of the month.

The overall flow diagram of the VGPM model is summarised in Figure.4.1.

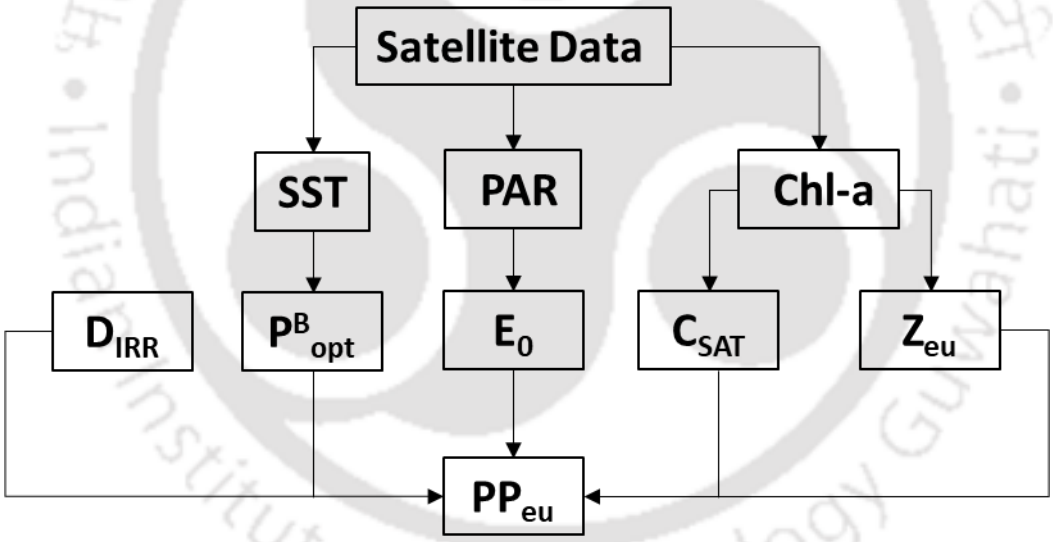

Figure. 4.1 Methodology flow diagram for ocean primary productivity calculation

The latitudinal (south to north) and longitudinal (west to east) gradient of the CO_2 fluxes distribution in relation to primary productivity and SST was carried out to understand the seasonal and spatial influence of the CO_2 uptake by biological activities and the temperature variations of sea water. Latitudinal and longitudinal averages of the satellite-derived primary productivity, SST, and flux values from both basins were extracted and plotted for pre-monsoon, monsoon, post-monsoon and winter seasons.

4.3 Results

4.3.1 Spatial and seasonal variability in Primary Productivity

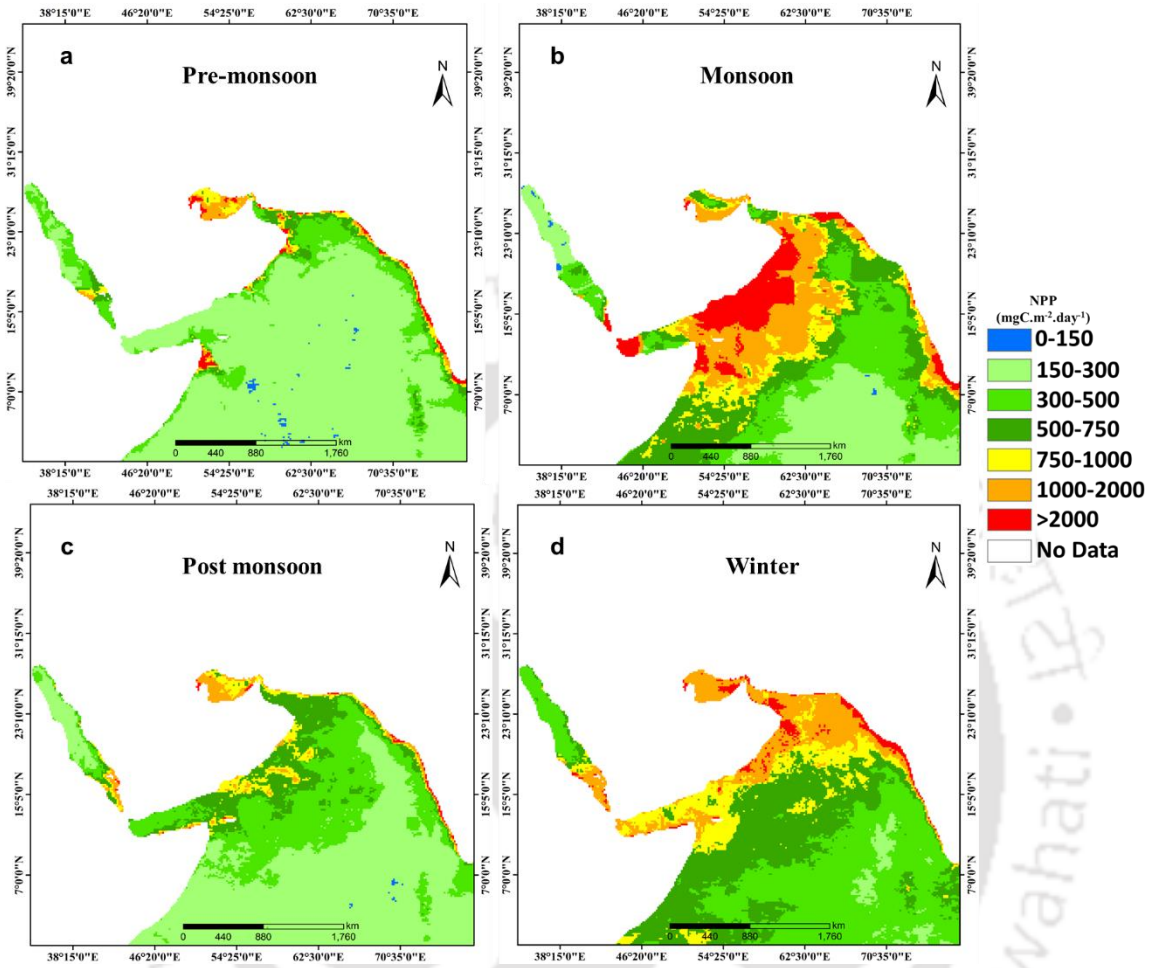

Figure.4.2 Spatio-temporal variation of ocean primary productivity over the Arabian Sea

Winter and monsoon seasons showed high productivity in the northern Arabian Sea. Winter productivity exhibited a wide range with average minimum values of 275 mgC m^{-2} day^{-1} in the eastern coast to a maximum of 2000 mgC m^{-2} day^{-1} in a the northern coast (Figure.4.2-d). Monsoon values ranged from 200 mgC m^{-2} day^{-1} on the east coast to 2500 mgC m^{-2} day^{-1} on the north-western coast (Figure.4.2-b). Pre (Figure.4.2-a) and post-monsoon (Figure.4.2-c) average values ranged from 150 – 600 mgC m^{-2} day^{-1}. High productivity can be the result of the monsoonal upwelling and winter convective mixing that bring nutrients from the subsurface hence triggering the ocean primary productivity, the absence of which caused a reduction in the productivity in pre-monsoon (Figure.4.2-a) and post-monsoon (Figure.4.2-c) seasons (Sarma et al., 2000; Barber et al., 2001; Marra and Barber, 2005).

High productivity is observed during winter in the north-eastern Arabian Sea, as observed by Madhupratap et al (1996). The winter cooling experienced by the northern Arabian Sea is characterised by sea surface temperature reduction and densification, leading to the formation of high salinity waters. This is followed by sinking and convective mixing, which brings nutrients to the surface waters from the thermocline, thus enhancing productivity (Chauhan et al., 2001). During winter, onshore and offshore chlorophyll blooms characterize the northern Arabian Sea, which also can result in high winter productivity (Dey and Singh, 2003). The highest productivity during monsoon was observed in the western region caused by the upwelling on the Oman coast (Barber et al., 2001).

Comparatively, less productivity was observed in the southern Arabian Sea, with maximum values in winter (250- 500 mgC m^{-2} day^{-1}) and minimum (150-200 mgC m^{-2} day^{-1}) in pre-monsoon season (Figure.4.2-a). The low productivity trend can be due to an increase in SST while going to the offshore regions and the resulting stratification in the surface layers and reduction in the upward transport of nutrients (Sarma, 2003). An increase in temperature also causes an increase in respiration rates and heterotrophic activities in the surface waters. The increased rates of microbial respiration and the time lag between production and respiration might have caused the reduced productivity (Sarma, 2003). Also, the nutrient concentration in the surface waters decreases offshore, and the mixed layer depth increases, which can result in reduced productivity (Sarma et al., 2000; takahashi et al., 2002; Marra and Barber, 2005). The western and northern regions were the highest productive regions in the Arabian Sea (Tang et al., 2002; Prasannakumar et al., 2009).

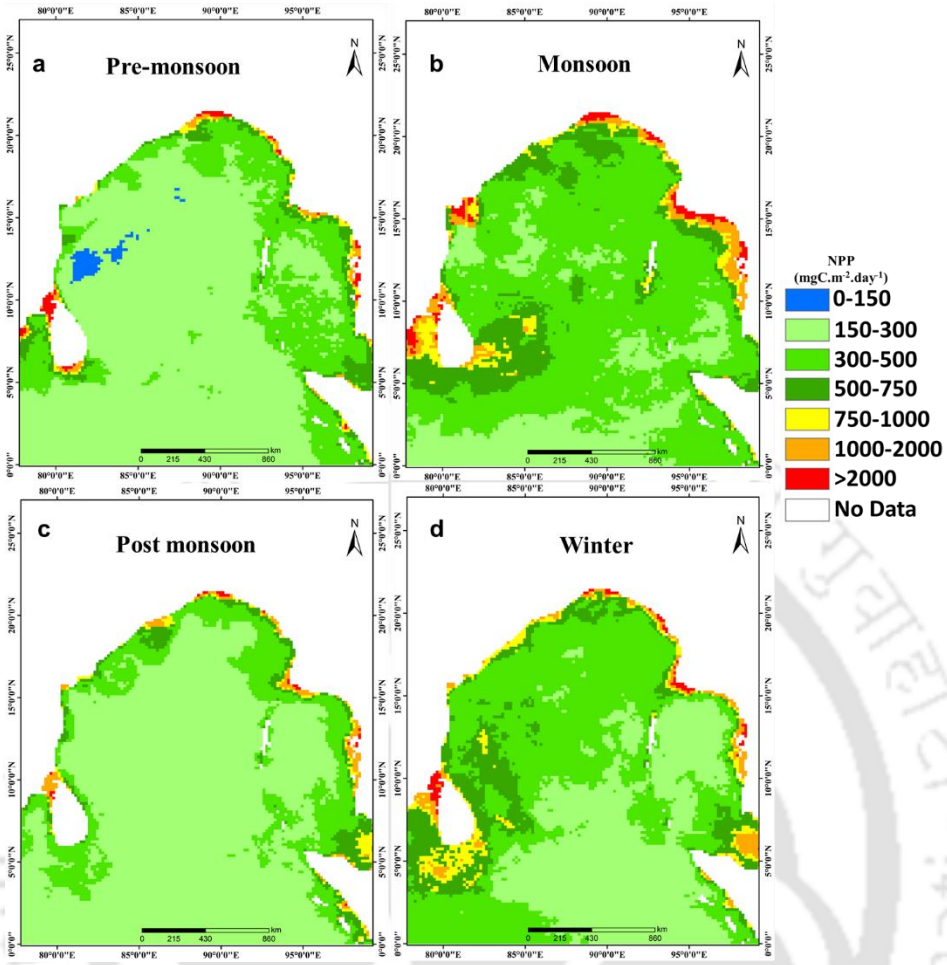

Figure.4.3 Spatio-temporal variation of ocean primary productivity over the Bay of Bengal

Primary productivity in BoB (Figure.4.3) was comparable to that of the southern Arabian Sea. Less values were observed in all seasons with an average range of 150-500 mgC m^{-2} day^{-1} with minimal fluctuation in spatial distribution. Intense precipitation and river runoff cause strong stratification in the BoB, as Unger et.al. (2003) reported. Stratification suppresses the vertical mixing process resulting in less nutrient content in surface waters lowering marine productivity (Rao et.al., 1994; George et.al., 1994; Kumar et.al., 1996). The hindrance of light by turbidity and cloud cover also affects productivity in BoB, as reported by Madhupratap et.al. (2003). The maximum values reaching up to the range 750-2000 mgC m^{-2} day^{-1} can be observed along the north east coast of BoB and the Sri Lanka coast; the nutrient availability from the river influx results in enhanced productivity in the former case, while the Ekman pumping triggered upwelling and monsoon chlorophyll blooms enhance the latter one (Murtugudde and Busalacchi, 1999; Vinayachandran et

al., 2004). The spatial and seasonal distribution of the average primary productivity values over the northern and southern Arabian Sea and BoB is summarised in Table 4.1.

Table 4.1. Spatial & Seasonal Distribution of Primary Productivity

Seasons	**Primary Productivity (mgC m^{-2} day^{-1})**			
	AS-N	**AS-S**	**BoB-N**	**BoB-S**
Pre-monsoon	150-600	150-200	120-500	200-300
Monsoon	200-2500	160-400	230-800	230-630
Post-monsoon	200-750	150-275	180-600	200-300
Winter	275-2000	250-500	200-600	160-600

4.3.2 CO_2 fluxes distribution in relation to ocean primary productivity

Seasonal variations in the south-north (S-N) and west-east (W-E) gradient of CO_2 fluxes were analysed in relation to the primary productivity to understand the significance of biological controls on the gas exchange at the sea surface in both the Arabian Sea and BoB. The S-N (Figure.4.4-a) distribution in the pre-monsoon season over the Arabian Sea showed a drop in the flux values over the mid-latitudes, with the lowest flux value observed to be 3 mmol m^{-2} day^{-1}, rising towards north and south, reaching up to a maximum of 7 mmol m^{-2} day^{-1} in the northern waters; a gradual northward increase in the productivity was observed. In the W-E gradient (Figure.4.4-b), the western and eastern coastal flux values recorded maximum (8 mmol m^{-2} day^{-1}) and the lowest (3 mmol m^{-2} day^{-1}) fluxes were observed over the western-central region. The productivity also exhibited western and eastern peaks, reaching a maximum of 350 mgC m^{-2} day^{-1} in the east, while the maximum values (373 mgC m^{-2} day^{-1}) were recorded over the western-central longitudes, accompanied by a fall in the flux values.

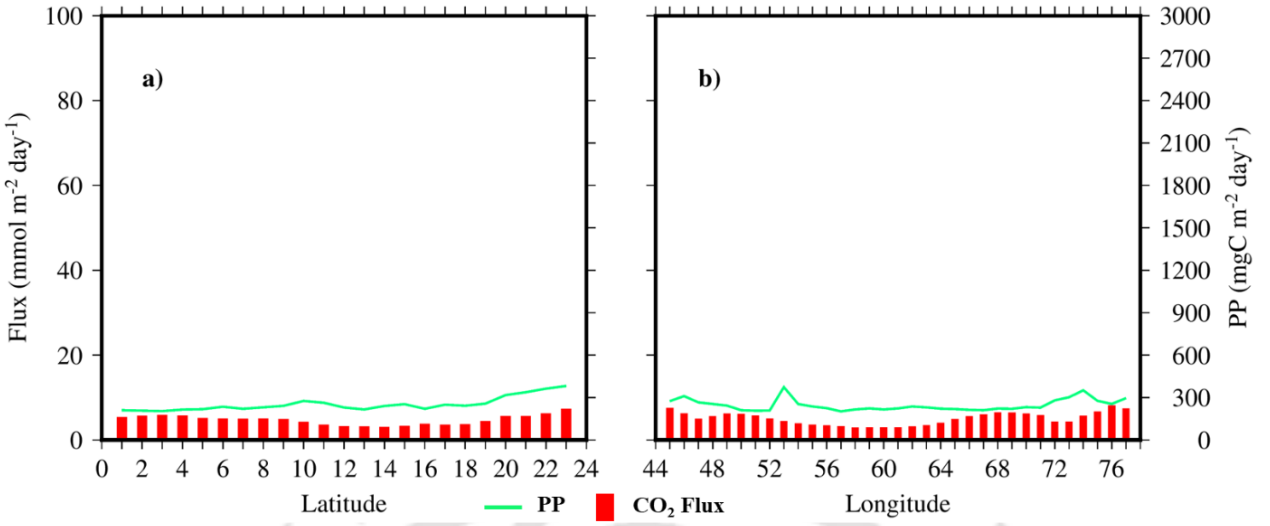

Figure.4.4 Spatial variations in pre-monsoon fluxes and primary productivity in the South-North and West-East directions over the Arabian Sea

In the monsoon season (Figure.4.5-a), both flux and productivity values peak over the upper central latitudes with a maximum flux value of 61 mmol m^{-2} day^{-1} and productivity of 2687 mgC m^{-2} day^{-1}, while the lowest values obtained over the southern waters with the CO_2 flux value falling to 14 mmol m^{-2} day^{-1} and productivity 365 mgC m^{-2} day^{-1}. Considering the W-E distribution (Figure.4.5-b), the productivity peaked over the western central region (2250 mgC m^{-2} day^{-1}), and high outflux (61 mmol m^{-2} day^{-1}) was identified towards the western coast.

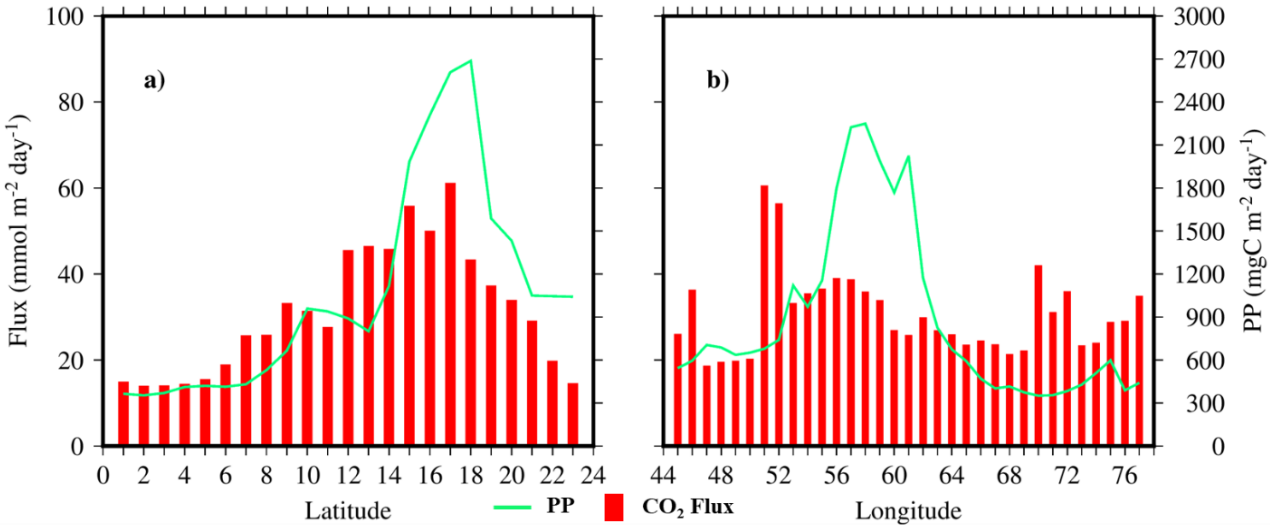

Figure.4.5 Spatial variations in monsoon fluxes and primary productivity in the South-North and West-East directions over the Arabian Sea

Post-monsoon productivity showed an increasing trend towards the upper latitudes, which also can be visible in the W-E distribution. In contrast, the fluxes decreased towards the north (Figure.4.6-a) while reaching maximum value (Figure.4.6-b) over the western coast of Arabian Sea. The northern productivity values reached up to 495 mgC m^{-2} day^{-1}, and the fluxes showed the lowest value of 2.6 mmol m^{-2} day^{-1}; the western coast observed the peak flux values around 8.2 mmol m^{-2} day^{-1}, while the highest productivity value of 402 mgC m^{-2} day^{-1} given by the central longitudinal averages.

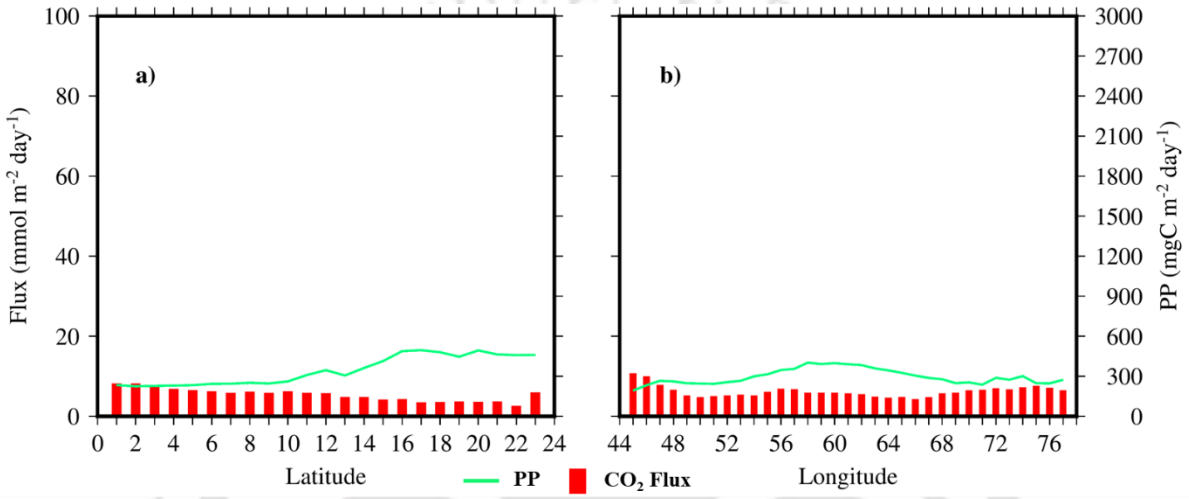

Figure.4.6 Spatial variations in post monsoon fluxes and primary productivity in the South-North and West-East directions over the Arabian Sea

Winter fluxes enhanced (Figure.4.7-a) over the mid-latitudes (30 mmol m^{-2} day^{-1}) and decreased over the southern waters (10 mmol m^{-2} day^{-1}); the productivity increased northward, reaching up to 1500 mgC m^{-2} day^{-1}, while lowest productivity value of 453 mgC m^{-2} day^{-1} was identified in the low latitudes. The W-E distribution of fluxes (Figure.4.7-b) peaked over the western and western-central Arabian Sea, with a maximum outflux around 37.4 mmol m^{-2} day^{-1}, dropping to 8.8 along the south west coast of India. Productivity was maximum (800 mgC m^{-2} day^{-1}) over the western longitudes, and lowest (359 mgC m^{-2} day^{-1}) towards the east.

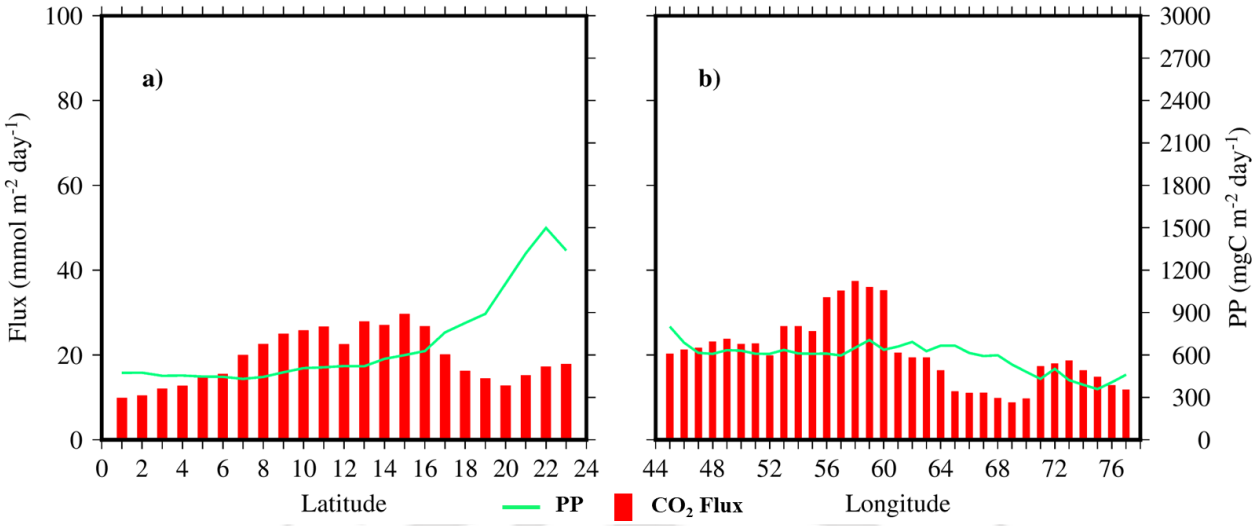

Figure.4.7 Spatial variations in winter fluxes and primary productivity in the South-North and West-East directions over the Arabian Sea

The maximum flux and productivity values observed over the northern and western Arabian Sea during winter and monsoon seasons can be attributed to the convective mixing and on-shore as well as off-shore upwelling. High productivity is associated with high respiration rates, elevating the surface CO_2. During monsoon, the maximum flux values were over the western coast owing to the Somali coast upwelling, which was transported towards the central and north-eastern waters by the Findlater Jet (Madhupratap et al, 1996; Sarma, 2003). This enhances the central and north-eastern fluxes. A reduction in monsoon fluxes towards the north is attributed to the high-nutrient, low-saline fresh water influx by river runoff in the Oman and Pakistan, lowering the fluxes due to reduced alkalinity while enhancing productivity (Sarma et al., 1998). The pre-monsoon distribution of fluxes and productivity did not show much trend since the absence of upwelling resulted in a lowering of both (Sarma et al., 2000; Marra and Barber, 2005). The increase in the flux values over the north might be due to the bacterial respiration enhancing the surface CO_2. In contrast, the absence of low salinity waters from the BoB increased the flux values over the western coast of India, increasing the southern fluxes (Sarma et al., 1998; Sarma et al., 2000; Sarma, 2003). Over the central and western Arabian Sea, the movement of low pCO_2 waters towards the north by the poleward surface circulation has lowered the fluxes (Sarma, 2003). The eastern and western productivity maximum was associated with a drop in the flux values, which can be due to the photosynthetic drawdown of surface CO2 (Madhupratap et al, 1996). The transport of high flux waters towards the south by the

reversing wind system during the post-monsoon could be behind the high values towards the south, also the CO_2 consumption by the high productivity over the western Arabian Sea might have resulted in the low flux values over this region (Beal et al., 2013). The winter fluxes were maximum over the western coast of the Arabian Sea, reducing over the south-west coast of India. The low saline waters from BoB entering the south-west coast might have led to the W-E gradient in flux values (Sarma, 2003).

In BoB, pre-monsoon fluxes (Figure.4.8-a) showed an air-sea transfer over the northern latitudes, while the trend reduced to the mid-latitudes, reversing towards the southern open ocean waters. The influx showed a maximum value up to -9.4 mmol m^{-2} day^{-1}, while the low latitude outfluxes reached 4 mmol m^{-2} day^{-1}. Productivity exhibited a spatial variation with lowest values over the southern and central latitudes, falling to 225 mgC m^{-2} day^{-1} while peaked towards the north (978 mgC m^{-2} day^{-1}). The W-E distribution of fluxes (Figure.4.8-b) has given the peak values (16 mmol m^{-2} day^{-1}) over the eastern BoB coast, while low value range (0.97-1.7 mmol m^{-2} day^{-1}) was observed over the central longitudes. Productivity was maximum over the western and eastern coasts with highest values obtained over the west (433 mgC m^{-2} day^{-1}); productivity dropped over the central open ocean waters to around 220 mgC m^{-2} day^{-1}.

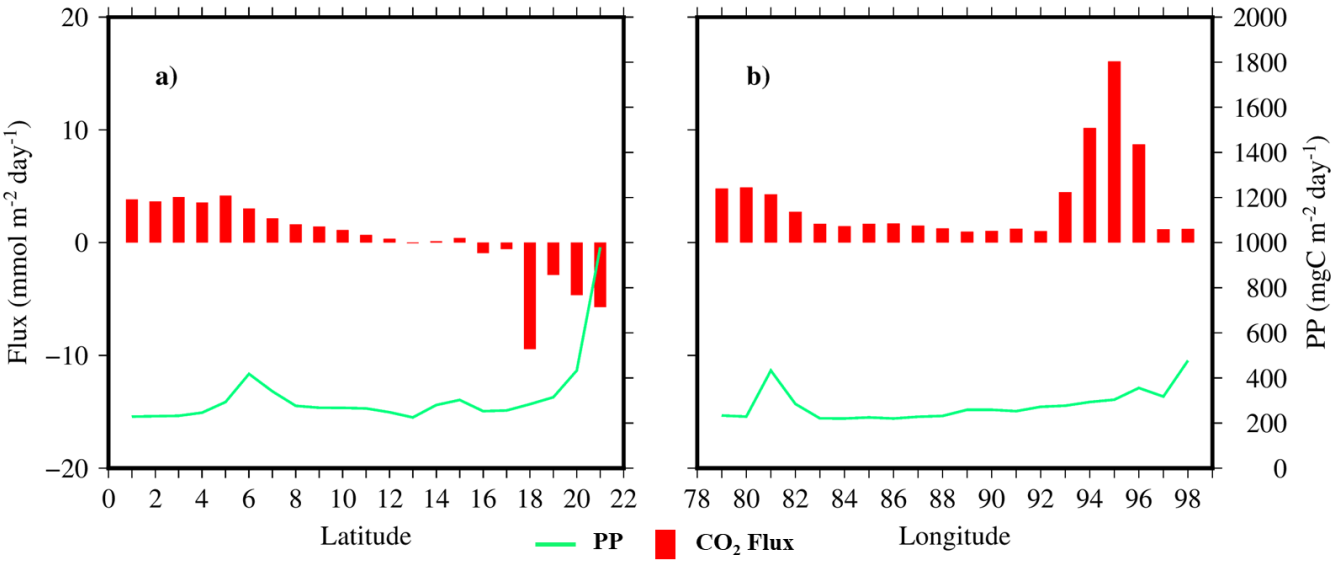

Figure.4.8 Spatial variations in pre-monsoon fluxes and primary productivity in the South-North and West-East directions over the Bay of Bengal

The monsoon trend reversed as compared to the pre-monsoon season, where the influx trend was observed towards the south (Figure.4.9-a) while the northern latitudes showed an average

outflux trend (1-17 mmol m^{-2} day^{-1}). Low outflux values (0.5-1.5 mmol m^{-2} day^{-1}) were observed towards the southern waters, while the north-east fluxes exhibited a positive values range. Towards the central BoB, a substantial influx trend can be observed, reaching a maximum value of -9.3 mmol m^{-2} day^{-1}. Productivity showed a similar trend in the S-N distribution (Figure.4.9-a) as that of the pre-monsoon, with the lowest values (270 mgC m^{-2} day^{-1}) observed over the southern latitudes, peaking over the northern waters (1541 mgC m^{-2} day^{-1}). The W-E distribution (Figure.4.9-b) showed an influx (-5 to -1.5 mmol m^{-2} day^{-1}) trend towards the western region, while the eastern waters exhibited a mixed scenario (-3 to 6.8 mmol m^{-2} day^{-1}). Primary productivity showed a peaking and falling trend along the W-E direction, with values ranging from 270 mgC m^{-2} day^{-1} over the extreme west, to 477 mgC m^{-2} day^{-1} over the eastern region.

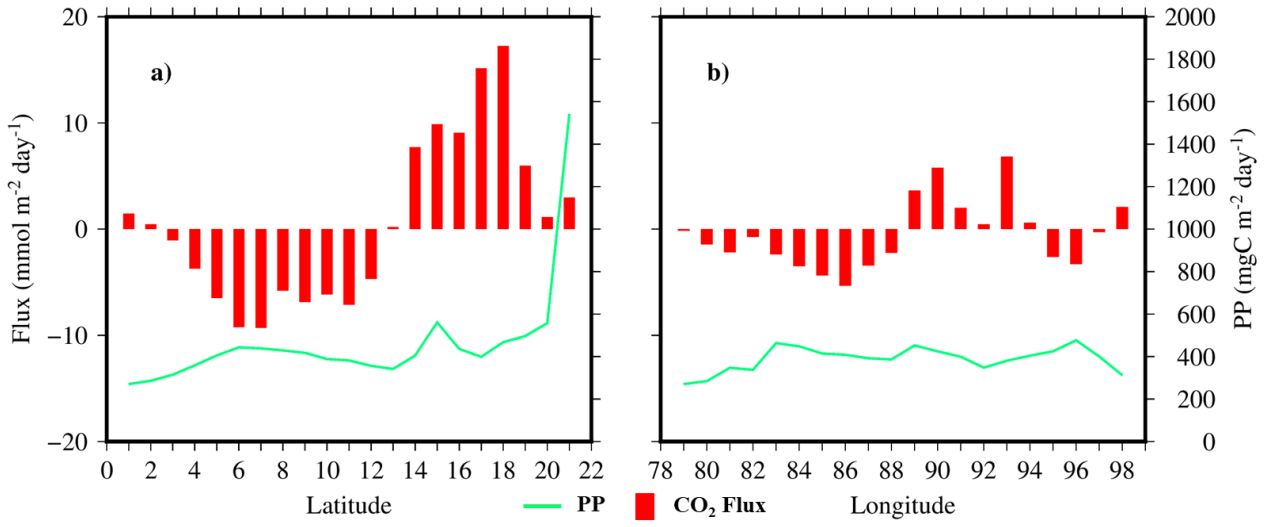

Figure.4.9 Spatial variations in monsoon fluxes and primary productivity in the South-North and West-East directions over the Bay of Bengal

Post-monsoon productivity also followed the S-N (Figure.4.10-a) increasing trend similar to pre-monsoon and monsoon values; while fluxes showed a mixed influx and outflux trend along the S-N direction, the western waters were observed to have an outflux trend, reversing towards east. The maximum productivity value obtained in the north was around 850 mgC m^{-2} day^{-1}, reducing to 218.5 mgC m^{-2} day^{-1} over the low latitudes. The highest influx values (-2.7 to -3.7 mmol m^{-2} day^{-1}) were observed over the upper-southern latitudes, while northern waters also showed the influx (-2.9 mmol m^{-2} day^{-1}) trend; 1.2-1.6 mmol m^{-2} day^{-1} outflux value range was obtained over the low latitudes, while the maximum fluxes values (3 mmol m^{-2} day^{-1}) found towards the north. The W-E distribution (Figure.4.10-b) gave maximum outflux values (5.9 mmol m^{-2} day^{-1}) over the western

region, reversing the trend towards the north, where the influx values peaked around -2.2 mmol m^{-2} day^{-1}. Increased productivity was observed in the east (501 mgC m^{-2} day^{-1}), whereas it dropped towards the west (213 mgC m^{-2} day^{-1}).

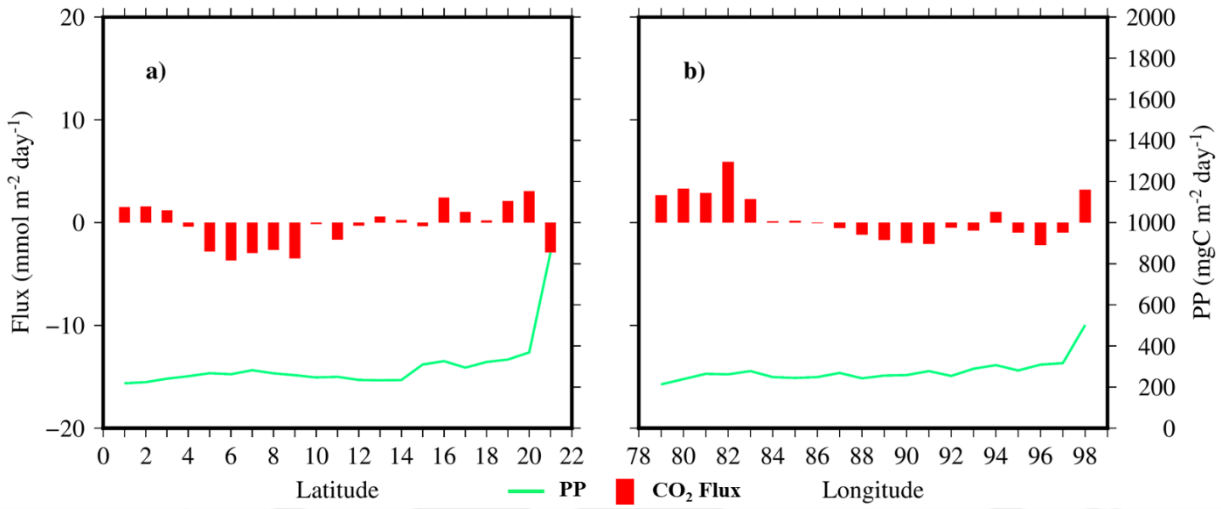

Figure.4.10 Spatial variations in post monsoon fluxes and primary productivity in the South-North and West-East directions over the Bay of Bengal

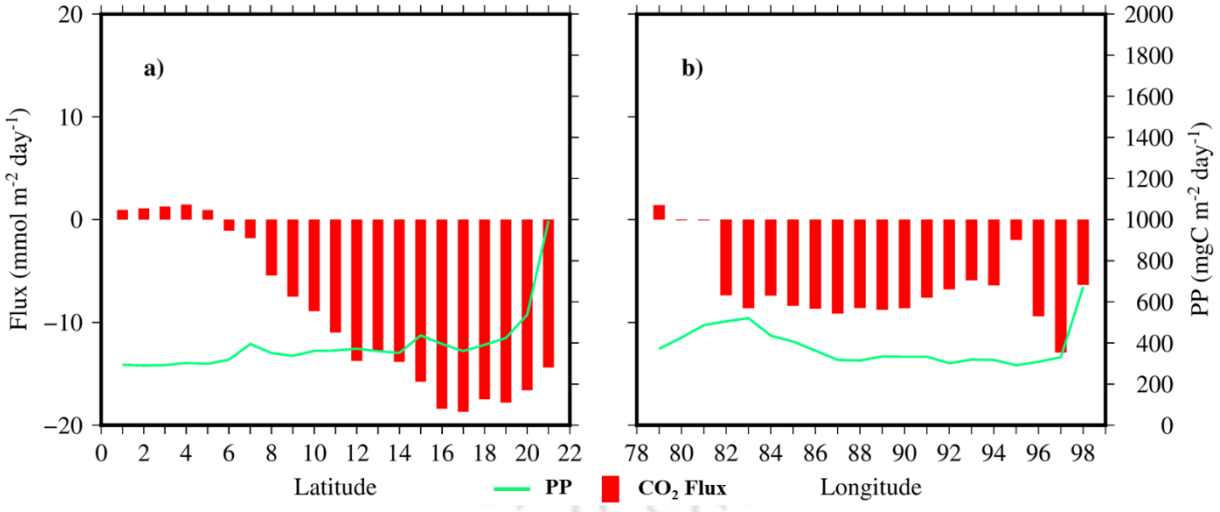

Figure.4.11 Spatial variations in winter fluxes and primary productivity in the South-North and West-East directions over the Bay of Bengal

Winter fluxes showed intense influx (-1 to -18.7 mmol m^{-2} day^{-1}) over the northern BoB, shifting to low outflux (0.9-1.4 mmol m^{-2} day^{-1}) trend over the low latitudes (Figure.4.11-a). Productivity repeated the previous S-N increasing trend with a value range of 293.7-993 mgC m^{-2} day^{-1}. The W-E distribution (Figure.4.11-b) exhibited a strong influx trend over the eastern (-1.97 to

-13 mmol m^{-2} day^{-1}) and central (-6 to -9 mmol m^{-2} day^{-1}) waters, with a slight outflux trend in the extreme west. The productivity peaked towards the western (521 mgC m^{-2} day^{-1}) and eastern (672 mgC m^{-2} day^{-1}) waters, lowering over the central (301 mgC m^{-2} day^{-1}) BoB.

In BoB, the maximum influx observed was in winter and the maximum outflux was in monsoon season, both in the north. The winter productivity was found to be maximum during monsoon and winter, with the highest values obtained for the monsoon season. During monsoon, the riverine influx brings a variety of organic and inorganic matter into the BoB, increasing bacterial respiration levels and increasing sea water CO_2 (Shanti et al., 2016). Due to the intense fresh water input from rivers and precipitation in monsoon, surface stratification establishes over the northern and central BoB, which usually hinders the upwelling of such subsurface CO_2 concentration (Madhupratap et al., 2003). Local eddies and the Ekman transport of the freshwater plume might disturb this stratification, which can enhance the surface pCO_2 levels compared to the atmosphere, leading to an outflux (Vinayachandran et al., 1996; Sarma et al., 2020). The strong influx over the central BoB in monsoon and the entire northern and central BoB might be attributed to the freshwater-induced surface stratification. During pre-monsoon season, the influence of the fresh water input is reduced, increasing the central and southern outflux. In post-monsoon, the reduction in the stratification and the transport of the northern low pCO_2 waters towards the central BoB result in an increase in outflux over the north-western BoB. The high productivity over the BoB basin is observed over the north eastern coast and along the Sri Lanka coast, which might be attributed to the coastal and Ekman transport induced- open ocean upwelling (Vinayachandran et al., 1996; McCreary et al., 2009).

4.3.3 CO_2 fluxes distribution in relation to sea surface temperature variability

The significance of S-N and W-E sea water thermal variations on the sea surface CO_2 fluxes distribution was analysed seasonally. Over the Arabian Sea, a strong S-N gradient (Figure.4.12-a) in pre-monsoon SST was visible, whereas the western and eastern SST values showed the lowest value of 27.7 °C increasing up to 31°C (Figure.4.12-b). However, a distinct W-E gradient was absent; a weak coast-open ocean gradient can be seen. Although a gradient did not exist, the lowest value (29.4 °C) was observed towards the western coastal waters, and the maximum SST (30.6 °C) was obtained in the east. While both fluxes and SST showed an increasing trend towards the low latitudes, the trend reversed in SST in the north, while fluxes lowered over the mid-latitudes. The

W-E distribution showed fluxes and SST peaks towards the west and east while dipping over the central Arabian Sea.

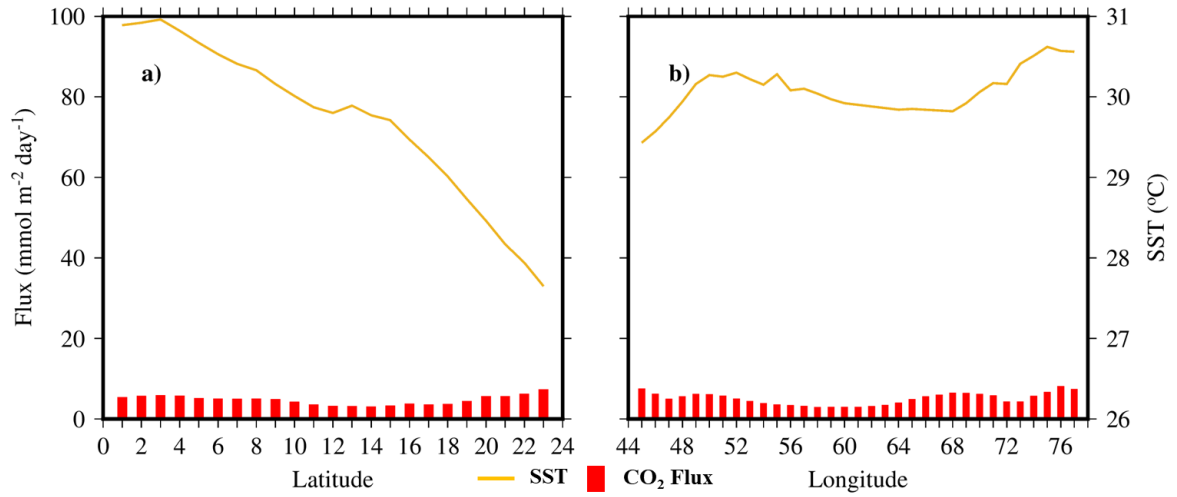

Figure.4.12 Spatial variations in pre-monsoon fluxes and SST in the South-North and West-East directions over the Arabian Sea

The monsoon SST values peaked towards the north and south, with maximum values reaching around 28.8 °C over the low latitudes (Figure.4.13-a); SST dropped over the mid-latitudes to 27.3 °C. The SST values showed a W-E gradient (Figure.4.13-b), from 26.3 °C in the west, reaching up to 29.6 °C in the eastern Arabian Sea. Monsoon season exhibited an inter-relation in the flux and SST distribution, both in the S-N and W-E direction.

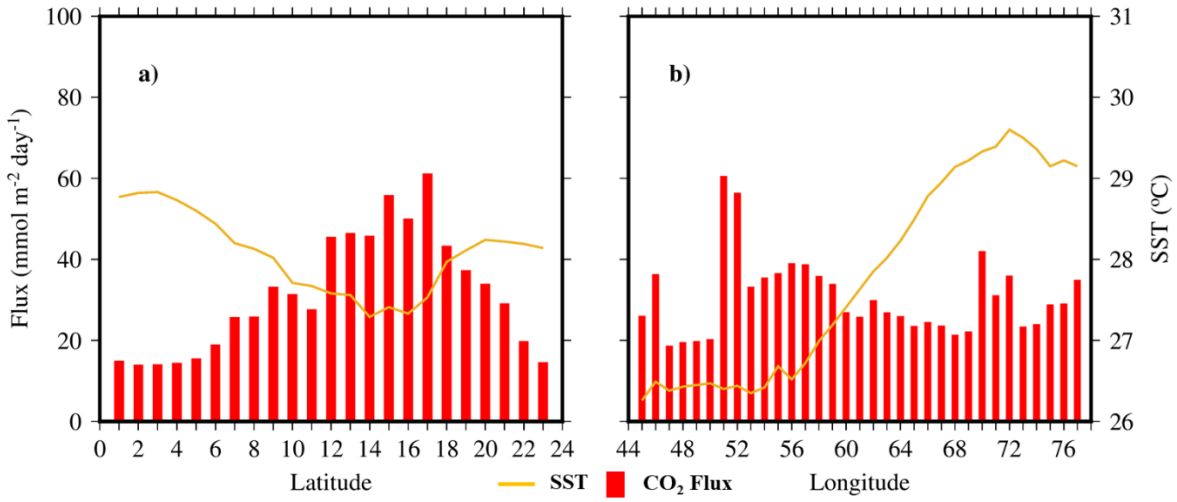

Figure.4.13 Spatial variations in monsoon fluxes and SST in the South-North and West-East directions over the Arabian Sea

Post-monsoon SST also followed the S-N and W-E monsoon trend, peaking towards the south and north (Figure.4.14-a), falling over the mid-latitudes, while a strong west-to-east gradient (Figure.4.14-b), with maximum values over the east, was evident. The highest SST values were observed towards the south around 29.4 °C, dropping to 28.4 °C over the central Arabian Sea; in the east, SST reached around 29.5 °C, dropping to 27°C towards the west. Flux and SST distribution showed a correlation in the S-N direction, whereas no particular trend was observed between their distribution in the W-E.

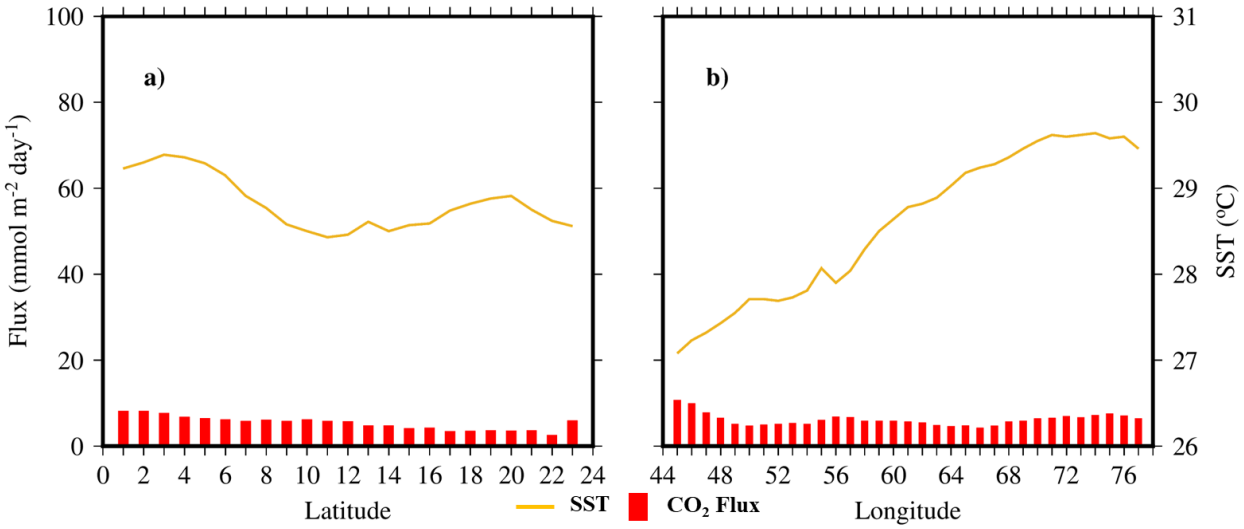

Figure.4.14 Spatial variations in post monsoon fluxes and SST in the South-North and West-East directions over the Arabian Sea

Winter values showed an S-N (Figure.4.15-a) gradient with maximum values obtained southward; northern SST lowered to 26 °C, increasing to 28.8 °C in the low latitudes. The W-E distribution (Figure.4.15-b) also exhibited increased SST values from west to east, with the value range 27.4-29.2 °C. In winter, the fluxes peaked over the west, lowering towards the east, thus, an inverse relation is visible in the W-E direction, whereas S-N direction did not show any specific trend between flux and SST distribution.

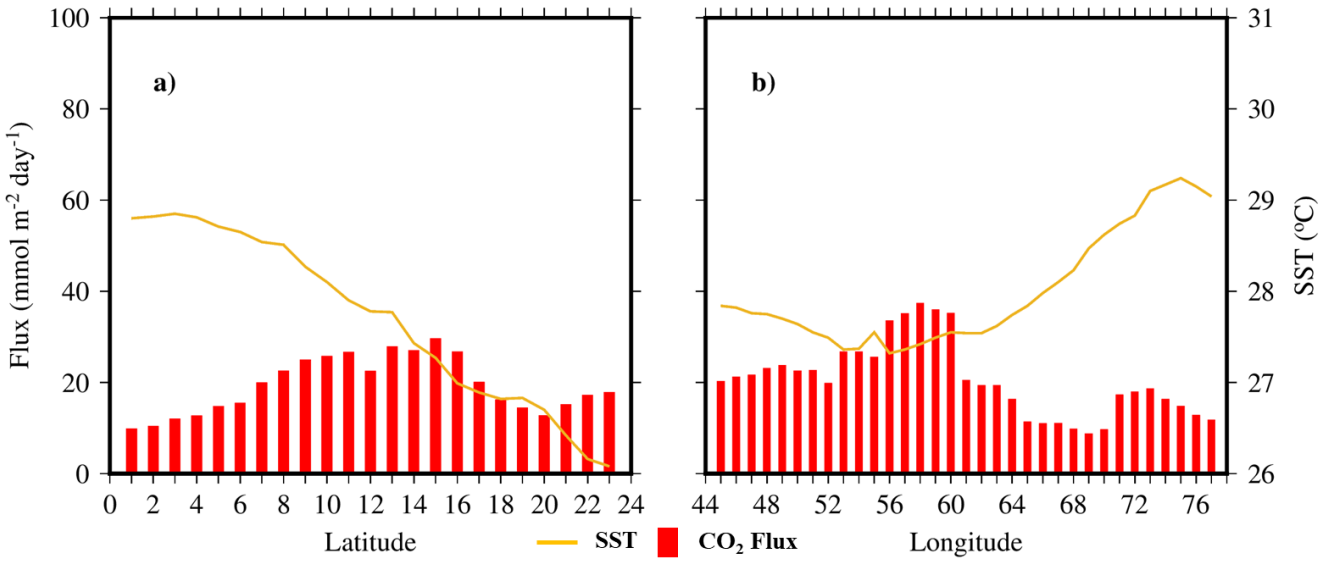

Figure.4.15 Spatial variations in winter fluxes and SST in the South-North and West-East directions over the Arabian Sea

Rao and Goswami (1988) reported that the primary and secondary peaks in SST values over the Arabian Sea were observed to be during the pre-monsoon and post-monsoon respectively. During both seasons, the maximum values were obtained over the low latitudes. The increased temperatures over the open ocean waters result in reduced CO_2 solubility, leading to enhanced fluxes; towards the north, the SST reduces while the bacterial respiration elevates the surface pCO_2, maintaining the outfluxes (Sarma et al., 1998; Sarma et al, 2000; Sarma, 2003). During monsoon, the open ocean upwelling brings the cold subsurface waters rich in CO_2 to the surface, thus enhancing the outfluxes; this could have resulted in the high fluxes in the mid-latitudes associated with low SSTs (Madhupratap et al., 1996; Sarma et al., 2000; Sarma, 2003). During post-monsoon season, western coastal areas show increased fluxes while a lowering in SST values could be due to localised upwelling processes. Towards the north, the increased SSTs establish a thermal stratification at the surface, reducing the fluxes (Sarma et al., 2000; Takahashi, 2002). Low SSTs over the western and northern Arabian Sea cause a convective mixing of the surface waters, leading to enhanced fluxes over these regions (Madhupratap et al., 1996; Sarma et al., 2000; Sarma, 2003).

BoB SST values during pre-monsoon season exhibited a strong S-N gradient (Figure.4.16-a); the values peaked (30.8 °C) over the southern latitudes, reducing towards the north (28.4 °C). The W-E distribution (Figure.4.16-b) showed maximum values reaching towards the western (30.5

°C) and eastern (30.7 °C) longitudes, dipping over the central BoB (29.7 °C). BoB fluxes followed the same spatial trend as SST, both in the S-N and W-E directions.

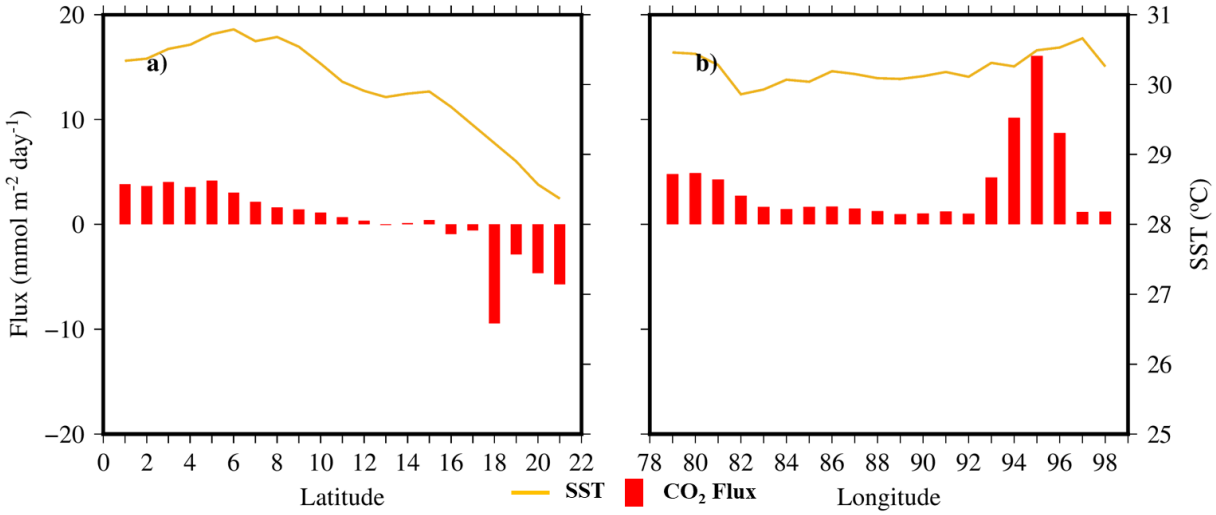

Figure.4.16 Spatial variations in pre-monsoon fluxes and SST in the South-North and West-East directions over the Bay of Bengal

Monsoon SST values tend to peak towards south and north (Figure.4.17-a) and west and east, while dropping over the central BoB (Figure.4.17-b). Southern and northern maximum reached around 30 °C, with the lowest value of 28.7 °C obtained over the mid-latitudes. The western and eastern SST values peaked around 29.7 °C and 30 °C, respectively, while the central SST values ranged from 29.2 to 29.6 °C. The S-N distribution showed an increased SST trend over the south, with high influx values, whereas a drop in SSTs over the mid-latitudes with enhanced outfluxes. In the W-E distribution, the high western influxes are accompanied by elevated SSTs, while eastern fluxes or SST values exhibit no specific trend.

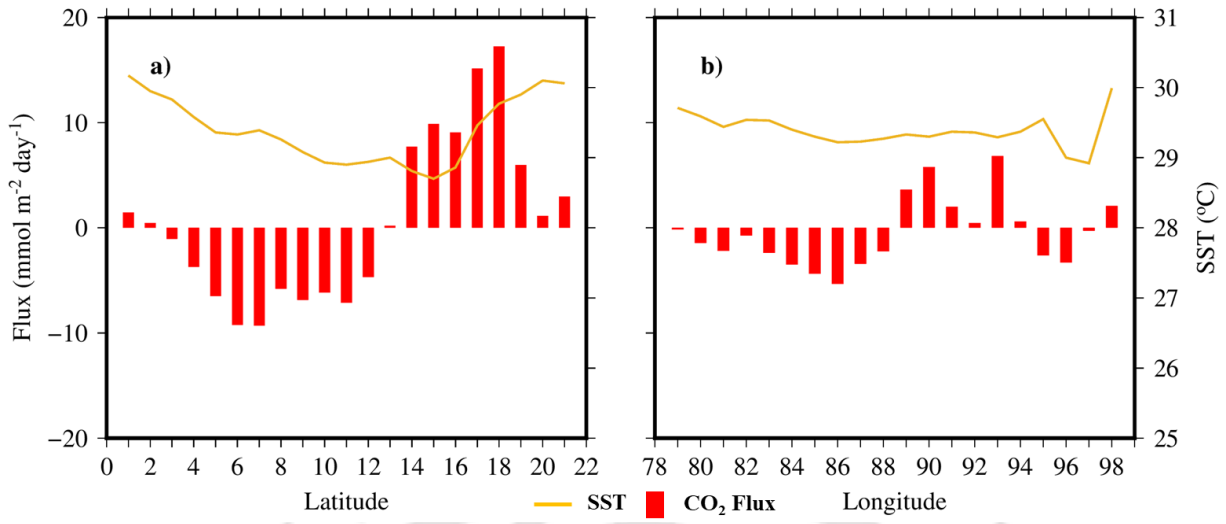

Figure.4.17 Spatial variations in monsoon fluxes and SST in the South-North and West-East directions over the Bay of Bengal

Post-monsoon values were high over the southern (29.85 °C), central (29.8 °C), and northern (29.9 °C) BoB, while lowest values (29 °C) obtained over the southern central latitudes (Figure.4.18-a). In the W-E direction (Figure.4.18-b), SST values reached a maximum of 30 °C towards the west and east, decreasing over the central (29.3 °C) BoB waters. Post-monsoon SSTs were observed to have a low spatial variation, both in the S-N and W-E directions. Both SST and flux values followed a similar spatial trend.

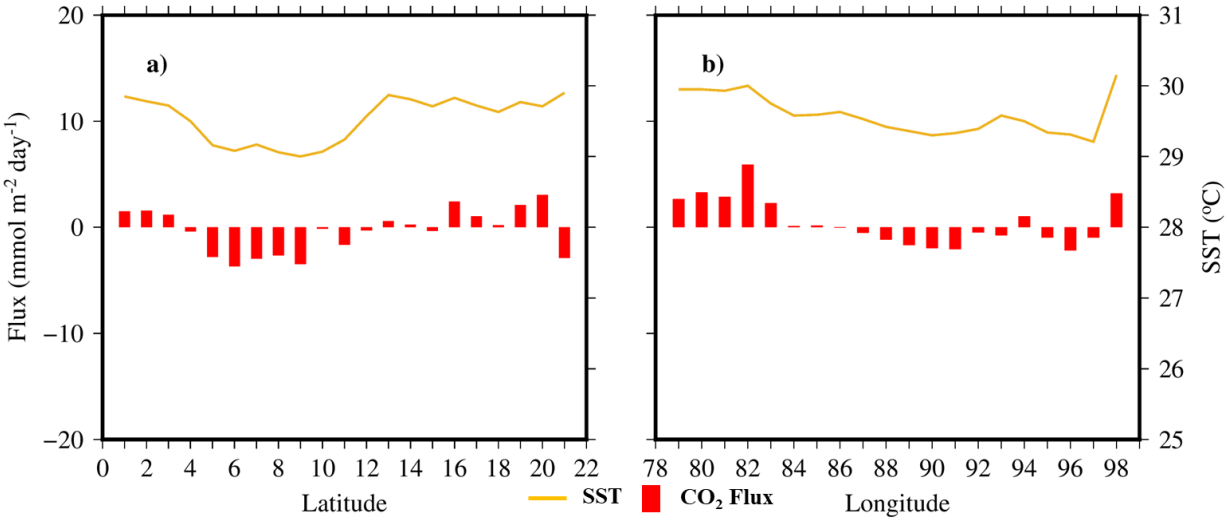

Figure.4.18 Spatial variations in post monsoon fluxes and SST in the South-North and West-East directions over the Bay of Bengal

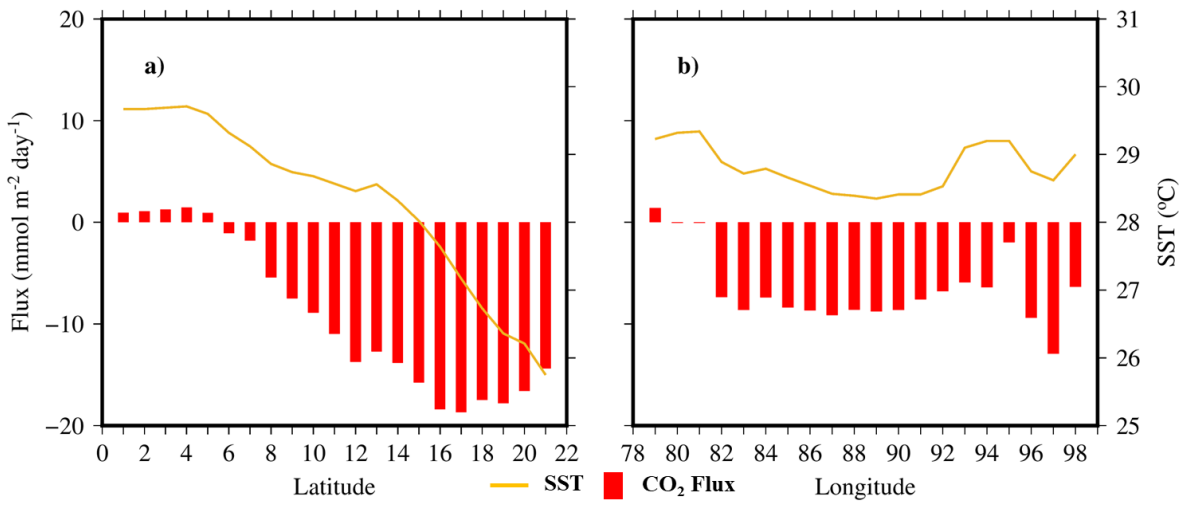

Figure.4.19 Spatial variations in winter fluxes and SST in the South-North and West-East directions over the Bay of Bengal

During the winter season, southern SSTs (29.6 °C) showed little to no variation while decreasing over the central to northern (25.8 °C) latitudes (Figure.4.19-a). The W-E distribution (Figure.4.19-b) showed the flux and SST values following a similar trend, with SSTs dropping (28.4 °C) over the central BoB, slightly increasing towards the west (29.3 °C) and east (29.2 °C).

The high insolation received during the pre-monsoon increases the SST values of the southern BoB, reducing the CO_2 flux solubility, thus enhancing the surface pCO_2, while the river influx in the north reduces the surface SSTs, while the salinity gradient establishes a surface stratification, thus lowering the northern fluxes (Behara and Vinayachandran, 2016; Shanthi et al., 2016). The enhanced monsoon fresh water input through river influx and precipitation extends the surface stratification towards the central BoB, lowering the SST values and fluxes, while north-west and north-east coastal wind action disturb the stratification, releasing the subsurface CO_2 towards the surface. Post-monsoon increases in SSTs over the south, central and northern BoB, along with the lowered intensity of the freshwater influx and the southward transport of low pCO_2 waters, enhances the temperatures and fluxes towards the north-west and southern waters. Winter monsoon-induced fresh water influx re-establishes the surface stratification in the north, accompanied by reduced winter SSTs, making this region act as a CO_2 sink while southern waters act as a weak source, mainly due to the lessening of the stratification southward, as well as the Ekman transport induced upwelling along the Sri Lanka coast (Vinayachandran et al., 1996; McCreary et al., 2009).

4.4 Summary and conclusion

High levels of primary production and sea-to-air CO_2 fluxes were observed during winter and monsoon seasons over the coastal waters of the Arabian Sea and BoB. With a decrease in production towards the open ocean region in the south, the CO_2 outgassing is also observed to be dropping. Even though marine production involves the utilization of dissolved CO_2, which contributes to the CO_2 partial pressure of sea water, monsoonal upwelling and winter convective mixing bring the CO_2 enriched subsurface waters and nutrients, thus enhancing the fluxes and productivity simultaneously. High production leads to high respiration rates and enhanced CO_2 levels in the surface waters.

The decreasing trend in productivity during the pre and post-monsoon seasons due to the absence of upwelling was also reflected in the fluxes. Warming of the waters will induce surface stratification and reduce the vertical mixing in the Arabian Sea, while the salinity gradient by the fresh water influx established surface stratification in BoB. Southern waters in BoB showed low productivity levels in post-monsoon while the fluxes have dropped considerably over the northern BoB during winter.

The increased summer insolation has elevated the SSTs over the open ocean waters in both the Arabian Sea and BoB, eventually lowering the CO_2 solubility, thus enhancing the fluxes. While winter and monsoon convective mixing and upwelling increase the outfluxes over the Arabian Sea, high fresh water input during summer and winter monsoons escalate the air-sea CO_2 influxes over the central to southern BoB and north-to-central BoB waters, respectively. With the introduction of a thermal or saline stratification, a layering of the water column occurs where the increased stability of the upper water layer hinders the gaseous as well as nutrient exchange from the subsurface layers to the surface. This process lowers the CO_2 outflux and productivity during pre-monsoon season in the Arabian Sea and monsoon season over the Bay of Bengal, towards the coastal waters. With a change in this stability of the upper water layer, due to change in temperature or salinity, or due to surface disturbances induced by wind driven ocean circulation, re-establishing of the water column mixing will result, leading to enhanced CO_2 outflux, along with the upwelling of nutrients, and increased productivity.

5

A regional model for basin-scale sea water pCO_2 estimation from in situ measurements

5.1 Introduction

The gradient of the partial pressures of CO_2 in the air and water interface is the primary factor in determining the CO_2 flux direction. The spatial and seasonal fluctuations are very large in the sea water CO_2 partial pressure as compared to the atmospheric pCO_2. The global range of sea water pCO_2 is around 150- 550 µatm which is around 60% below and above the atmospheric pCO_2. The CO_2 partial pressures in sea water are primarily regulated by the temperature changes and variations in the CO_2 concentrations in water due to biological activities. Other factors that control the sea water partial pressure include sea surface salinity, nutrient concentrations and mixed layer depth (Takahashi et al, 2002; Padhy et al, 2016).

Empirical models for pCO_2 using in situ observations of sea surface parameters such as SST, Chl-a, and salinity were derived for the northern Pacific Ocean (Stephens et al., 1995; Ono et al., 2004; Sarma et al., 2006), where the algorithm using single parameter i.e., SST showed a comparatively high RMSE of 26 µatm while a three-variable algorithm including SST, SSS and Chl-a provided a better RMSE value in the range 17-23 µatm. Cosca et al (2003) included nutrients along with SST, SSS, and Chl-a resulting in an enhanced accuracy of pCO_2 model results (12 µatm) in the Pacific Ocean. The single parameter algorithm developed for Greenland by Hood and Merlivat (1999) using SST yielded an RMSE value range of 7-10 µatm and the two-variable model from SST and Chl-a by Zhu et al (2009) over the northern South China Sea, Zui et al (2012) over the Huanghai and Bohai Sea and Padhy et al (2016) in the Hooghly Estuary provided 4.6 µatm, 13.45 µatm, and 18 µatm accuracy respectively. Jang et al (2017) used a wide range of parameters such as DIC, SST, salinity, mixed layer depth, and Chl-a over the East Sea, Japan to provide an accuracy of 4.6 µatm. pCO_2 model for the global oceans was developed by Liu and Xie (2014) using SST, Salinity, Chl-a with an accuracy of 16 µatm. All these studies suggest that for different oceanic regions, the defining

or controlling factors of the sea surface pCO_2 can vary, depending on the geographical and climatological setup of these regions.

5.2 Data and methods

5.2.1 Multiple Regression

Ship measurements of SST, SSS and pCO_2 for Arabian Sea and BoB were extracted from Global Ocean Surface Water Partial Pressure of CO_2 Database prepared using the measurements taken during 1957-2018 period (Takahashi et al., 2019) and provided by the National Centers for Environmental Information, NOAA. Multiple regression method was applied to derive the relationship between the predictor variables SST and SSS and the criterion variable sea water pCO_2. As the initial step, linear regression method was used, i.e., each of the predictor variables were regressed with the pCO_2 to determine the individual significance of each on the pCO_2 variability. The model assumes a linear relationship between the dependent and independent variable. The model was again improved by applying the polynomial regression with each parameter. Further, multiple linear regression (MLR) was used to understand the combined effect of the predictor variables on the criterion variable which assumes linear relation of SST and SSS on pCO_2. The model can be expressed as equation 5.1 (Pedhazur, 1982; Adamowski et al, 2012).

$$Y= a+\beta_1*i \ +\ldots\ldots\ldots\ldots+ \ \beta_k*k \qquad (5.1)$$

where, a is the intercept, β is the slope, and k is the number of observations.

This is followed by the implementation of multiple polynomial regression (MPR) due to the complex non-linear trends of oceanographic variables; multiple polynomial regression is normally used for quick and accurate prediction of randomly occurring events (Ivakhnenko, 1970). The model can be expressed as equation 5.2.

$$Y= a+\beta_1*i+ \beta_2*j+\beta_3*i^2 +\beta_4*j^2 +\ldots\ldots\ldots\ldots..+\beta_k*i*j \qquad (5.2)$$

where, a is the intercept, β is the slope, and k is the number of observations.

The models for each basin were trained and validated using the same data series; a total of well-distributed 60,000 samples were used as training points and 3000 samples as testing points for the Arabian Sea whereas, 3000 training points and 600 testing points were used for BoB and a second order polynomial function was applied.

5.2.2 Random Forest

The Random Forest Regressor (RFR) is a prediction model that uses a collection of randomized base regression trees to make aggregated regression estimates. The random forest (RF) method assesses the relative importance of the independent variables on the variations of the criterion variable and can detect the non-linear relationships between them. The model calculates estimations by aggregating the individual predictions of each tree, with EΘ[.] representing the expectation with respect to the random parameter, given X i.e., input features matrix. The RFR combines these random trees to form the aggregated regression estimate, as given in equation 5.3 by Bikia et al. (2021).

$$\bar{r}_n(X) = E\Theta[r_n(X, \Theta)] \quad (5.3)$$

where Θ = [Θ1, . . ., ΘN] are independent and identically distributed (i.i.d.) random variables outputs of each tree. To grow the trees, bootstrapping is applied to the training data to create a regression tree for each bootstrap sample, with estimators randomly sampled and the best split chosen at each node. This formal structure allows for accurate and reliable predictions in various applications. This method is capable of handling large predictor datasets and is insensitive to the outliers in such data sets. It is also flexible in order to fitting multi-period datasets (Bikia et al., 2021; Bolotin et al., 2022). It is a machine learning-based technique that utilizes bootstrapped sample of the data to build regression trees which are further combined to produce model-averaged fit. Correlation between the trees is less in this technique since the number of available random predictors at each node is kept small, thus reducing the error rate (Leach et al., 2018). The RF model structure can be represented as Figure.5.1.

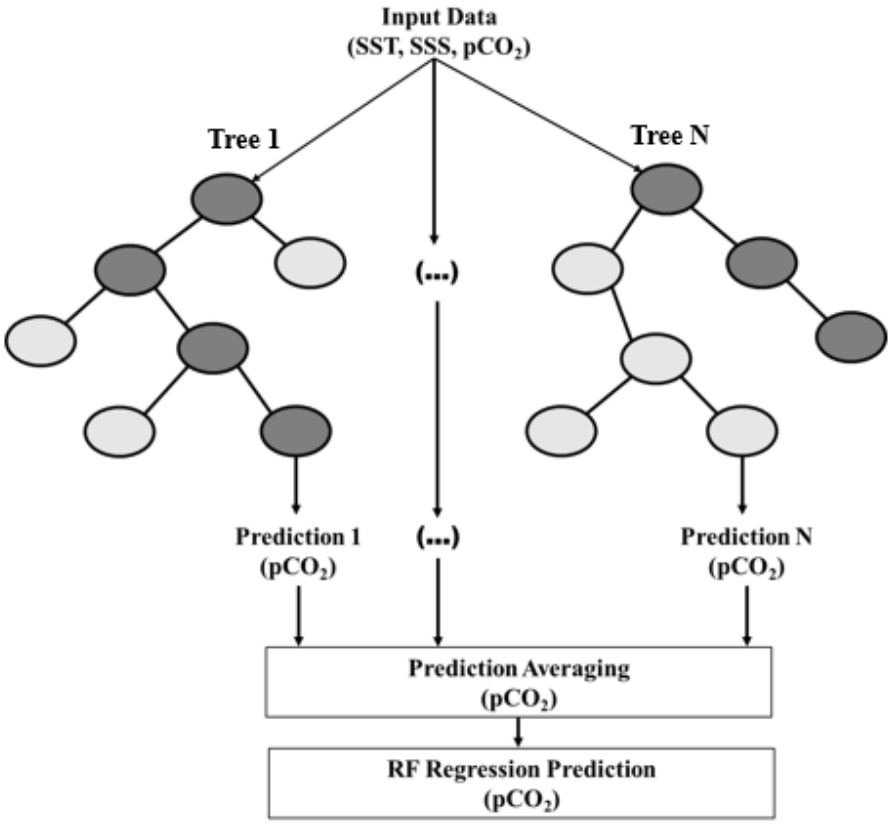

Figure.5.1 Random Forest Model Structure

The dataset for each basin was divided into 70% training and 30% testing samples, and the random forest regressor function is applied to each basin training dataset. A total of 500 trees were constructed for each training sample with pCO_2 as the predictand variable, and SST and SSS as predictors; the number of the trees was selected through repeated trial-and-error. The fitted model was validated using the testing samples for both basins. The details of the parameters used in the RF model are given in Table 5.1.

Table 5.1. Model Parameter Details for the Random Forest Regression

RF Model Parameters	
Number of Estimators	500
Loss Function	Mean Squared Error
Tree Depth	30
Maximum Features	Square Root
Bootstrap	True

5.3 Results

5.3.1 Multiple Regression

The individual linear regression of SST and SSS with pCO_2 gave a coefficient of determination value of 0.26 for SST and 0.12 for SSS over the Arabian Sea, whereas, BoB obtained slightly better R^2 values of 0.49 for SST and 0.3 for SSS. Applying the polynomial function of order 2 provided slightly better values for Arabian Sea SST i.e., 0.3 while the coefficient of determination value for SSS remained the same (R^2=0.12). However, the BoB model produced significantly improved results with an R^2 value of 0.6 for SST and 0.38 for SSS. This must be due to the better representation of sea surface pCO_2 distribution of BoB in relation to SST and SSS as compared to the Arabian Sea. The application of multiple linear regression techniques on these datasets yielded an R^2 value of 0.4 for the Arabian Sea and 0.7 for BoB. These models were further improved through the implementation of a multiple polynomial regression model of order 2. The results of the final model fitting showed a coefficient of determination value of 0.70 for the Arabian Sea and 0.76 for BoB. Validation of the fitted model using the testing samples obtained R^2= 78 and RMSE= 10.7 µatm for Arabian Sea (Figure.5.2) and R^2= 0.79 and RMSE= 6 µatm for BoB (Figure.5.3). The model for Arabian Sea and BoB sea water pCO_2 can be expressed as equation 5.4 and 5.5 respectively.

$$pCO_{2(AS)} = 22490-713.2\ SST-678.1SSS+3.759SST^2+3.959SSS^2+14.07 \quad (5.4)$$

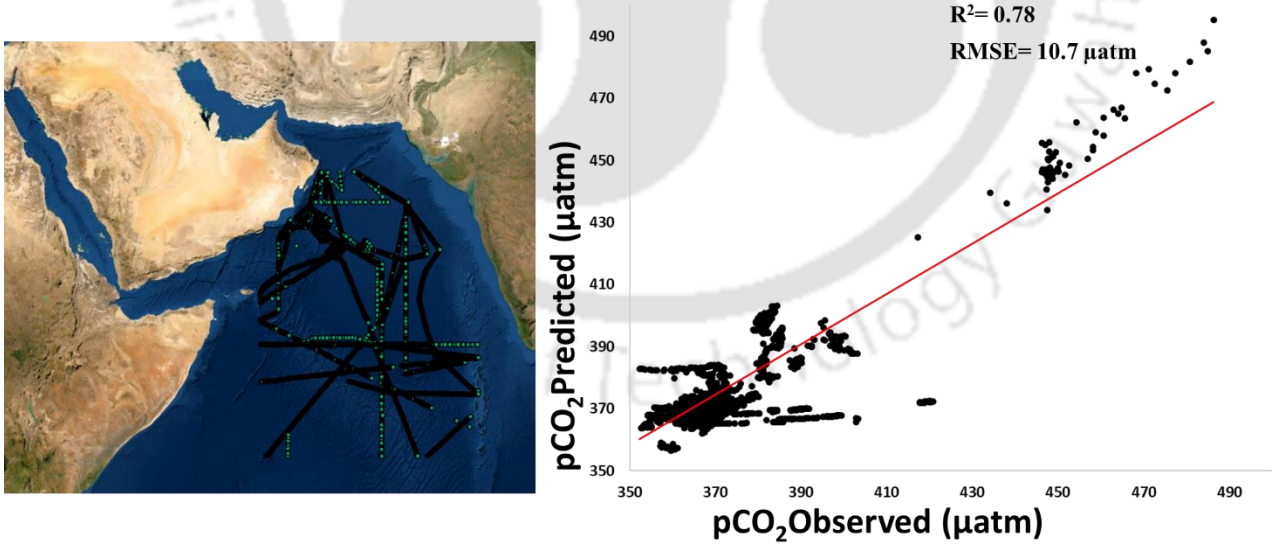

Figure.5.2 pCO_2 model (MPR) validation-Arabian Sea

$$pCO_{2(BoB)} = -291.229+17.4199\ SST+6.4648SSS-1.2899SST^2-0.8243SSS^2+2.0 \quad (5.5)$$

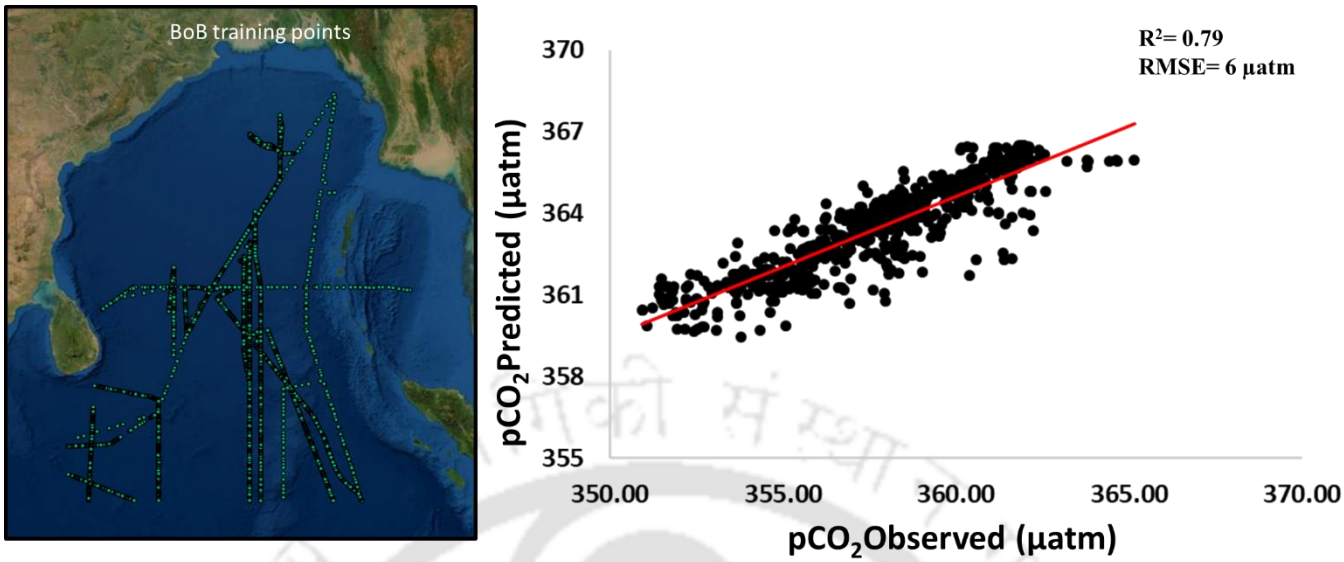

Figure.5.3 pCO_2 model (MPR) validation- Bay of Bengal

5.3.2 Random Forest

The pCO_2 model fitting using the multiple regression techniques was further improved using the machine learning-based random forest. Results suggested a far better representation of the predictor-predictand relationship by the RF method. Model validation provided a coefficient of determination value of 0.98 for both the basins, while RMSE values of 0.05 µatm and 0.06 µatm for the Arabian Sea (Figure.5.4) and BoB (Figure.5.5) respectively.

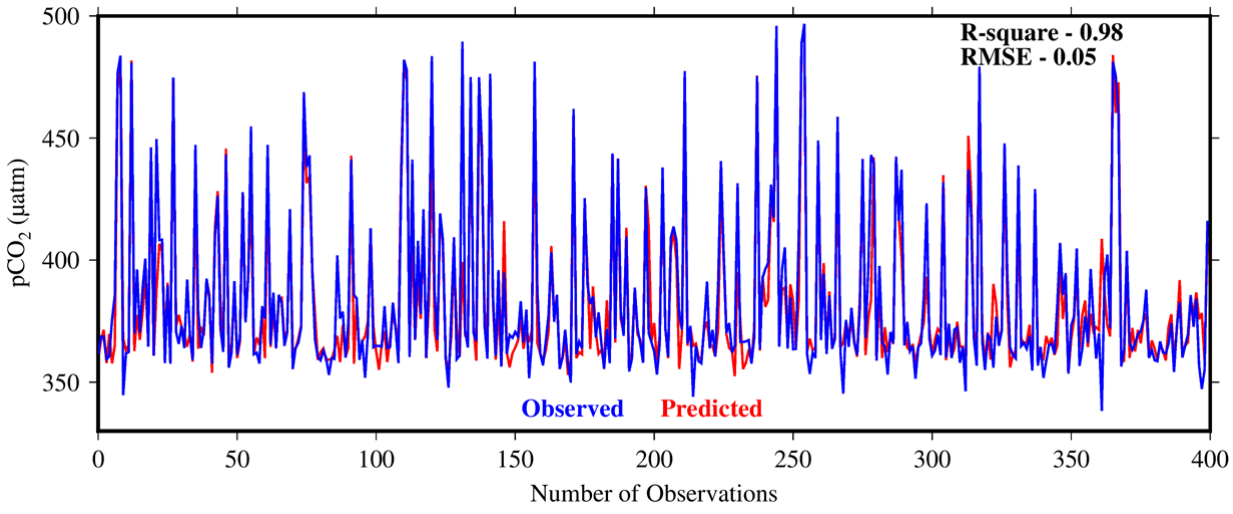

Figure.5.4 pCO_2 model (RF) validation-Arabian Sea

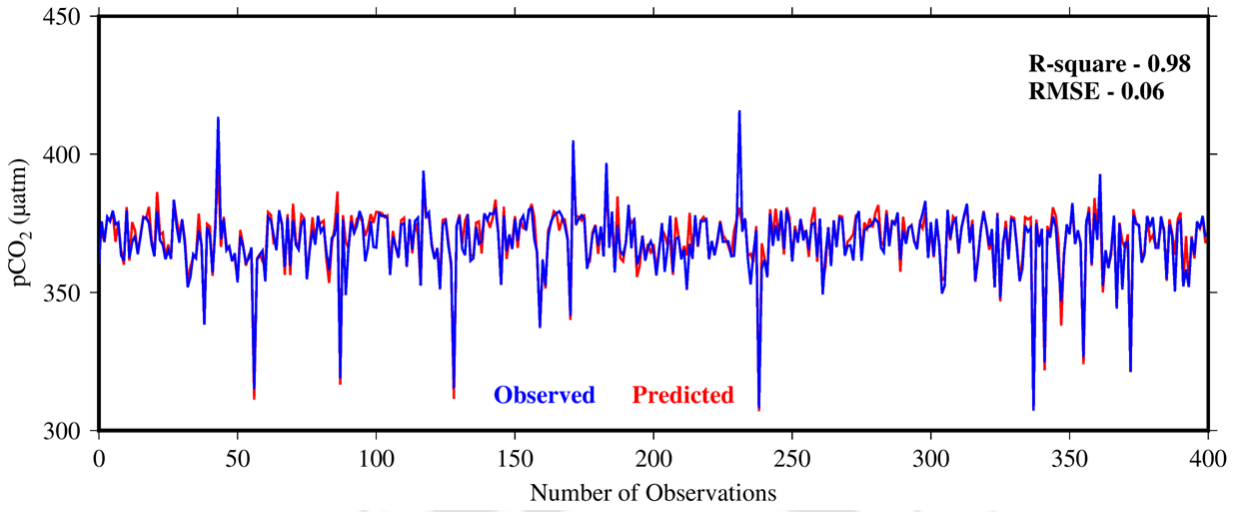

Figure.5.5 pCO_2 model (RF) validation- Bay of Bengal

The controls of thermal and saline characteristics of the sea water on the sea surface pCO_2 distribution were observed to be better represented by the RF function. This function can be effectively used to predict the sea water pCO_2 using satellite or climatological datasets of SST and SSS over the western and eastern basins of the Indian Ocean.

5.4 Summary and Conclusions

Sea water pCO_2 is one of the most significant factors governing the exchange of CO_2 gas at the marine-atmosphere interface. Observations on sea water pCO_2 over global oceanic regions were made through field surveys and sampling, however, the spatial and temporal resolution of the data collected is very low, considering the vastness of the global ocean. The key factors governing the pCO_2 variations change with geographic location and climatic conditions. The two sub-basins of the Indian Ocean exhibit varying nature of surface CO_2 dynamics since the Arabian Sea is a perennial source while BoB acts as a CO_2 sink. This contrast leads to the development of separate algorithms to derive the sea water pCO_2 for the Arabian Sea and BoB. Ship observations of SST, SSS, and pCO_2 were used to derive the relationship of thermal and saline variations on the partial pressure distribution. The multiple polynomial regression method provided a model fit result with moderate accuracy for both basins, which was further improved using the random forest regression method. The relationship of the predictor variables SST and SSS with the sea surface pCO_2 is better represented by the random forest function, providing better accuracy for both basins, probably due to the non-linear nature of the pCO_2 variation with seasonal as well as spatial trends in SST and SSS.

6

Impacts of nutrient dynamics, sea surface temperature, and wind speed anomalies on the air-sea exchange of CO_2 over the Indian Ocean

6.1 Introduction

River discharge is one of the primary sources of dissolved inorganic nutrients (DIN), such as nitrate, phosphate, and silicate, in the marine environment. Coastal oceans also receive nutrients through aerosol deposition, coastal upwelling, and eddies. These nutrient supplies enrich marine primary production to a great extent. Other than these natural sources, anthropogenic activities, such as extensive use of fertilizers in agricultural fields, plantation of leguminous plants, and domestic and industrial sewage contribute to the nutrient supply in coastal systems. In the case of the coastal Indian Ocean, the Bay of Bengal receives significantly higher nutrient input annually, as compared to the Arabian Sea. This is attributed to the fact that the catchment regions of BoB obtain about 78% of the fertilizer application (Krishna et al, 2016). The major nutrient input in the Arabian Sea is the eolian dust storms from the western land masses (Ramaswamy and Nair, 1994).

Particle fluxes to the BoB are controlled by the seasonal variability of river discharge and marine biogenic production; the maximum particle and freshwater flux occur during the southwest monsoon as reported by Ittekkot et al (1991). Particle fluxes in the Arabian Sea are caused by wind mixing processes and in BoB by river discharge. High fresh water and nutrient input were observed in BoB in SW monsoon. Annual fluxes are higher in BoB compared to the Arabian Sea (Ramaswami & Nair, 1994). High biogenic and lithogenic particle fluxes were observed during the NE and SW monsoon season in the Bay of Bengal (Ramaswami et al., 1997). Wind-driven coastal upwelling and river discharge during SW monsoon increase phytoplankton biomass while productivity is reduced by light limitation in the Bay of Bengal (Gomes et al., 2000). Analysis of the nutrient dynamics in the Arabian Sea and BoB was carried out to understand the role of the nutrient influx and their distribution in the spatial and seasonal variations in basin primary productivity and fluxes.

The influence of the SST and windspeed anomalies on the sea water pCO_2 distribution was also analyzed to understand the impact of such events on the air-sea exchange of CO_2 gas. With an increase in SST, there will be a thermal stratification of the surface water layer which will hinder the outflux of CO_2, whereas, a lowering of the SST can lead to densification of the surface waters, leading to convective mixing and enhanced CO_2 outflux. The increased SST can also result in decreased CO_2 solubility, thus a reduction in the air-sea influx. These scenarios can be affected by the sea surface windspeed variation. An increased wind action can cause the turbulence of the surface water layer, thus enabling the upwelling process, hence manifesting an increased CO_2 outflux (Madhupratap et al., 1996; Takahashi et al., 2002; Sarma, 2003).

6.2 Data and methods

Data for nitrate, phosphate, and silicate were procured from the National Centers for Environmental Information (NOAA) World Ocean Atlas 2018 database (WOA18). Monthly data of spatial resolution 1° for each of the nutrient parameters has been downloaded and averaged to get the seasonal datasets. The WOA18 objectively analyzed climatology data consists of the variable mean fields at standard depth levels; since the nutrient availability at the top depth levels is almost zero, the data from the depth of 600m, i.e., the layer of maximum nutrient content (Rozanov and Bykova, 1967), was extracted for analyzing the basin-wide nutrient distribution. Each of the nutrient parameters was analyzed for its spatial and seasonal variation, with respect to the ocean's primary productivity and flux distribution.

The European Center for Medium-Range Weather Forecast Reanalysis (ECMRWF) ERA-5 windspeed and SST data sets of spatial resolution 25 km were procured for 30 years (1980-2012) and anomaly maps were derived from a consecutive overlapping 3-month period. The peak warm and cold events were identified from the anomaly maps using the Oceanic Nino Index concept i.e., SST values higher than 0.5 °C denote a warm event and lower than -0.5 °C denote a cold event. The anomaly data were plotted against the CO_2 partial pressure data (1980-2012) from the Coupled Model Intercomparison Project (CMIP) 5 historical database to analyze the significant changes in partial pressure with respect to these events. This specific time period of 1980-2012 has been chosen in order to match with that of the historical data period of the CMIP5 data.

6.3 Results

6.3.1 Analysis of the nutrient dynamics with respect to primary productivity and CO_2 fluxes

6.3.1.1 Nitrate

Maximum nutrient concentrations (30.5-32 µM) can be observed over the western and open ocean waters of the Arabian Sea in all the seasons (Figure.6.1). This must be due to the input from the aeolian deposition from the Oman region (Srinivas and Sarin, 2013). The pre-monsoon concentrations are comparatively low (24-29 µM) over the north-eastern coast, followed by the post-monsoon (25-29 µM). While the nutrient is getting replenished during the south-west and north-east monsoons through river influx in the north and eastern parts, the inter-monsoon seasons face a depletion due to the high productivity during the monsoon period due to upwelling and winter convective mixing. Also, the presence of denitrifying cyanobacteria is another major factor in the lowering of subsurface dissolved nitrate levels (Bange et al., 2005). Southern concentrations were observed to be almost unfluctuating due to the low productivity and absence of the upwelling process.

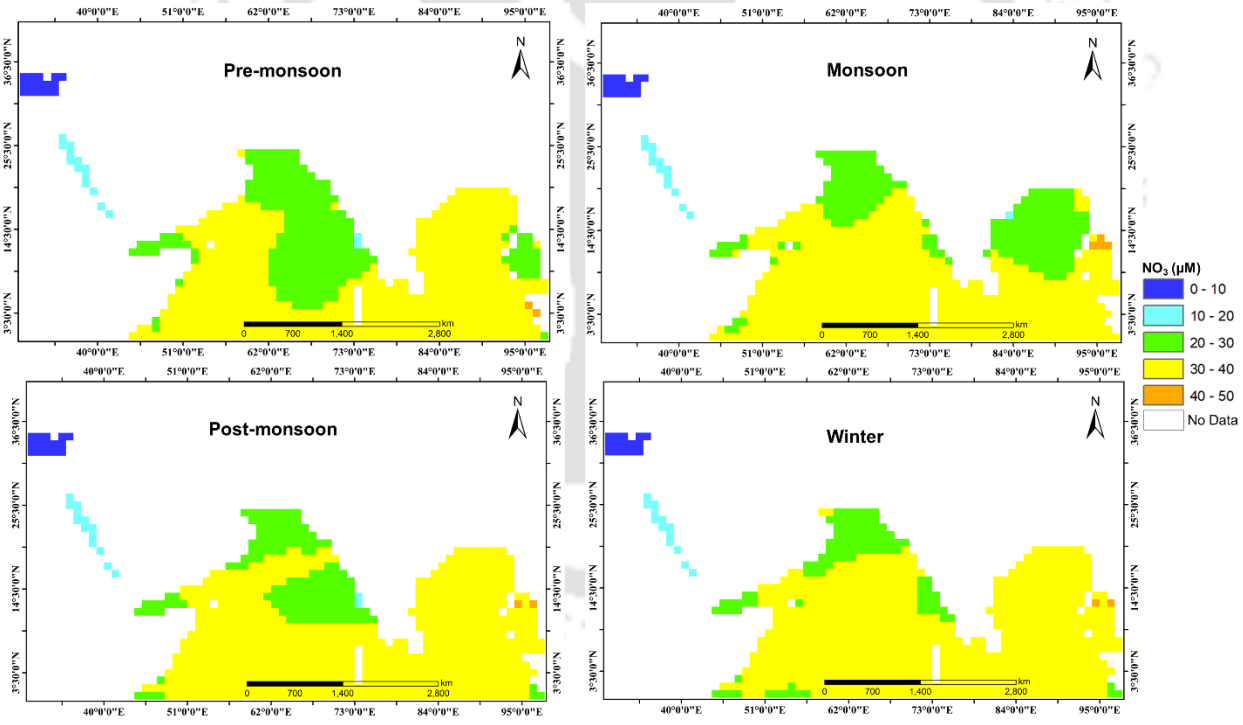

Figure.6.1 Spatio-temporal distribution of Nitrate

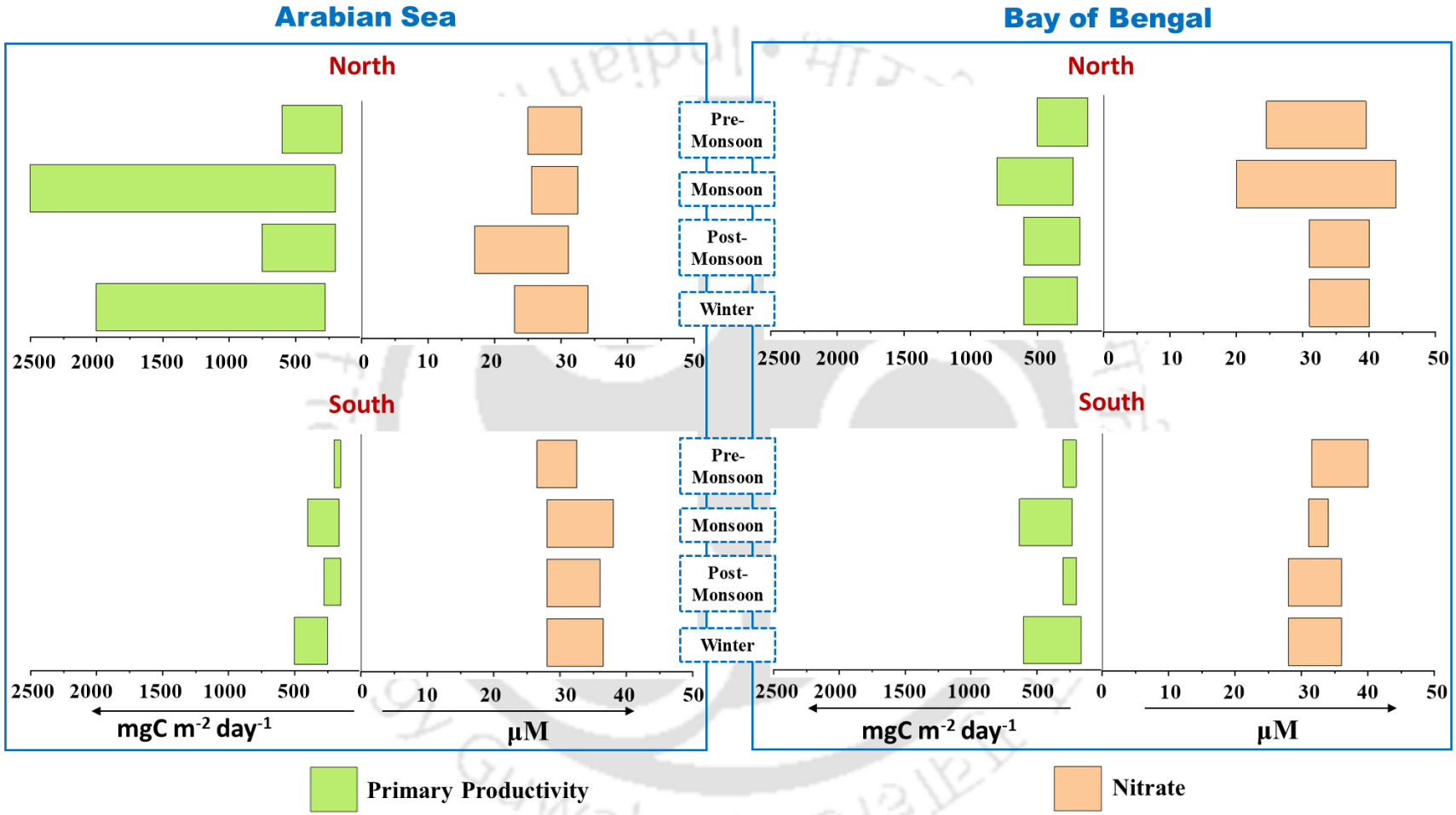

Figure.6.2 Nitrate Distribution Vs. Productivity

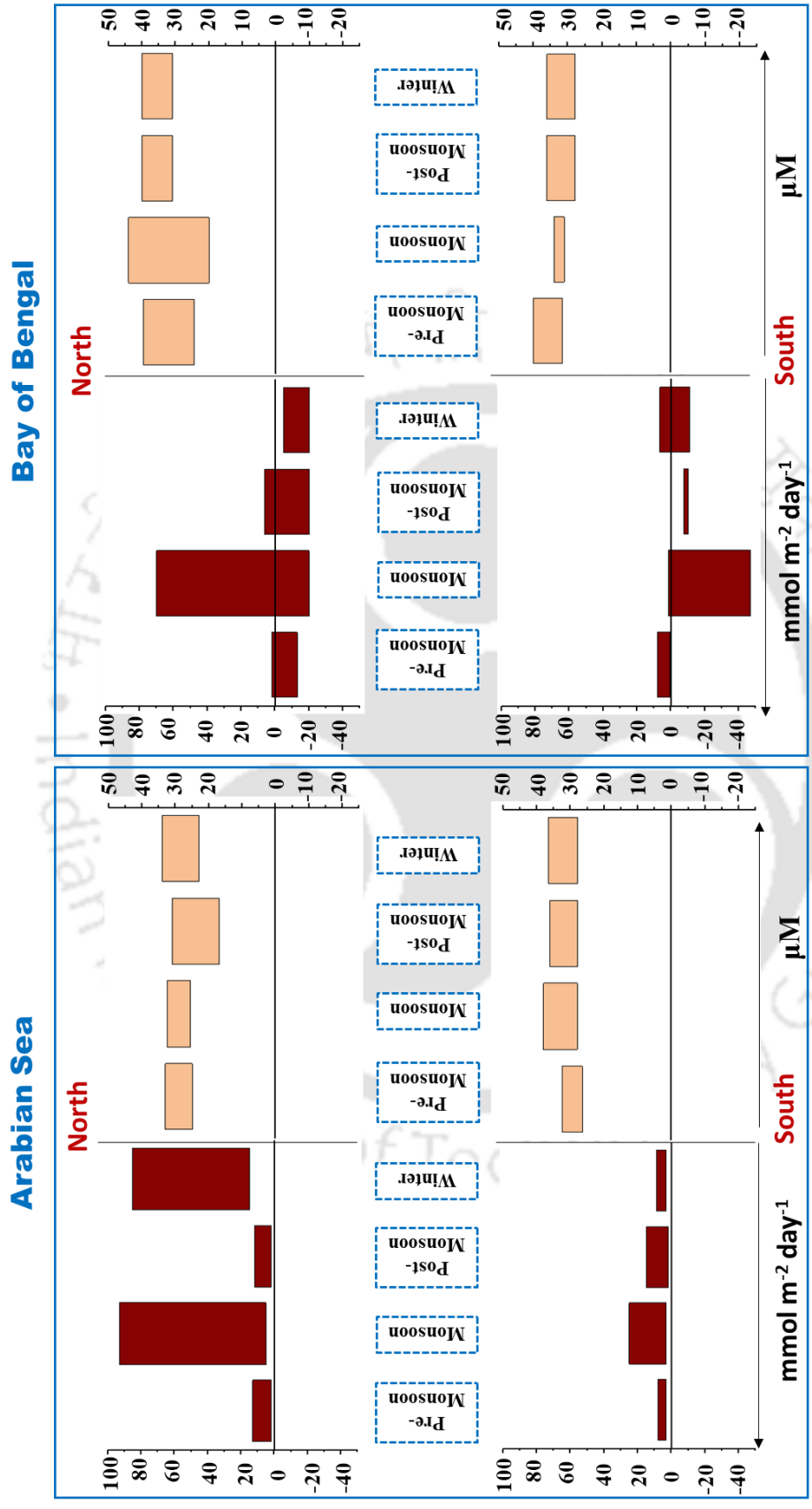

Figure.6.3 Nitrate Distribution Vs. CO_2 Flux

BoB showed high nitrate concentrations (32-40 µM) in the south during all seasons and in the north except in monsoon season (Figure.6.1). The relatively high productivity along with the monsoon currents which bring the northern influx of nutrients towards the southern part could be the reason behind this reduction, while low productivity along with high nutrient input causes the comparatively high nutrient content in the south (Murtugudde and Busalacchi, 1999; Vinayachandran et al., 2004).

The analysis of the nitrate distribution in relation to productivity and CO_2 fluxes is given in Figure.6.2 and Figure.6.3 respectively. The northern values of nitrate concentration show high variability in both basins as compared to the south, due to high primary productivity in the Arabian Sea and high nutrient influx in BoB. Monsoon nitrate values were observed to be low in the northern Arabian Sea than in the south, whereas the primary productivity showed the opposite trend. Intense upwelling during monsoon reduces the subsurface nitrates while increasing the surface CO_2 fluxes. Also, the input of the nutrient is mainly from the northern and eastern river influx and western aeolian deposition which is consumed by the high productivity rates during monsoon. This, along with the upwelling and bacterial denitrification causes the subsurface nitrate concentrations to reduce. Further, these processes lead to the depletion of the post-monsoon concentrations. Low southern fluxes and high nutrient concentrations could be associated with the absence of the upwelling process and reduced productivity. In BoB, the monsoon influx of nutrients in the north gets transported towards the south during the post-monsoon, with the weakening of the south-westerlies (Shetye et al., 1996), thus increasing the southern nitrate concentrations during the post-monsoon. Fluxes show a negative trend due to the river influx thus the BoB basin is characterized by high CO_2 uptake along with high nutrient concentrations. Only the northern monsoon fluxes showed high outflux values, which could be attributed to the open ocean upwelling, while the northern monsoon nitrate range also showed low values which could be due to the upwelling process lowering the subsurface concentrations. The winter nitrate values were comparable to that of the post-monsoon; although the winter productivity is high, the nutrient influx during winter monsoon can maintain the subsurface concentrations. CO_2 influx over the entire north during winter is also associated with the freshwater input, thus lowering the values. Reduced productivity in the pre-monsoon might have caused the high subsurface nitrates due to less consumption of the winter monsoon input.

6.3.1.2 Phosphate

High concentrations of phosphate (2.5-3 µM) were observed over the northern Arabian Sea in all the seasons (Figure.6.4). Monsoon and winter showed low levels of phosphate (1.7-2.4 µM) towards the south-west while high concentrations can be observed in the post-monsoon (2.5-2.7 µM) season. River influx might be the reason behind high concentrations in the northern and eastern parts, while dry depositions enhance the nutrient concentrations over the western and central Arabian Sea (Srinivas and Sarin, 2013). Also, the high productivity along the western and eastern coast of the Arabian Sea during winter could have depleted the subsurface nutrient levels, thus lowering the values in the pre-monsoon season (Sarma, 2003).

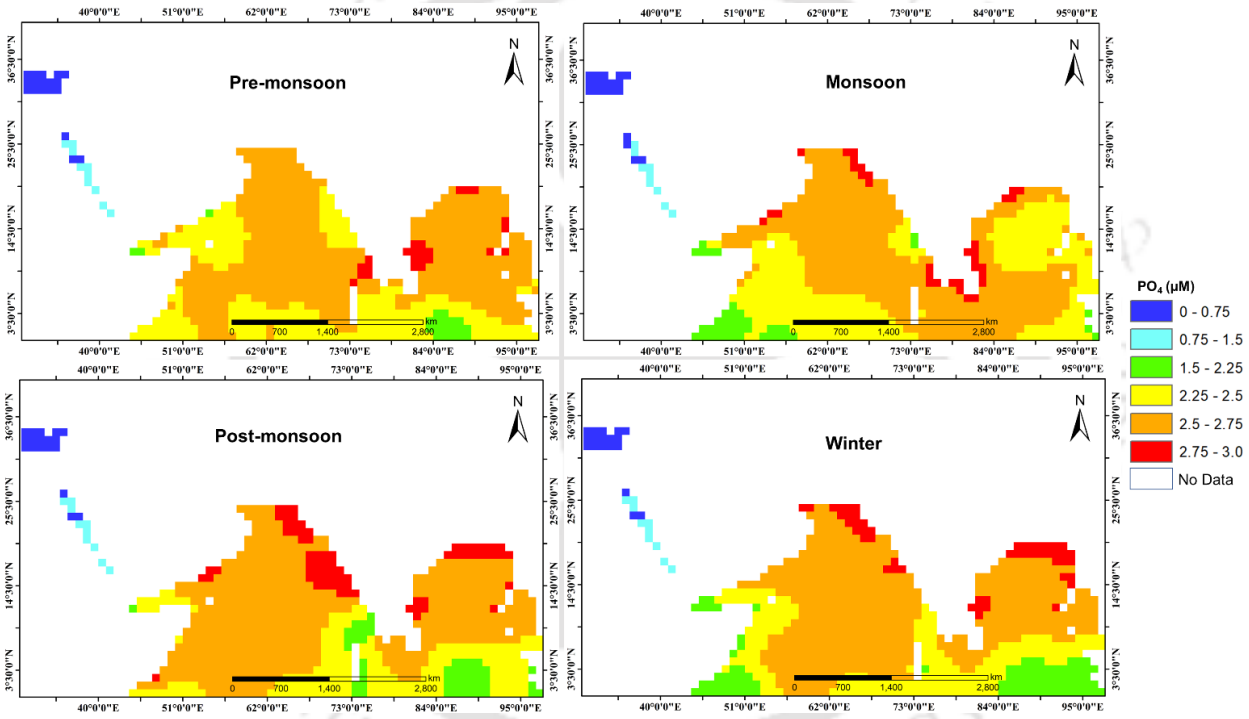

Figure.6.4 Spatio-temporal distribution of Phosphate

BoB showed high northern values (2.6-2.9 µM) during post-monsoon and winter followed by pre-monsoon, while monsoon values were reduced to 2.3-2.5 µM range over most of the northern part (Figure.6.4). The surface values are high during summer as compared to winter months in the northern Indian Ocean due to upwelling processes which can be due to the depletion of the monsoon phosphate levels (Conkright et al., 2000). The high river influx bringing nutrients during the monsoon season would result in the sinking and settling of the same to the subsurface, thus increasing the post-monsoon values.

Analysis of the phosphate distribution with respect to the productivity and CO_2 fluxes is given in Figure.6.5 and Figure.6.6 respectively. The replenishment of phosphate in the Indian Ocean is reported to be high during the summer months, which is clearly visible from the seasonal distribution in the north while, the southern concentrations vary with the ocean circulation (Conkright et al., 2000). The northern Arabian Sea observed similar trends in productivity and phosphate concentrations, as the monsoonal input and surface upwelling increased the phosphate availability for primary production while the dry deposition and river influx enhanced the nutrient concentrations. The decreasing trend in the nutrient in the inter-monsoon periods was also followed by the productivity in the northern basin. Maximum nutrient variation in the values can be visible for the monsoon and winter values in the northern Arabian Sea; this could be attributed to the high input as well as high consumption of the nutrient in the northern waters. The high flux values due to the upwelling and convective mixing can also be associated with the corresponding high nutrient consumption. BoB showed maximum nutrient concentration in the pre-monsoon and monsoon seasons with maximum productivity in the monsoon. This increased utilization of the monsoon nutrient concentration might have resulted in the lowering of the post-monsoon levels. The northern high fluxes in connection with the open ocean upwelling can also be associated with the high monsoon productivity and surface phosphate concentrations over the BoB. Since there is comparatively less nutrient input in the winter months, the winter productivity further reduced the phosphate concentrations.

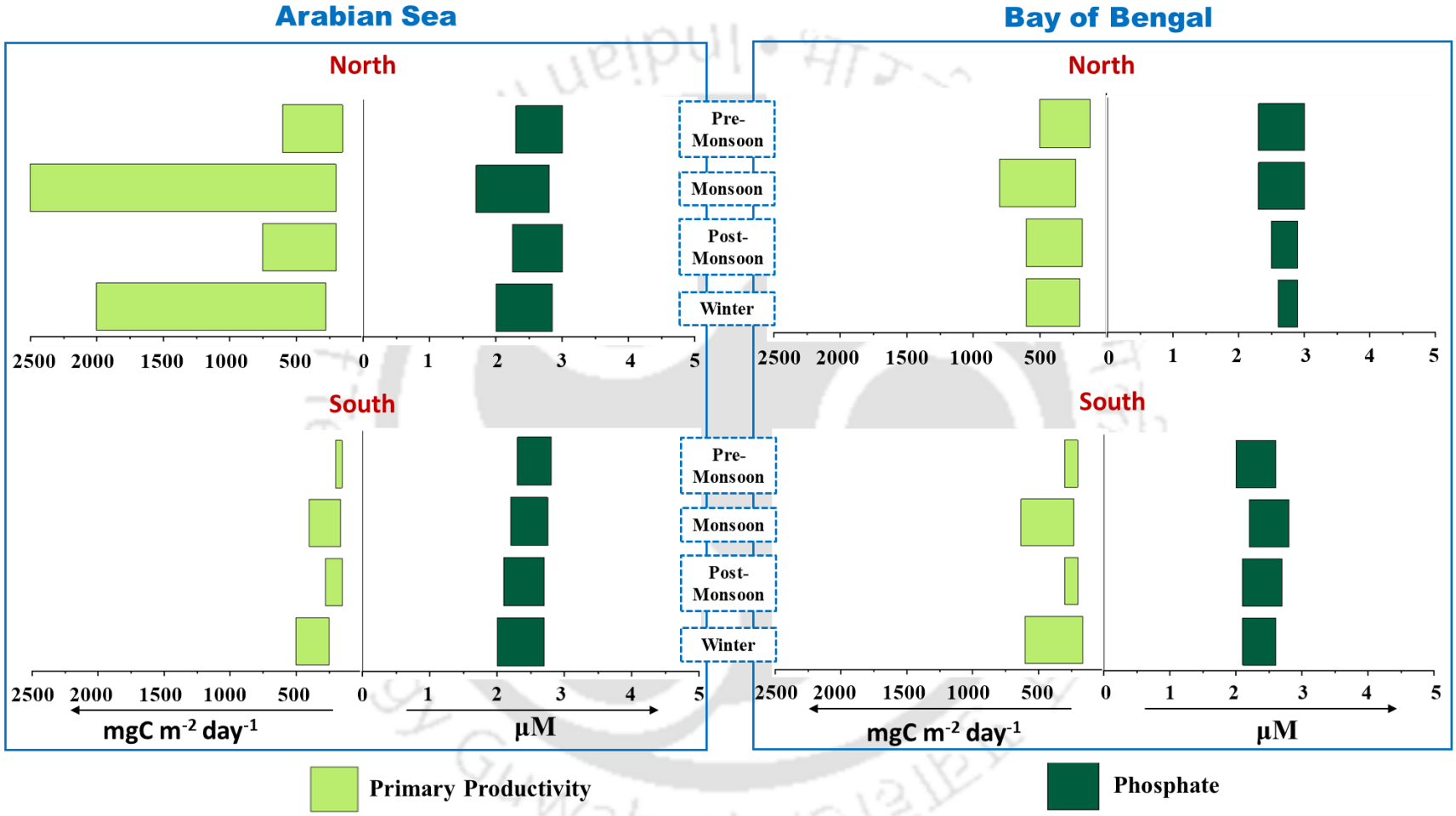

Figure.6.5 Phosphate Distribution Vs. Productivity

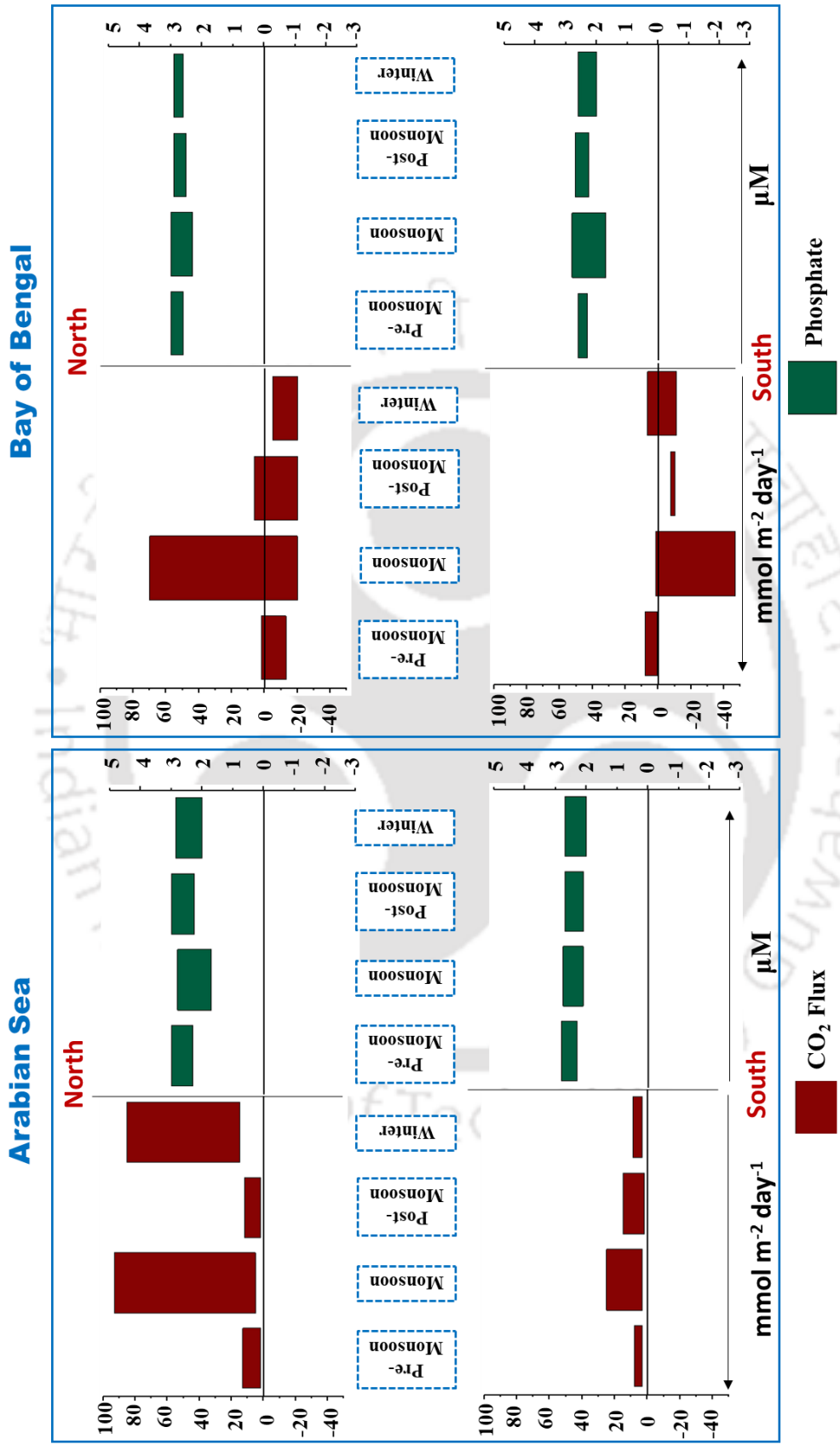

Figure.6.6 Phosphate Distribution Vs. CO_2 Flux

6.3.1.3 Silicate

In all seasons, BoB showed comparatively high silicate concentrations (50-65 µM) than the Arabian Sea, (Figure.6.7) due to the high influx of land-derived nutrients. Also, the utilization of the silicate by the diatoms leading to nutrient limitation in the Arabian Sea (Young and Kindle, 1994). In the Arabian Sea, the maximum concentrations (50-55 µM) can be observed towards the central part, while depletion over the coastal waters; this might be due to the coastal upwelling and associated high productivity. In BoB, northern concentrations were identified to be high (50-65 µM) while reducing towards the south. The silicate-utilizing phytoplankton species are mainly concentrated over the intense upwelling regions, hence their presence in the northern BoB, characterized mainly by the surface stratification would be low (Young and Kindle, 1994; Schiebel et al., 2004).

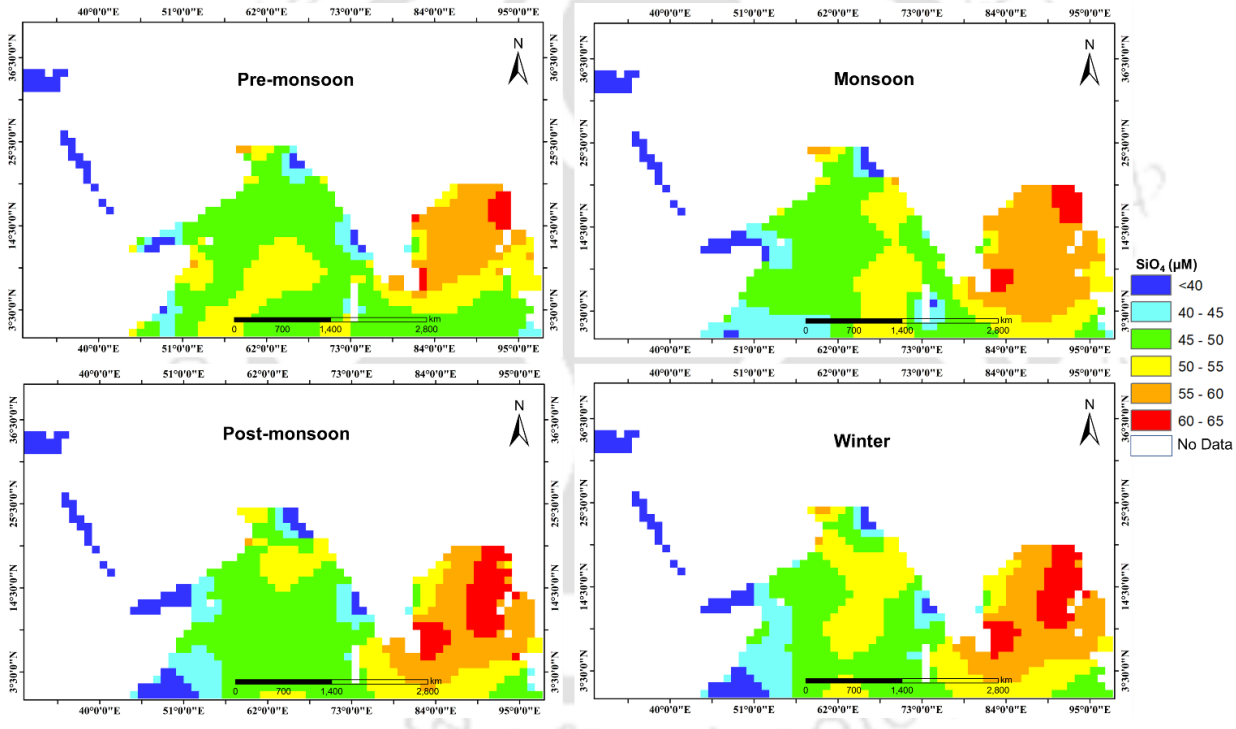

Figure.6.7 Spatio-temporal distribution of Silicate

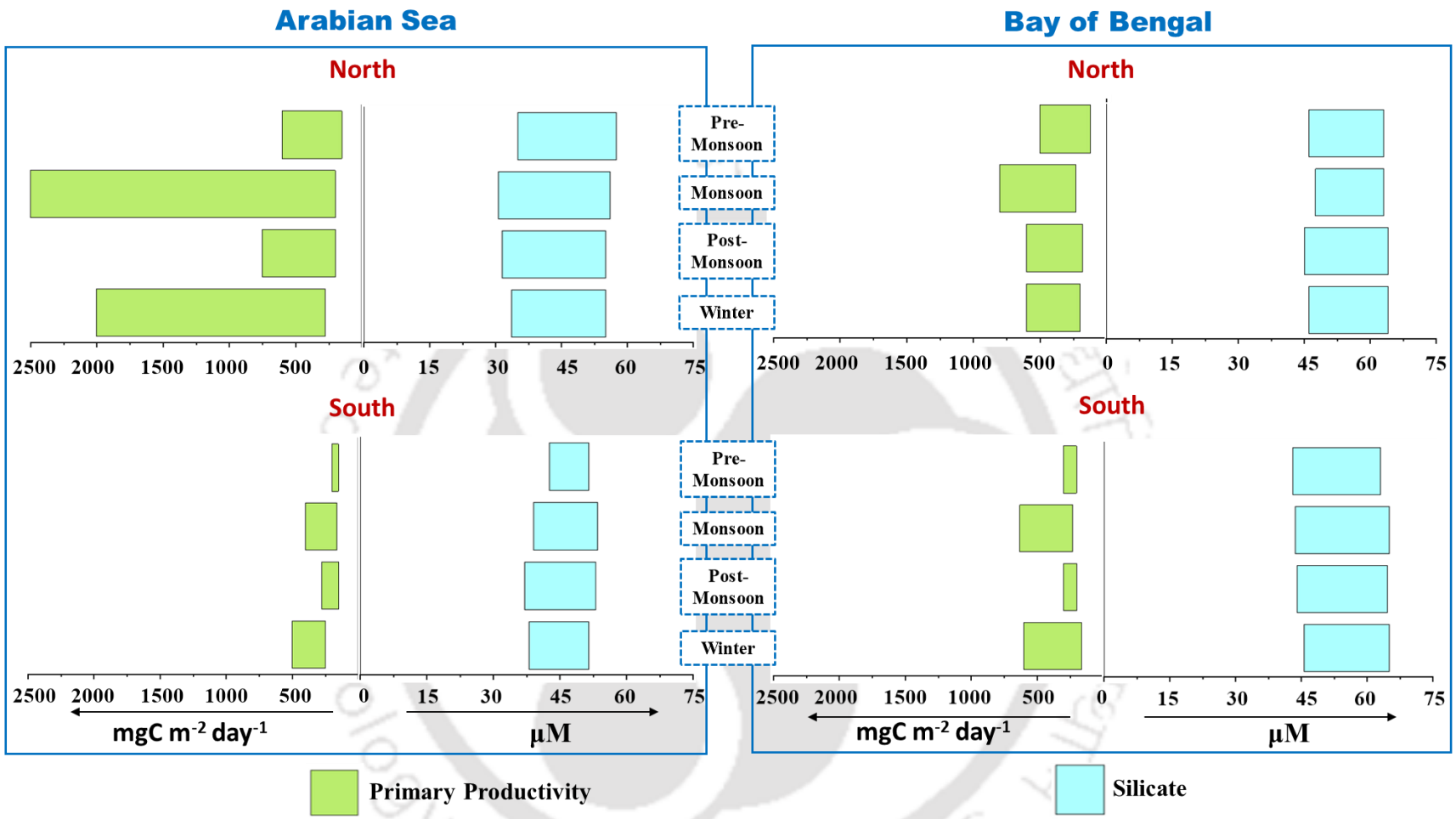

Figure.6.8 Silicate Distribution Vs. Productivity

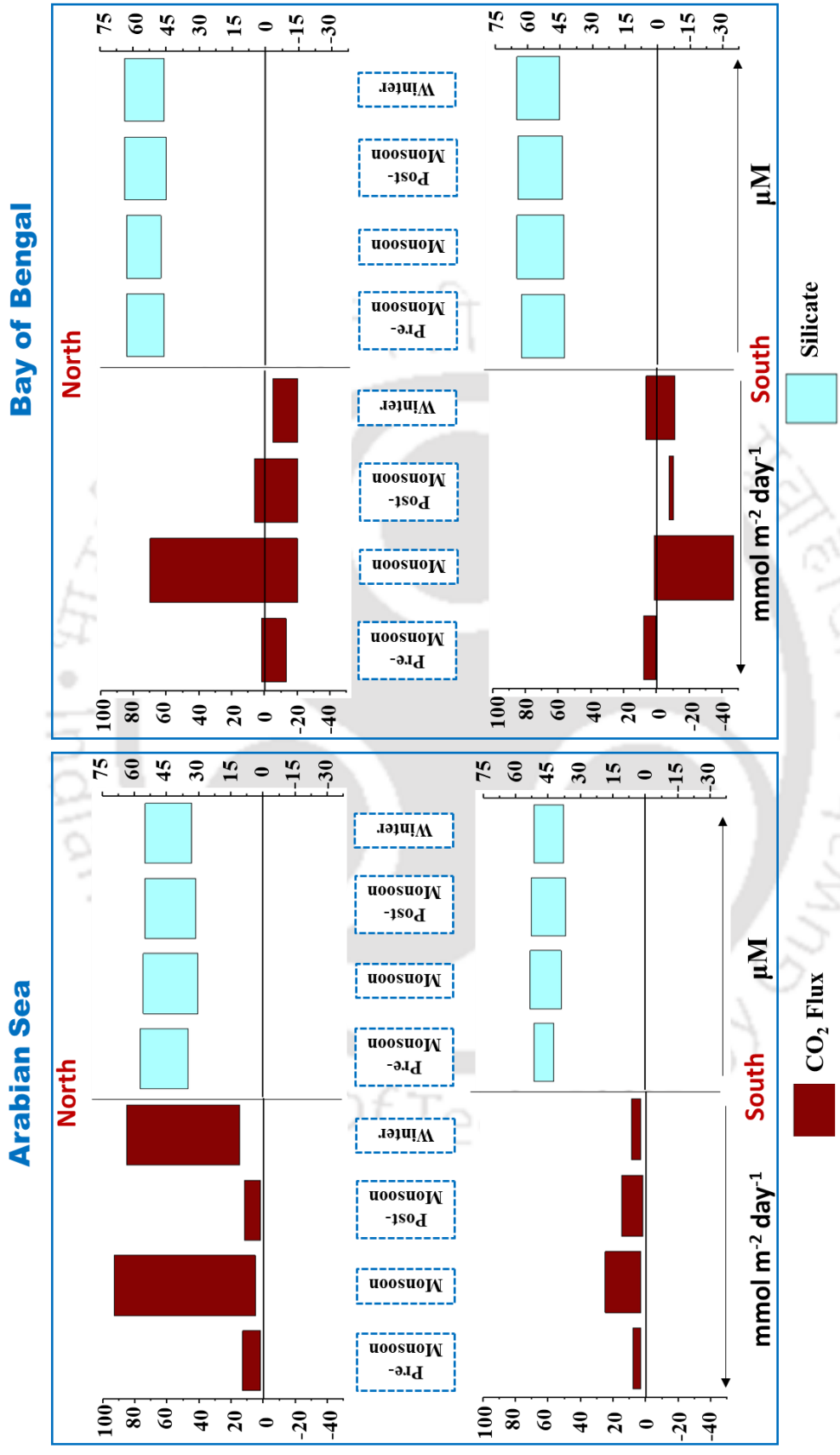

Figure.6.9 Silicate Distribution Vs. CO_2 Flux

Analysis of the silicate distribution in relation to productivity and CO_2 fluxes are given in Figure.6.8 and Figure.6.9 respectively. The northern Arabian Sea showed comparatively low silicate concentrations in all the seasons while BoB was observed to have high silicate levels. Monsoon concentrations were found to have a high-value range in the northern Arabian Sea due to the high consumption rate of the nutrient by the silicate-utilizing plankton species i.e., diatoms in the upwelling regions of this basin (Young and Kindle, 1994; Schiebel et al., 2004). The high monsoon CO_2 fluxes in the upwelling northern waters can also be associated with the high nutrient uptake and the resulting enhanced productivity. BoB waters showed comparatively less silicate consumption while high land influx was observed through river input, which contributes to the relatively high nutrient concentration. While the value range varied for the northern Arabian Sea silicate concentrations, the BoB showed almost comparable concentrations in both northern and southern waters.

6.3.2 Influence of sea surface temperature and wind speed anomalies on the sea surface pCO_2 distribution

6.3.2.1 Arabian Sea

The SST anomaly maps (Figure.6.10) showed significant warm peak events for the March-April-May and April-May-June periods and cool peak events for August-September-October and September-October-November periods for the Arabian Sea. Anomaly maps for SST, wind speed, and sea surface pCO_2 were analyzed to understand the impact of warm and cool peak events on the air-sea exchange of CO_2.

The warm SST anomaly (Figure.6.11) was found to have a significant influence on the pCO_2 distribution over the Arabian Sea, where increased temperatures, along with low weak winds were associated with reduced pCO_2 values in the east coast and central basin due to thermal stratification of the surface. An increased wind anomaly might have caused a turbulent action leading to disturbance in the surface stratification and hence an increase in the pCO_2 in southern waters. Along the west coast, the surface pCO_2 was observed to be high even though the wind action is very weak; this can be due to the high productivity over this region resulting in high levels of respiration, thus increasing the surface pCO_2 (Sarma et al, 2000; Sarma, 2003).

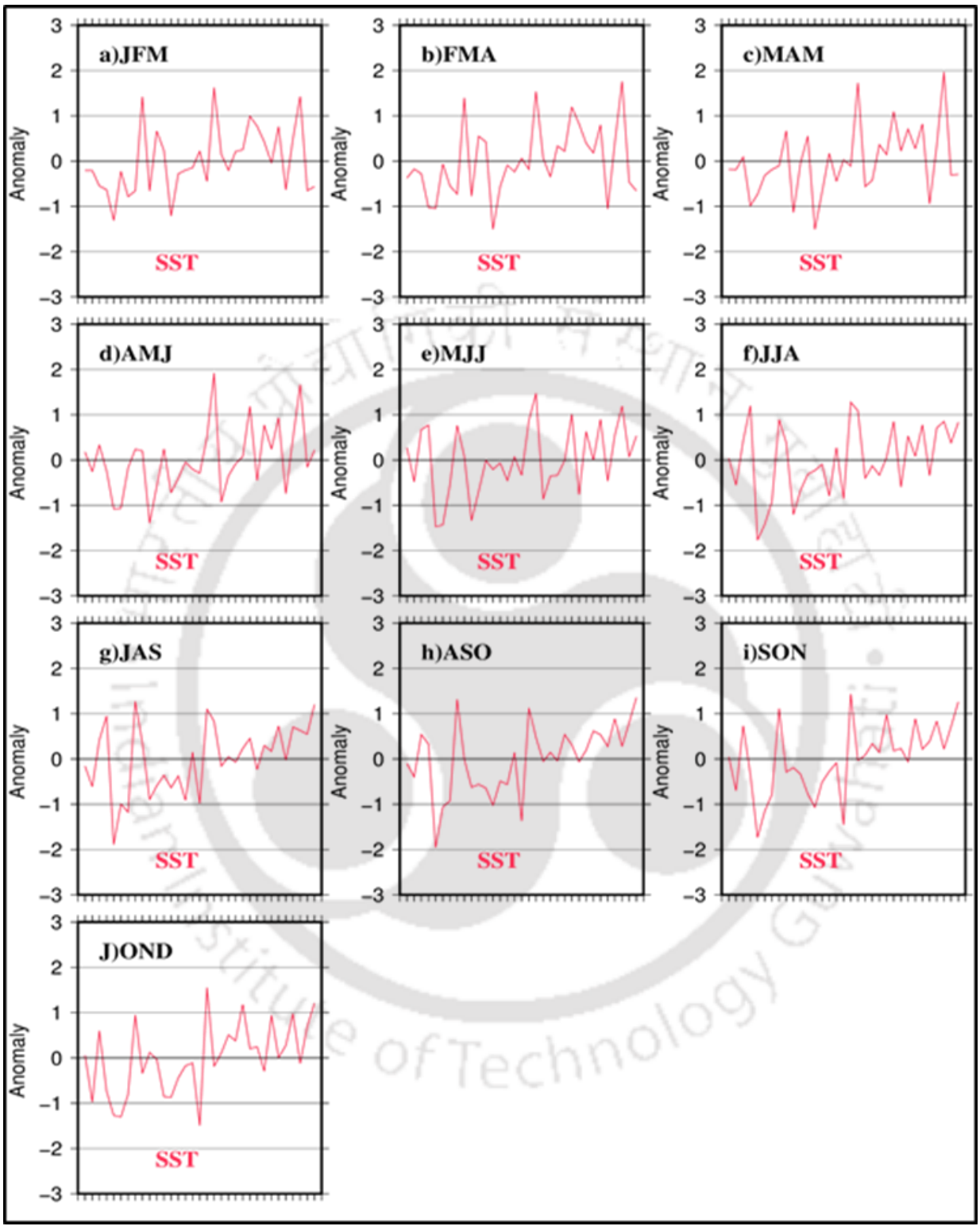

Figure. 6.10 SST anomaly map for Arabian Sea

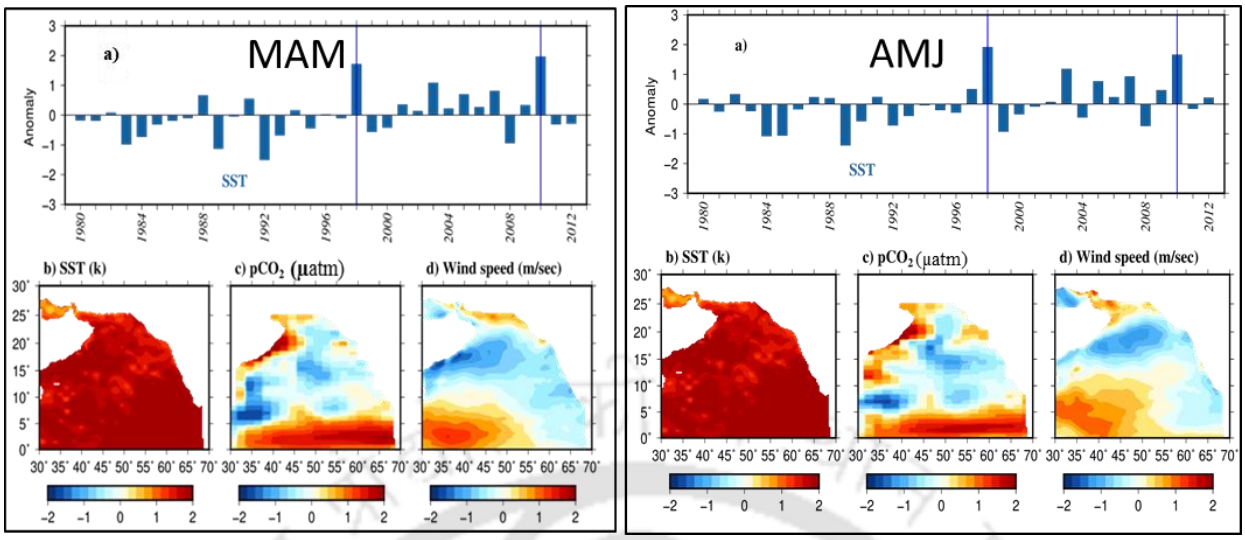

Figure. 6.11 Impact of warm SST and wind anomaly on pCO_2sw in the Arabian Sea

The cool SST anomaly (Figure.6.12) event was observed to enhance the coastal pCO_2 in the north and west; lowering of the surface temperature could trigger the convective mixing (Takahashi et al., 2002; Sarma, 2003). The strong wind action over the north could have also contributed to the increased surface pCO_2 in this region. Also, the positive wind anomaly associated with the monsoon season in the eastern Arabian Sea could have resulted in the upwelling, thus enhancing the surface pCO_2 along the west and south-west coast of India (Sarma, 2000; Sarma, 2003).

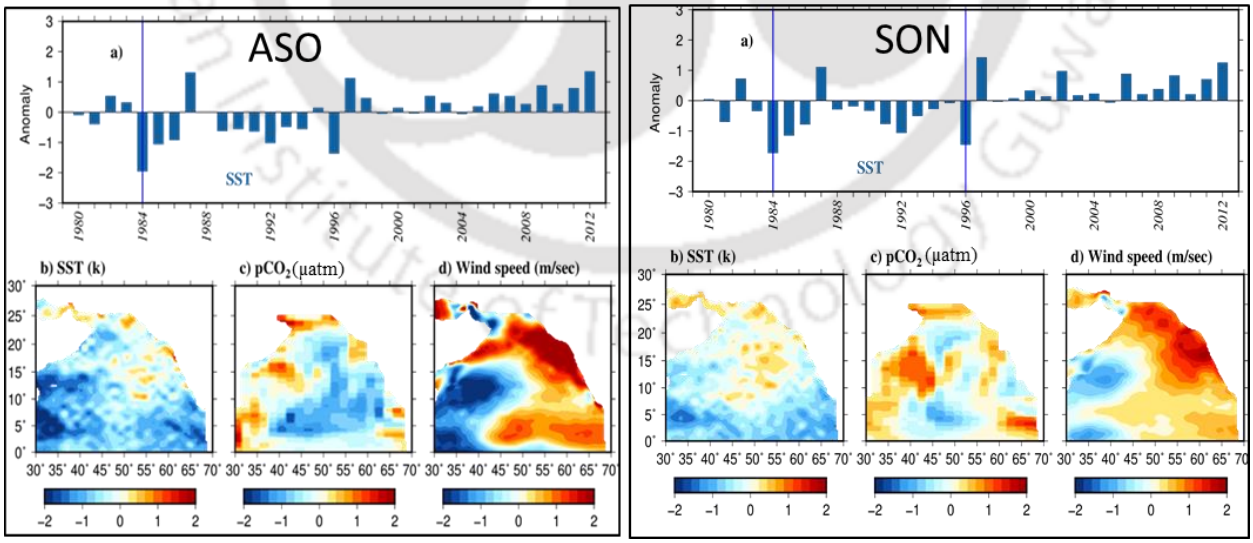

Figure. 6.12 Impact of cool SST and wind anomaly on pCO_2sw in Arabian Sea

6.3.2.2 Bay of Bengal

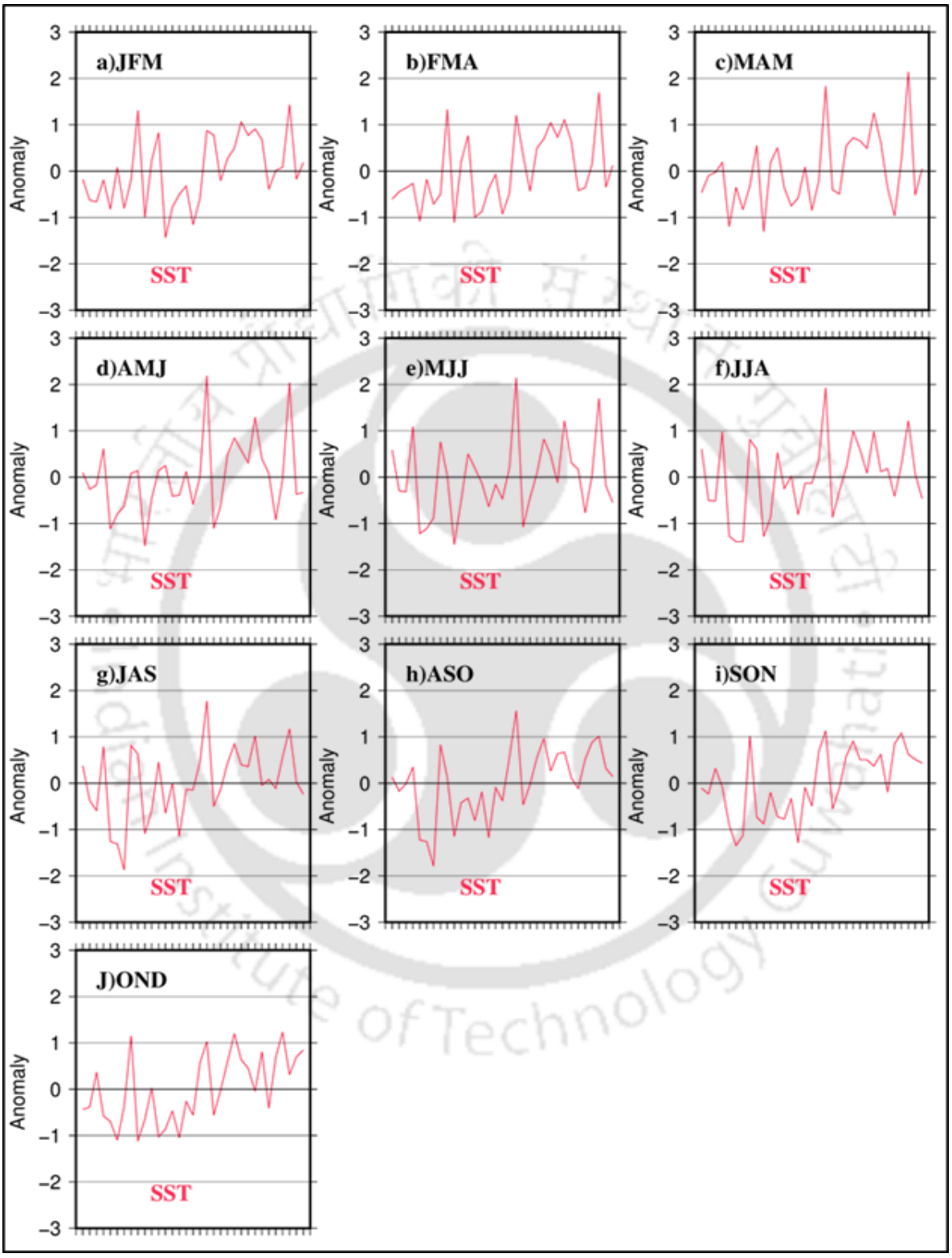

Figure. 6.13 SST anomaly map for Bay of Bengal

In the BoB, warm peak events were identified for March-April-May, April-May-June and May-June-July periods (Figure.6.13) from the SST anomaly plots. Warm anomaly event over the BoB basin is found to have a positive effect on the coastal as well as southern waters (Figure. 6.14). This might be attributed to the escaping of gaseous CO_2 as a result of the evaporation of surface waters. The wind is found to be strong along the north and west coastal area, which can induce a turbulent action, thus enhancing surface pCO_2. However, the weak winds over the eastern coast of BoB were found to have not much impact on the surface pCO_2 distribution. Also, the wind speeds over the southern BoB can be observed to gradually increase from the March-April-May period towards May-June-July, however, the fluxes were found to be strong over the south irrespective of the wind speeds. Here the evaporative process is found to have a better impact on the surface pCO_2.

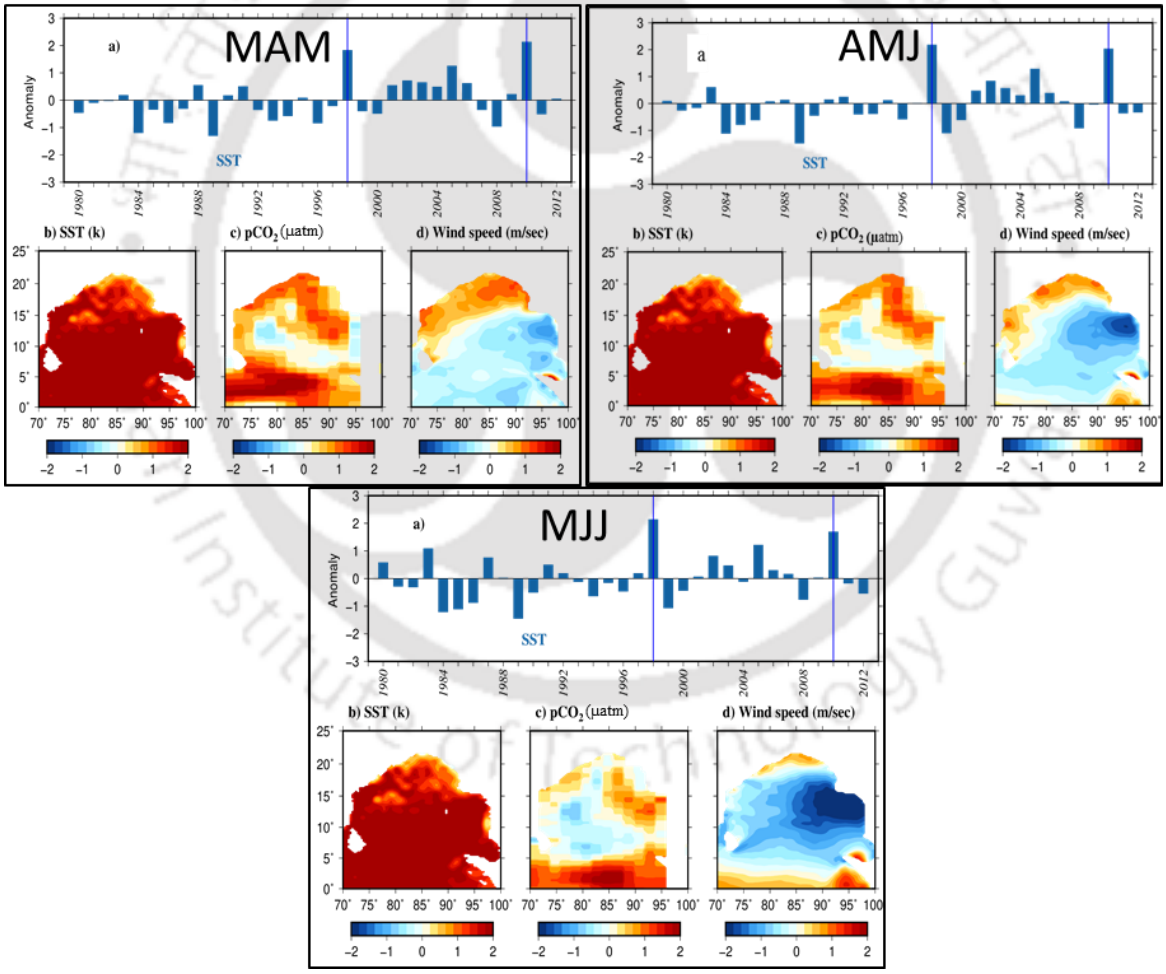

Figure. 6.14 Impact of warm SST and wind anomaly on pCO_2sw in Bay of Bengal

Cool SST anomaly event (Figure.6.15) along with strong winds over the open ocean is observed to enhance the pCO_2sw over the southern waters, however, the high pCO_2 values over the northern coast and central BoB waters must be associated with the monsoon-induced coastal and open ocean upwelling. The increase in temperatures over the central BoB also indicates the possible upwelling region where the subsurface warm waters are brought to the surface (Vinayachandran et al., 1996; Sarma et al., 2020).

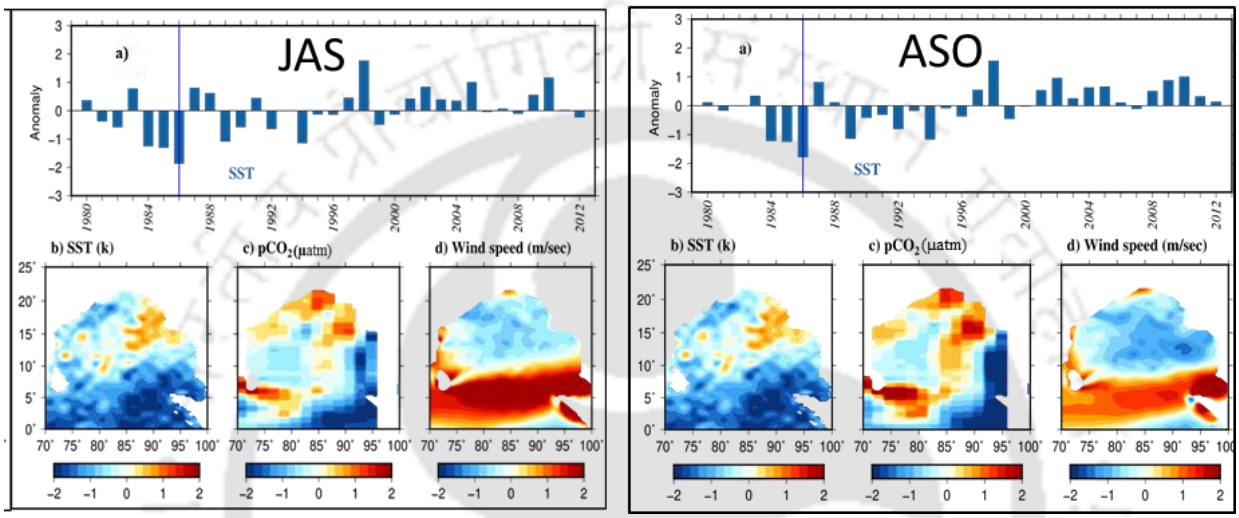

Figure. 6.15 Impact of cool SST and wind anomaly on pCO_2sw in the Bay of Bengal

6.4 Summary and Conclusion

The nutrient dynamics over the northern Indian Ocean were studied in order to understand their role in the spatial and seasonal distribution of ocean primary productivity and CO_2 fluxes. All three nutrients analyzed, i.e., nitrate, phosphate, and silicate, showed high concentrations over the BoB while maximum productivity was observed in the Arabian Sea. The intense influx of nutrients by the river discharge reasons this nutrient maximum in BoB while the surface stratification caused by fresh water input hinders proper upwelling over the northern waters rich in nutrients. This leads to low productivity in the BoB, whereas, the northern and eastern river influx during monsoon and the western aeolian deposit supply nutrients to the Arabian Sea which are utilized by the high photosynthetic activity over this basin. The maximum nutrient uptake can be observed over the upwelling regions where high productivity along with intense CO_2 fluxes was identified. BoB waters are characterized by negative fluxes, indicating an air-sea CO_2 uptake, owing to surface stratification. The influence of SST and windspeed anomalies on the air-sea CO_2 exchange showed

warm events over the Arabian Sea, along with weak winds have caused a reduction in surface pCO_2 which could be due to thermal stratification; however, strong winds led to increased surface pCO_2, caused by the turbulence action. Cooler SSTs with strong winds over the Arabian Sea increased surface pCO_2 resulting from convective mixing and upwelling. In BoB, enhanced surface pCO_2 was observed from the evaporative effect of warm anomalies with turbulent action of strong winds. Also, the cool events associated with strong winds were found to increase the pCO_2 which might be resulted from convective mixing.

7

Summary and Conclusions

7.1 Conclusions

- The spatial and seasonal distribution of sea surface pCO_2 and air-sea CO_2 fluxes over the western and eastern sub-basins of the Indian Ocean were analyzed to understand the contrasting CO_2 gas exchange trends between the two basins. Latitudinal distribution of sea surface partial pressures in relation to SST, SSS, and Chl-a distribution showed the dominance of biological forcings during the inter-monsoon seasons while physico-chemical factors influence the pCO_2 distribution during monsoon and winter seasons in the Arabian Sea; in BoB, biological controls were observed to be strong during pre-monsoon, post-monsoon and winter, while monsoonal pCO_2 is affected by physical forcings. High-temperature dependence was observed during pre-monsoon and winter seasons in the Arabian Sea, whereas, BoB showed a high correlation with temperature trends in all seasons. Salinity was not found to have much impact on the latitudinal pCO_2 distribution in the Arabian Sea, while, a moderate to high correlation was observed over BoB. Monsoon and winter seasons resulted in enhanced outfluxes in the Arabian Sea, whereas, the freshwater influx due to intense precipitation manifests surface stratification in BoB, thus reducing the surface pCO_2 and enhancing the influx of CO_2 from air to water. The Arabian Sea was observed to act as a perennial CO_2 source with a maximum average outflux of 93 mmol m^{-2} day^{-1} in monsoon, and BoB acted as an intense sink in winter while the maximum influx value of -47 mmol m^{-2} day^{-1} observed during monsoon season in southern BoB.
- The significance of ocean primary productivity and SST variability over the CO_2 flux distribution was analyzed; both productivity and fluxes were observed to be maximum during monsoon and winter seasons due to upwelling and convective mixing processes, while thermal stratification reduce the surface flux and nutrient availability in pre- and post-monsoon seasons. High productivity resulted in monsoon and winter seasons enhancing the

photosynthetic drawdown of surface CO_2 in the inter-monsoon period, causing a reduction in CO_2, while the increase in primary production is also associated with increased respiration rates, which enhances the CO_2 in the sea waters. Increased summer insolation reduces the CO_2 water solubility, leading to increased outflux, while winter reduction in SSTs induces surface convective mixing, releasing the subsurface CO_2. Increased surface temperatures can also result in reduced fluxes due to thermal stratification.

- The regional sea surface pCO_2 algorithm derived from ship measurements of pCO_2, SST, and SSS using multiple polynomial regression and random forest function showed better prediction accuracy by the latter technique. The linear and polynomial relationship between the SST and SSS with the sea water pCO_2 trends were comparatively higher in the BoB due to the high dependency of pCO_2 distribution on the thermal and salinity variations, while biological activities play a key role in the Arabian Sea. The non-linear relationship of the SST and SSS trends on surface pCO_2 variations was properly modelled by the random forest method, where both basins show very high validation accuracy, with a coefficient of determination value of 0.98 and RMSE value of 0.05-0.06 µatm.
- Nutrient dynamics over the Indian Ocean revealed maximum concentrations of nitrate, phosphate, and silicate over the BoB whereas, high productivity was observed over the Arabian Sea. The heavy river input of nutrients results in the high nutrient content of BoB, however, the freshwater-induced stratification and surface water turbidity due to sediment transport results in reduced light penetration in BoB water rich in nutrients, thus reducing the primary productivity.
- Analyzing the impact of SST and wind anomalies over the surface CO_2 distribution showed positive temperature and negative wind anomalies together reduce the surface pCO_2 over the Arabian Sea, due to surface stratification, while warm events coupled with strong winds enhance sea surface pCO_2. Cool events with positive wind anomalies cause convective mixing-induced outflux. BoB showed high sea surface pCO_2 during warm and cool anomalies in combination with strong winds.

7.2 Limitations and recommendations

- Field validation of the results is missing in this study, especially for the surface pCO_2 algorithm

- Incorporating in situ observations of Chlorophyll-a as a predictor parameter for the sea surface pCO_2 would improve the predictions since biological forcings are key factors in governing the sea water pCO_2 in the Indian Ocean.
- Seasonal sampling and analysis of the nutrient concentrations in both Arabian Sea and BoB waters would provide a better understanding of the nutrient scenario.
- Sampling and analysis of the aeolian deposition of nutrients are significant to understand their composition as well as their importance in ocean productivity.

LIST OF PUBLICATIONS:

Research Articles Published:

1) **Lekshmi, K.,** Bharti, R., and Mahanta, C., (2021). Dynamics of Air-Sea CO_2 Fluxes and their Trends in The Global Context. Current Science.
2) Dixit, A., **Lekshmi, K.**, Bharti, R., and Mahanta, C., (2019). Net sea-Air CO_2 fluxes and modeled partial pressure of CO_2 in open ocean of Bay of Bengal. IEEE Journal of Selected Topics in Applied Earth Observations and Remote Sensing.

Research Articles Under Review:

3) **Lekshmi, K.,** Bharti, R., and Mahanta, C., (2022). Significance of physico-chemical and biological parameters on spatio-temporal pCO_2 distribution in the northeastern Indian Ocean (*under review in Journal of Indian Society of Remote Sensing*).
4) Lekshmi K., Bharti, R., and Mahanta, C., (2023). Biological and thermohaline controls on sea surface pCO_2 over north-western Indian Ocean (*Under review in Ocean Dynamics*)

Research Articles to be Submitted:

5) Estimation of CO_2 partial pressures and air-sea CO_2 fluxes over the east and west sub-basins of the northern Indian Ocean using in situ and satellite observations
6) An investigation of nutrient dynamics and ocean primary productivity on the spatio-temporal distribution of CO_2 fluxes over the northern Indian Ocean
7) Influence of warm and cool events on the spatial and seasonal variability of sea surface CO_2 partial pressures over the northern Indian Ocean

Conferences:

i.) **Lekshmi, K.,** Bharti, R., & Mahanta, C., Significance of biological forcing on the spatio-temporal variability of carbon dioxide fluxes over the Northern Indian Ocean. EGU23-15166, EGU General Assembly 2023.

ii.) **Lekshmi, K.,** Bharti, R., & Mahanta, C., Biogeochemical Impacts on Seasonal CO_2 Flux Distribution over Northern Indian Ocean. Ocean Sciences Meeting, 2022.

iii.) **Lekshmi, K.,** Bharti, R., & Mahanta, C., Spatio-Temporal Distribution of Carbon Dioxide Partial Pressure in the Bay of Bengal. IEEE International Geoscience and Remote Sensing Symposium Yokohama, Japan 67 2019

iv.) **Lekshmi, K.,** Mishra, A., Bharti, R., & Mahanta, C., Seasonal Variability Analysis of Sea Water pCO_2 Over North Western Indian Ocean AGU Fall Meeting Washington, D.C. 2018.

v.) Dixit, A., **Lekshmi, K.,** Bharti, R., & Mahanta, C., Basin Scale pCO_2 Distribution in Case 1 Waters: An Investigation from Bay of Bengal, India. IEEE International Geoscience and Remote Sensing Symposium Valencia, Spain, 2018.

vi.) Dixit, A., **Lekshmi, K.,** Bharti, R., & Mahanta, C., A technique for estimation of partial pressure of carbon dioxide in the Bay of Bengal. Ocean Sciences Meeting Portland, Oregon 2018.

REFERENCES

Adamowski, J., Chan, H.F., Prasher, S.O., Zielinski, B.O., & Sliusarieva, A. (2012). Comparison of multiple linear and nonlinear regression, autoregressive integrated moving average, artificial neural network, and wavelet artificial neural network methods for water demand forecasting in Montreal, Canada. Water Resources Research, 48: 1-14. W01528. doi:10.1029/2010WR009945.

Amol, P., Vinayachandran, P. N., Shankar, D., Thushara, V., Vijith, V., Chatterjee, A., & Kankonkar, A. (2020). Effect of freshwater advection and winds on the vertical structure of chlorophyll in the northern Bay of Bengal. Deep Sea Research Part II: Topical Studies in Oceanography, 179, 104622.

Babu, M. T., Sarma, Y. V. B., Murty, V. S. N., & Vethamony, P. (2003). On the circulation in the Bay of Bengal during northern spring inter-monsoon (March–April 1987). Deep Sea Research Part II: Topical Studies in Oceanography, 50(5), 855-865.

Balino, B.M., Fasham, M.J.R & Bowles, M.C., (2000). Ocean biogeochemistry and global change: JGOFS research highlights 1988-2000, IGBP, ICSU, Stockholm, Sweden.

Bange, H. W., Naqvi, S. W. A., & Codispoti, L. A. (2005). The nitrogen cycle in the Arabian Sea. Progress in Oceanography, 65(2-4), 145-158.

Barber, R.T., Marra, J., Bidigare, R.C., Codispoti, L.A., Halpern, D., Johnson, Z., Latasa, M., Goericke, R & Smith, S.L. (2001). Primary productivity and its regulation in the Arabian Sea during 1995, Deep-Sea Research II, 48,1127-1172.

Bates, N. R. (2007). Interannual variability of the oceanic CO_2 sink in the subtropical gyre of the North Atlantic Ocean over the last 2 decades, Journal of Geophysical Research, 112 (C09013), 26p, doi:10.1029/2006JC003759.

Beal, L. M., Hormann, V., Lumpkin, R., & Foltz, G. R. (2013). The response of the surface circulation of the Arabian Sea to monsoonal forcing. Journal of Physical Oceanography, 43(9), 2008-2022.

Behara, A., & Vinayachandran, P. N. (2016). An OGCM study of the impact of rain and river water forcing on the Bay of Bengal. Journal of Geophysical Research: Oceans, 121(4), 2425-2446.

Behara, A., Vinayachandran, P. N., & Shankar, D. (2019). Influence of rainfall over eastern Arabian Sea on its salinity. Journal of Geophysical Research: Oceans, 124(7), 5003-5020.

Behrenfeld, M. J., & Falkowski, P. G. (1997). Photosynthetic rates derived from satellite-based chlorophyll concentration. Limnology and oceanography, 42(1), 1-20.

Bernstein, L., Bosch, P., Canziani, O et al., 2007. An assessment of the Intergovermental Panel on Climate Change, Climate Change 2007: Synthesis Report, www.ipcc.ch/pdf/assessment-report/ar4/syr/ar4-syr.pdf

Bikia, V., Rovas, G., Pagoulatou, S., & Stergiopulos, N (2021). Determination of aortic characteristic impedance and total arterial compliance from regional pulse wave velocities using machine learning: an in-silico study, Frontiers in Bioengineering and Biotechnology, 9(649866), doi:10.3389/fbioe.2021.649866.

Bindoff, N.L., Willebrand, J., Artale, V., Cazenave, A., Gregory, J., Gulev, S., Hanawa, K., Le Quere, C., Levitus, S., Nojiri, Y., Shum, C.K., Talley, L.D., & Unnikrishnan, A., 2007. Observations: Oceanic Climate Change and Sea level, Climate Change, Cambridge University Press, Cambridge, United Kingdom and New York, NY, USA

Bolotin, L. A., Summers, B. M., Savoy, P., & Blaszczak, J. R. (2022). Classifying freshwater salinity regimes in central and western US streams and rivers. Limnology and Oceanography Letters.

Botkin, D.B., & Keller, E.A. (2000). Environmental Science, Earth as a Living Planet, 3rd edition, John Wiley & Sons, Inc, 649p.

Brian, J.S., & Stephen, C.P. (1995). The blue planet: an introduction to earth system science, John Wiley & Sons, Inc. NewYork.

Buesseler, M., Bowles, M., & Joyce, K. (2013). U.S.JGOFS brochure, U.S. JGOFS planning and data management office, Wooda Whole, Massachusetts, USA.

Caldera, K., & Wickett, M.E. (2003). Anthropogenic carbon and ocean pH, Nature Brief Communications, 425:365.

Chauhan, P., Nagur, C.R.C., Mohan, M., Nayak, S.R., & Navalgund, R.R. (2001). Surface chlorophyll-a distribution in Arabian Sea and Bay of Bengal using IRS-p4 Ocean Colour Monitor satellite data, Current Science, 80(2), 127-129.

Chester, R. (2000). Marine Geochemistry, 2nd edition, Blackwell Science Ltd, Osney Mead, Oxford OX2 0EL, 506p.

Ciais, P., Sabine, C., Bala, G., Bopp, L., Brovkin,V., Canadell, J., Chhabra, A., DeFries, R., Galloway, J., Heimann, M., Jones, C., Le Quéré, C., Myneni, R.B., Piao, S., & Thornton, P. (2013). Carbon and Other Biogeochemical Cycles. In: Climate Change 2013: The Physical Science Basis. Contribution of Working Group I to the Fifth Assessment Report of the Intergovernmental Panel on Climate Change [Stocker, T.F., D. Qin, G.-K. Plattner, M. Tignor, S.K. Allen, J. Boschung, A. Nauels, Y. Xia, V. Bex and P.M. Midgley (eds.)]. Cambridge University Press, Cambridge, United Kingdom and New York, NY, USA.

Conkright, M. E., Gregg, W. W., & Levitus, S. (2000). Seasonal cycle of phosphate in the open ocean. Deep Sea Research Part I: Oceanographic Research Papers, 47(2), 159-175.

Cosca, C.E., Feely, R.A., Boutin, J., Etcheto, J., McPhaden, M.J., Chavez, F.P., & Strutton, P.G. (2003). Seasonal and interannual CO_2 fluxes for the central and eastern equatorial Pacific Ocean as determined from fCO_2-SST relationships, Journal of Geophysical Research, 108 (C8), 3278, doi:10.1029/2000JC000677.

Da vila, M.G., Casiano, J.M.S., & Da vila, E.F.G. (2007). Interannual variability of the upper ocean carbon cycle in the north east Atlantic Ocean, Geophysical Research Letters, 34.

Dey, S., & Singh, R.P. (2003). Comparison of chlorophyll distributions in the northeastern Arabian Sea and southern Bay of Bengal using IRS-P4 Ocean Color Monotor data, Remote Sensing of environment, 85, 424-428.

Dickson, A.G.,& Goet, C. (1994). DOE 1994, Handbook of methods for the analysis of various parameters of the carbon dioxide system in seawater, version 2, ORNL/CDIAC-74.

Dickson, A.G., Sabine, C.L., & Christian, J.R. (2007). Guide to best practices for ocean CO_2 measurements, PICES Special Publication, 3, 1-191.

Dixit, A., K, L., Bharti, R., & Mahanta.C. (2018). Basin scale estimation of partial pressure of carbon dioxide in case 1 waters of Bay of Bengal, International Geoscience and Remote Sensing symposium, Velencia, Spain, 23-27 July.

Dixit, A., K, L., Bharti, R., & Mahanta.C. (2019). Net sea-air CO_2 fluxes and modelled partial pressure of CO_2 in open ocean of BoB. IEEE Journal of Selected Topics in Applied Earth Observation and remote Sensing., 12(7), 2462-2469. doi: 10.3402/tellusb.v64i0.10961.

Falkowski, P.,Scholes, R.J., Boyle, E., Canadell, J., Canfield, D., Elser, J., Gruber, N., Hibbard, K., Hogberg, P., Linder, S., Mackenzie, F.T., Moore III, B., Pedersen, T., Rosenthal, Y., Seitzinger, S., Smetacek, V and Steffen, W. (2000). The Global Carbon Cycle: A Test of Our Knowledge of Earth as a System, Science, New Series, 290(5490), 291-296.

Feely, R. A., Wanninkhof, R., McGillis, W., Carr, M. E., & Cosca, C. E. (2004). Effects of wind speed and gas exchange parameterizations on the air-sea CO_2 fluxes in the equatorial Pacific Ocean. Journal of Geophysical Research: Oceans, 109(C8).

Feely, R.A., Sabine, C.L., Takahashi, T., & Wanninkhof,R . (2001). Uptake and Storage of Carbon Dioxide in the Ocean: The Global CO_2 Survey, Oceanography, 14(4), 18-32

Feely, R.A., Takahashi, T., Wanninkhof, R., McPhaden, M. J., Cosca, C. E., Sutherland, S. C., & Carr, M. (2006). Decadal variability of the air-sea CO_2 fluxes in the equatorial Pacific Ocean, Journal of Geophysical Research, 111(C08S90), 1-16, doi:10.1029/2005JC003129.

Feely, R.A., Wanninkhof, R., Takahashi, T., & Tans,P. (1999). The influence of El Niño on the equatorial Pacific contribution to atmospheric CO_2 accumulation, Nature, 398, 597–601.

Fletcher, S. M., Gruber, N., Jacobson, A. R., Gloor, M., Doney, S. C., Dutkiewicz, S., Gerber, M., Follows, M., Joos, F., Lindsay, K., Menemenlis, D., Mouchet, A., Muller, S.A., & Sarmiento, J. L. (2006). Inverse estimate of oceanic sources and sinks of natural CO_2 and their implied oceanic transport. J Geophys Res, 21.

George, M.D., Kumar, M.D., Naqvi, S.W.A., Banerjee, S., Navrekar, P.V., deSousa, S.N. and Jayakumar. D.A., 1994, Study of the carbon dioxide system in the northern Indian Ocean during premonsoon, Marine Chemistry, 47, 243-254pp.

Goes, J. I., Saino, T., Oaku, H., Ishizaka, J., Wong, C. S., & Nojiri, Y. (2000). Basin scale estimates of sea surface nitrate and new production from remotely sensed sea surface temperature and chlorophyll. Geophysical research letters, 27(9), 1263-1266.

Goet, C., Beauverger, C., Brunet, C., & Poisson, A. (1991). Distribution of carbon dioxide partial pressure in surface waters of the Southwest Indian Ocean, Tellus, 43(b), 1-11.

Goetz, P.W. (1987). The New Encyclopedia Britannica, Vol. 1, Encyclopedia Britannica Inc, Chicago.

Gomes, H.R, Goes, J.I and Saino,T. (2000). Influence of physical processes and freshwater discharge on the seasonality of phytoplankton regime in the Bay of Bengal, Continental Shelf Research, 20, 313-330.

Gopalakrishna, V. V., Murty, V. S. N., Sengupta, D., Shenoy, S., & Araligidad, N. (2002). Upper ocean stratification and circulation in the northern Bay of Bengal during southwest monsoon of 1991. Continental Shelf Research, 22(5), 791-802.

Gray, A. R., Johnson, K. S., Bushinsky, S. M., Riser, S. C., Russell, J. L., Talley, L. D., Wanninkhof, R., Williams, N.L., & Sarmiento, J. L. (2018). Autonomous biogeochemical floats detect significant carbon dioxide outgassing in the high-latitude Southern Ocean. Geophysical Research Letters, 45(17), 9049-9057.

Han, W., & McCreary Jr, J. P. (2001). Modeling salinity distributions in the Indian Ocean. Journal of Geophysical Research: Oceans, 106(C1), 859-877.

Hood, E. M., Merlivat, L., & Johannessen, T. (1999). Variations of JEO and air-sea flux of in the Greenland Sea gyre using high-frequency time series data from CARIOCA drift buoys, Journal of Geophysical Research, 1049(C9), 20, 571-20,583.

Horst, D.S., & Mathias Z. (2006). Marine Geochemistry, 2nd edition, Springer-Verlag Berlin Heidelberg.

Ittekkot, V., Nair, R. R., Honjo, S., Ramaswamy, V., M. Bartsch, Manganini, S. and Desai, B. N. (1991). Enhanced particle fluxes in Bay of Bengal induced by injection of fresh water, Nature, 351, 385–387, doi:10.1038/351385a0.

Ivakhnenko, A. G. (1970). Heuristic self-organization in problems of engineering cybernetics. Automatica, 6(2), 207-219.

Jang,E., Im, J., Park, G., & Park,Y. (2017). Estimation of Fugacity of Carbon Dioxide in the East Sea Using In Situ Measurements and Geostationary Ocean Color Imager Satellite Data, Remote Sensing, 9 (821), doi:10.3390/rs9080821, 23p.

Jensen, J.R. (1996). Introductory Digital Image Processing: A Remote Sensing Perspective (2nd ed.). Chapter 6, Image Preprocessing: Radiometric and Geometric Correction. Upper Saddle River, NJ: Prentice-Hall.,107- 137.

Kortzinger, A., Duinker, J.C., & Mintrop, L. (1997). Strong CO_2 emissions from the Arabian Sea during south-west monsoon , Geophysical Research Letters, 24(14), 1763-1766.

Kortzinger, A., Send, U., Lampitt, R. S., Hartman, S., Wallace, D. W. R., Karstensen, J., Villagarcia, M. G., Llina, O., & DeGrandpre, M. D. (2008). The seasonal pCO_2 cycle at 49N/16.5W in the northeastern Atlantic Ocean and what it tells us about biological productivity, Journal of Geophysical Research, 113 (C04020), doi:10.1029/2007JC004347.

Krishna, M.S., Prasad, M.H.K., Rao, D.B., Viswanadham, R., Sarma, V.V.S.S., & Reddy, N.P.C. (2016). Export of dissolved inorganic nutrients to the northern Indian Ocean from the Indian monsoonal rivers during discharge period, Geochimica et Cosmochimica Acta, 172, 430–443.

Kumar, M. D., Naqvi, S. W. A., George, M. D., & Jayakumar, D. A. (1996). A sink for atmospheric carbon dioxide in the northeast Indian Ocean, Journal of Geophysics Research, 101(18), 121–125.

Kumar, S. P., & Narvekar, J. (2005). Seasonal variability of the mixed layer in the central Arabian Sea and its implication on nutrients and primary productivity. Deep Sea Research Part II: Topical Studies in Oceanography, 52(14-15), 1848-1861.

Kumar, S. P., & Prasad, T. G. (1999). Formation and spreading of Arabian Sea high-salinity water mass. Journal of Geophysical Research: Oceans, 104(C1), 1455-1464.

Kumar, S.P., Muraleedharan, P. M., Prasad, T. G., Gauns, M., Ramaiah, N., de Souza, S. N., Sardesai, S. and Madhupratap, M. (2002). Why is the Bay of Bengal less productive during summer monsoon compared to the Arabian Sea?, Geophysical Research Letters, 29(24,2235): 88.1-88.4. doi:10.1029/2002GL016013.

Landschutzer, P. (2014). Variability of the global ocean carbon sink (1998 through 2011), Ph.D thesis, School of Environmental Sciences, University of East Anglia, 184p.

Landschützer, P., Gruber, N., & Bakker, D. C. (2016). Decadal variations and trends of the global ocean carbon sink. Global Biogeochemical Cycles, 30(10), 1396-1417.

Leach, T. H., Beisner, B. E., Carey, C. C., Pernica, P., Rose, K. C., Huot, Y., Brentrup, J.A., Domaizon, I., Grossart, H-P., Ibelings, B.W., Jacquet, S., Kelley, P.T., Rusak, J.A., Stockwell, J.D., Straile, D., & Verburg, P. (2018). Patterns and drivers of deep chlorophyll maxima structure in 100 lakes: The relative importance of light and thermal stratification. Limnology and Oceanography, 63(2), 628-646.

Lee, K., Wanninkhof, R., Feely, R. A., Millero, F. J., & Peng, T. H. (2000). Global relationships of total inorganic carbon with temperature and nitrate in surface seawater. Global Biogeochemical Cycles, 14(3), 979-994.

Levitus, S., Conkright, M. E., Reid, J. L., Najjar, R. G., & Mantyla, A. (1993). Distribution of nitrate, phosphate and silicate in the world oceans. Progress in Oceanography, 31(3), 245-273.

Liu, T.W., & Xie, X. (2014). Ocean Surface Carbon Dioxide Fugacity Observed from Space, JPL Publication 14-15, National Aeronautics and Space Administration, Jet Propulsion Laboratory California Institute of Technology Pasadena, California, 18p.

Lutgens, F.K., & Tarbuck, E.J. (2004). The Atmosphere: An Introduction to Meteorology, 9th edition, Prentice Hall, New Jersey, 434p.

Madhupratap, M., Gauns, M., Ramaiah, N., Kumar, S. P., Muraleedharan, P. M., De Sousa, S. N., Sardessai, S., & Muraleedharan, U. (2003). Biogeochemistry of the Bay of Bengal: physical, chemical and primary productivity characteristics of the central and western Bay of Bengal during summer monsoon 2001. Deep Sea Research Part II: Topical Studies in Oceanography, 50(5), 881-896.

Madhupratap, M., Prasannakumar, S., Bhattathiri, P.M.A., Kumar, M.D., Raghukumar, S., Nair, K.K.C., & Ramaiah, N. (1996). Mechanism of the biological response to winter cooling in the northeastern Arabian Sea, Nature, 384, 549-552.

Marra, J., & Barber, R.T. (2005). Primary productivity in the Arabian Sea: A synthesis of JGOFS data, Progress in Oceanography, 65, 159-175.

Martiny, A.C., Vrugt1,J.A., & Lomas, M.W. (2014). Concentrations and ratios of particulate organic carbon, nitrogen, and phosphorus in the global ocean, Nature Scientific Data, 1(140048), 7p, doi: 10.1038/sdata.2014.48.

Matsushita, B., Yang, W., Chang, P., Yang, F., & Fukushima, T. (2012). A simple method for distinguishing global case-1 and caes-2 waters using SeaWiFS measurements, ISPRS Journal of Photogrmmetry and Remote Sensing, 69, 74-87.

McCreary, J. P., Murtugudde, R., Vialard, J., Vinayachandran, P. N., Wiggert, J. D., Hood, R. R., Shankar, D., & Shetye, S. (2009). Biophysical processes in the Indian Ocean. Indian Ocean biogeochemical processes and ecological variability, 185, 9-32.

McNeil, B.I., Metzl,N., Key,R.M., Matear,R.J., & Corbiere,A. (2007). An empirical estimate of the Southern Ocean air-sea CO2 flux, Global Biogeochemical Cycles, 21(GB3011), doi:10.1029/2007GB002991.

Metzl, N., Brunet, C., Jabaud-Jan, A., Poisson, A., & Schauer, B. (2006). Summer and winter air–sea CO_2 fluxes in the Southern Ocean, Deep-Sea Research I, 53, 1548–1563.

Midorikawaa, T., Umedaa, T., Hiraishia, N., Ogawaa, K., Nemotoa, K., Kuboa, N., & Masao Ishiib, M. (2002). Estimation of seasonal net community production and air–sea CO_2 flux based on the carbon budget above the temperature minimum layer in the western subarctic North Pacific, Deep-Sea Research I, 49, 339–362.

Millero, F.J., & Poisoon, A. (1981). International one-atmosphere equation of state of seawater, Deep-Sea Research, 28A (6), 625-629.

Mongwe, N., Vichi, M., & Monteiro, P. (2018). The seasonal cycle of pCO_2 and CO_2 fluxes in the Southern Ocean: diagnosing anomalies in CMIP5 Earth system models. Biogeosciences, 15(9), 2851-2872.

Murtugudde, R., & Busalacchi, A. J. (1999). Interannual variability of the dynamics and thermodynamics of the tropical Indian Ocean. Journal of Climate, 12(8), 2300-2326.

Murty, V. S. N., Sarma, Y. V. B., Rao, D. P., & Murty, C. S. (1992). Water characteristics, mixing and circulation in the Bay of Bengal during southwest monsoon. Journal of Marine Research, 50(2), 207-228.

Oliveira, R. R., Pezzi, L. P., Souza, R. B., Santini, M. F., Cunha, L. C., & Pacheco, F. S. (2019). First measurements of the ocean-atmosphere CO_2 fluxes at the Cabo Frio upwelling system region, Southwestern Atlantic Ocean. Continental Shelf Research, 181, 135-142.

Olsen, A., Bellerby, R.G.J., Johannessen, T., Omar, A.M and Skjelvan, I. (2003). Interannual variability in the wintertime air-sea flux of carbon dioxide in the northern North Atlantic, 1981-2001, Deep-Sea Resaerch I, 50,1323-1338.

Ono, T., Saino, T., Kurita, N., & Sasaki, K. (2004). Basin-scale extrapolation of shipboard pCO_2 data by using satellite SST and Chla, International Journal of Remote Sensing, 25 (19), 3803–3815.

Orselli, I.B.M., Kerr, R., de Azevedo, J. L.L., Galdino, F., Araujo, M., & Garcia, C.A.E. (2019). The sea-air CO_2 net fluxes in the South Atlantic Ocean and the role played by Agulhas eddies, Progress in Oceanography, 170: 40-52.

Padhy, P. C., Nayak, R. K., Dadhwal, V. K., Salim, M., Mitra, D., Chaudhury, S. B., Rao, P. R., Rao, K. H., & Dutt, C.B. S. (2016). Estimation of partial pressure of carbon dioxide and air-sea fluxes in Hooghly estuary based on in situ and satellite observations, Journal of Indian Society of Remote Sensing, 44(1), 135–143, doi:10.1007/s12524-015-0459-z.

Pedhazur, E. J. (1982), Multiple Regression in Behavioral Research: Explanation and Prediction, Holt, Rinehart and Winston, New York.

Prasad, T. G., & Ikeda, M. (2002). A numerical study of the seasonal variability of Arabian Sea high-salinity water. Journal of Geophysical Research: Oceans, 107(C11), 18-1.

Prasannakumar, S., Roshin, R.P., Narvekar, J., Kumar, P.K.D., & Vivekanandan, E. (2009). Response of the Arabian Sea to global warming and associated regional climate shift, Marine Environmental Research, 68, 217-222.

PreethiLatha, T., Rao, K.H., Sarma, V.V.S.S., Dutt, C.B.S., Seetaram, P., Dhadwal, V.K., Choudhury, S.B., Manna, S. and Nagamani, P.V. (2015). Estimation of Air-Sea CO_2 Flux in the Coastal Waters of Visakhapatnam, Journal of Indian Society of Remote Sensing, 43(3), 647–652.

Prentice, I.C., Farquhar, G.D., Fasham, M.J.R., Goulden, M.L., Heimann, M., Jaramillo, V.J., Kheshgi, H.S., Le Quéré, C., Scholes, R.J., & Wallace, D.W.R. (2001). The Carbon Cycle and Atmospheric Carbon Dioxide, Contribution of Working Group I to the Third Assessment Report of the Intergovernmental Panel on Climate Change, Cambridge University Press, Cambridge, United Kingdom and New York, NY, USA.

Ramaiah, N., Raghukumar, S., & Gauns, M. (1996). Bacterial abundance and production in the central and eastern Arabian Sea. Current Science, 878-882.

Ramaswamy, V., & Nair, R.R. (1994). Fluxes of material in the Arabian Sea and Bay of Bengal-Sediment trap studies, Proceedings of Indian Academic Society (Earth Planet. Sci.), 103 (2), 189-210.

Ramaswamy, V., Kumar, V. B., Parthiban, G., Ittekkots, V., & Nair, R. R. (1997). Lithogenic fluxes in the Bay of Bengal measured by sediment traps, Deep-Sea Research I, 44(5), 793-810.

Rao, C.K., Naqvi, S.W.A., Kumar, M.D., Varaprasad, S.J.D., Jayakumar, A., George, M.D., & Singbal, S.Y.S. (1994). Hydrochemistry of Bay of Bengal: Possible reason for a different water column cycling of carbon and nitrogen from the Arabian Sea, Marine Chemistry, 47, 279-290.

Rao, K. G., & Goswami, B. N. (1988). Interannual variations of sea surface temperature over the Arabian Sea and the Indian monsoon: A new perspective. Monthly Weather Review, 116(3), 558-568.

Roy, R., Rao, K. H., Latha, T. P., Dadhwal, V. K., Sarma, V. V. S. S., Nagamani, P. V., Choudhury, S.B., & Pondala, S. (2017). Satellite and In situ observations of a phytoplankton bloom from coastal Bay of Bengal: Role in pCO_2 modulation. Journal of the Indian Society of Remote Sensing, 45(3), 513-524.

Rozanov, A. G., & Bykova, V. S. (1967). Distribution of nitrates and nitrites in the water of north Indian Ocean Naval Oceanographic Office NSTL station MS.

Sadhuram, Y., & Murty, T. V. R. (2012). Carbon dioxide emissions from Indian monsoonal estuaries, Geophysical Research Letters, 39, L03602, 5p, doi:10.1029/2011GL050709.

Samanta, D., Hameed, S. N., Jin, D., Thilakan, V., Ganai, M., Rao, S. A., & Deshpande, M. (2018). Impact of a narrow coastal Bay of Bengal sea surface temperature front on an Indian summer monsoon simulation. Scientific reports, 8(1), 1-12.

Sarangi, R.K. (2011). Impact of cyclones on the Bay of Bengal chlorophyll variability using remote sensing satellites. Indian Journal of Geo-marine Sciences., 40(6), 794-801.

Sardessai, S., Maya, M.V., Shetye, S., Kumar, S.P., Fernandes, V., Paul, J and Ramaish, N. (2010), Environmental controls on the seasonal carbon dioxide fluxes in the northeastern Indian Ocean, Indian Journal of Marine Sciences, 39(2), 192-200.

Sarma, V. V. S. S., Rajula, G. R., Durgadevi, D. S.L., Kumar, S.G., & Loganathan, J. (2020). Influence of eddies on phytoplankton composition in the Bay of Bengal, Continental Shelf Research, 208, 104241.

Sarma, V. V. S. S., Krishna, M. S., Rao, V. D., Viswanadham, R., Kumar, N. A., Kumari, T. R., Gawade, L., Ghatkar, S., & Tari, A. (2012). Sources and sinks of CO_2 in the west coast of Bay of Bengal, Series B, Chemical and Physical Meteorology, Tellus B, 64, 10961, doi: 10.3402/tellusb.v64i0.10961.

Sarma, V. V. S. S., Kumar, M. D., Gauns, M., & Madhupratap, M. (2000). Seasonal controls on surface pCO_2 in the central and eastern Arabian Sea. Journal of Earth System Science, 109(4), 471-479.

Sarma, V. V. S. S., Lenton, A., Law, R. M., Metzl, N., Patra, P. K., Doney, S., Lima, I. D., Dlugokencky, E., Ramonet, M., & Valsala, V. (2013). Sea–air CO_2 fluxes in the Indian Ocean between 1990 and 2009, Biogeosciences, 10, 7035–7052, doi:10.5194/bg-10-7035-2013.

Sarma, V. V. S. S., Saino ,T., Sasaoka, K., Nojiri, Y., Ono, T., Ishii, M., Inoue, H. Y.,& Matsumoto, K. (2006). Basin-scale pCO_2 distribution using satellite sea surface temperature, Chl a, and climatological salinity in the North Pacific in spring and summer, Global Biogeochemical Cycles, 20 (GB3005), doi:10.1029/2005GB002594.

Sarma, V. V. S. S. (1998). Variability in forms and fluxes of carbon dioxide in the Arabian Sea, Ph.D. thesis, Goa Univ., Goa, India.

Sarma, V.V.S.S. (2003). Monthly variability in surface pCO_2 and net air-sea CO_2 flux in the Arabian sea, Journal of Geophysical Research, 108(C8).

Sarma, V.V.S.S., Kumar, M.D., & George M.D. (1998). The central and eastern Arabian sea as a perennial source of atmospheric carbon dioxide, Tellus, 50B, 179-184.

Sarma, V.V.S.S., Kumar, M.D., Gauns, M and Madhupratap, M., 2000. Seasonal controls on surface pCO_2 in the central and eastern Arabian Sea, Proc. Indian Acad. Sci (Earth Planet. Sci.), 109 (4), 471-479.

Sarma,V. V. S. S., Viswanadham, R., Rao, G. D., Prasad, V. R., Kumar, B. S. K.,Naidu, S. A., Kumar, N. A., Rao, D. B., Sridevi, T., Krishna, M. S., Reddy, N. P. C.,Sadhuram, Y., & Murty, T. V. R. (2012). Carbon dioxide emissions from Indian monsoonal estuaries, Geophysical Research Letters, 39 (L03602), 5p, doi:10.1029/2011GL050709.

Schiebel, R., Zeltner, A., Treppke, U. F., Waniek, J. J., Bollmann, J., Rixen, T., & Hemleben, C. (2004). Distribution of diatoms, coccolithophores and planktic foraminifers along a trophic gradient during SW monsoon in the Arabian Sea. Marine Micropaleontology, 51(3-4), 345-371.

Shankar, D., Vinayachandran, P. N., & Unnikrishnan, A. S. (2002). The monsoon currents in the north Indian Ocean. Progress in oceanography, 52(1), 63-120.

Shanthi, R., Poornima, D., Naveen, M., Thangaradjou, T., Choudhury, S. B., Rao, K. H., & Dadhwal, V. K. (2016). Air-sea CO_2 flux pattern along the southern Bay of Bengal waters, Dynamics of Atmospheres and Oceans, 76, 14-28.

Sharada, M.K., Swathi, P.S., Yajnik, K.S., & Devasena, C.K. (2008). Role of biology in the air–sea carbon flux in the Bay of Bengal and Arabian Sea, Journal of Earth System Sciences, 117(4), 429–447.

Shetye, S. R., & Shenoi, S. (1988). Seasonal cycle of surface circulation in the coastal north Indian Ocean. Proceedings of the Indian Academy of Sciences-Earth and Planetary Sciences, 97(1), 53-62.

Shetye, S. R., Gouveia, A. D., Shankar, D., Shenoi, S. S. C., Vinayachandran, P. N., Sundar, D., Michael, G.S., & Nampoothiri, G. (1996). Hydrography and circulation in the western Bay

of Bengal during the northeast monsoon. Journal of Geophysical Research: Oceans, 101(C6), 14011-14025.

Shetye, S. R., Gouveia, A. D., Shenoi, S. S. C., Sundar, D., Michael, G. S., & Nampoothiri, G. (1993). The western boundary current of the seasonal subtropical gyre in the Bay of Bengal. Journal of Geophysical Research: Oceans, 98(C1), 945-954.

Shetye, S. R., Shenoi, S. S. C., Gouveia, A. D., Michael, G. S., Sundar, D., & Nampoothiri, G. (1991). Wind-driven coastal upwelling along the western boundary of the Bay of Bengal during the southwest monsoon. Continental Shelf Research, 11(11), 1397-1408.

Sheu, D. D., W.-C. Chou, C.-L. Wei, W.-P. Hou, G. T. F. Wong, & C.-W. Hsu. (2010). Influence of El Niño on the sea-to-air CO_2 flux at the SEATS time-series site, northern South China Sea, J. Geophys. Res., 115 (C10021), 1-19, doi:10.1029/2009JC006013.

Shukla, J. (1975). Effect of Arabian sea-surface temperature anomaly on Indian summer monsoon: A numerical experiment with the GFDL model. Journal of Atmospheric Sciences, 32(3), 503-511.

Solomon, S., Qin, D., Manning, M., Chen, Z., Marquis, M., Averyt, K.B., Tignor, M., & Miller, H.L. (2007). Contribution of Working Group to the Fourth Assessment Report of the Intergovernmental Panel on Climate Change, Cambridge University Press, Cambridge, United Kingdom and New York, NY, USA.

Srinivas, B., & Sarin, M. M. (2013). Atmospheric deposition of N, P and Fe to the Northern Indian Ocean: Implications to C-and N-fixation. Science of the total environment, 456, 104-114.

Stephens, M.P., Samuels, G., Olson, D.B., Fine, R.A. and Takahashi, T. (1995). Sea-air flux of CO_2 in the North Pacific using shipboard and satellite data, Journal of Geophysical Research, 100 (C7), 13,571-13,583.

Sutton, A. J., Wanninkhof, R., Sabine, C. L., Feely, R. A., Cronin, M. F., & Weller, R. A. (2017). Variability and trends in surface seawater pCO_2 and CO_2 flux in the Pacific Ocean. Geophysical Research Letters, 44(11), 5627-5636.

Takahashi, T., Olaffson, J., Goddard, J.D., Chipman, D.W., & Sutherland, S.C. (1993). Seasonal Variation of CO_2 and nutrients in the High-Latitude Surface Oceans: A Comparative Study, Global Biogeochemical Cycles, 7(4), 843-878.

Takahashi, T., Sutherland, S. C., & Kozyr, A. (2019). Global ocean surface water partial pressure of CO_2 database: Measurements performed during 1957–2018 (version 2018). NOAA/NCEI/OCADS NDP-088 (V2018) Rep., 25 pp., https://www. ncei. noaa. gov/access/ocean-carbon-data-system/oceans/LDEO_Underway_Database/NDP-088_V2018. pdf.

Takahashi, T., Sutherland, S.C., Sweeney, C Poisson, A., Metzl, N., Tilbrook, B., Bates, N., Wanninkhof, R., Freely, R.A., Sabine, C., Olafsson, J., & Nojiri, Y. (2002). Global sea-air CO_2 flux based on climatological surface ocean pCO_2, and seasonal biological and temperature effects, Deep-sea research II, 49. 1601-1622.

Takahashi, T., Sutherland, S.C., Wanninkhof, R., Sweeney. C., Freely, R.A., Chipman, D.W., Hales, B., Friederich,G., Chavez, F., Sabine, C., Watson, A., Bakker, D.C.E., Schuster, U., Metzl, N., Inoue, H.Y., Ishii,M., Midorikawa, T., Nojiri, Y., Kortzinger, A., Steinhoff,T., Hoppema, M., Olafsson, J., Arnarson, T.S., Tilbrook, B., Johannessen, T., Olsen, A., Bellerby, R., Wong, C.S., Delille, B., Bates, N.R ., & debar, H.W. (2009). Climatological mean and decadal change in surface ocean pCO_2, and net sea-air CO_2 flux over the global oceans, Deep Sea Research II, 56, 554-577.

Takahashi,T., Freely, R.A., Weiss, R.F., Wanninkhof, R.H., Chipman, D.W., Sutherland, S.C., & Takahashi, T.T. (1997). Global air-sea flux of CO_2: An estimate based on measurements of sea-air pCO_2 difference, Colloquium Paper, Proc. Natl. Acad. Sci. USA, 94, 8292-8299.

Takamura, T. R., Inoue, H. Y., Midorikawa, T., Ishii, M., & Nojiri, Y. (2010). Seasonal and inter-annual variations in pCO_2sea and air-sea CO_2 fluxes in mid-latitudes of the western and eastern North Pacific during 1999-2006: Recent results utilizing voluntary observation ships. Journal of the Meteorological Society of Japan. Ser. II, 88(6), 883-898.

Tang, D., Kawamura, H ., & Luis, A.J. (2002). Short-term variability of phytoplankton blooms associated with a cold eddy in the northwestern Arabian Sea, Remote Sensing of Environment, 81, 82-89.

Thushara, V., & Vinayachandran, P. N. (2016). Formation of summer phytoplankton bloom in the northwestern Bay of Bengal in a coupled physical-ecosystem model, Journal of Geophysical Research: Oceans, 121(12), 8535-8550.

Unger, D., Ittekkot, V., Schafer, P., Tiemann, J., & Rescheke, S. (2003). Seasonality and interannual variability of particle fluxes to the deep Bay of Bengal: Influence of riverine input and oceanographic processes, Deep Sea Research, Part II,50, 897-923pp.

Valsala, V., Maksyutov, S., Telszewski, M., Nakaoka, S., Nojiri, Y., Ikeda, M., Murtugudde, R., Climate impacts on the structures of the North Pacific air-sea CO_2 flux variability, Biogeosciences, 2012b, 9, 477-492, doi: 10.5194/bg-9-477-2012.

Valsala, V., & Makyutov, S. (2013) Interannual variability of air-sea CO_2 flux in the north Indian Ocean, Ocean Dynamics, 63, 165-178, doi: 10.1007/s10236-012-0588-7.

Valsala, V., Makyutov, S., & Murtugudde, R. (2012a). A window for carbon uptake in the southern subtropical Indian Ocean, Geophysical Research Letters, 39, doi:10.1029/2012GL052857.

Valsala, V., & Murtugudde, R. (2015). Mesoscale and intraseasonal air-sea CO_2 exchanges in the Western Arabian Sea during boreal summer, Deep Sea Research Part I, 103, 101-113, doi: 10.1016/j.dsr.2015.06.001.

Valsala, V., Roxy, M., Ashok, K., & Murtugudde, R. (2014). Spatio-temporal characteristics of seasonal to multidecadal variability of pCO_2 and air-sea CO_2 fluxes in the equatorial Pacific Ocean, Journal of Geophysical Research: Oceans, 119, 8987-9012, doi: 10.1002/2014JC010212.

Velasco, E., & Roth, M. (2010). Cities as net sources of CO_2: Review of atmospheric CO_2 exchange in urban environments measured by eddy covariance technique, Geography Compass, 4, 1238–1259.

Vinayachandran, P. N., & Mathew, S. (2003). Phytoplankton bloom in the Bay of Bengal during the northeast monsoon and its intensification by cyclones. Geophysical Research Letters, 30(11).

Vinayachandran, P. N., Chauhan, P., Mohan, M., & Nayak, S. (2004). Biological response of the sea around Sri Lanka to summer monsoon. Geophysical Research Letters, 31(1).

Vinayachandran, P. N., Masumoto, Y., Mikawa, T., & Yamagata, T. (1999). Intrusion of the southwest monsoon current into the Bay of Bengal. Journal of Geophysical Research: Oceans, 104(C5), 11077-11085.

Vinayachandran, P. N., McCreary Jr, J. P., Hood, R. R., & Kohler, K. E. (2005). A numerical investigation of the phytoplankton bloom in the Bay of Bengal during Northeast Monsoon. Journal of Geophysical Research: Oceans, 110(C12).

Vinayachandran, P. N., Murty, V. S. N., & Ramesh Babu, V. (2002). Observations of barrier layer formation in the Bay of Bengal during summer monsoon. Journal of Geophysical Research: Oceans, 107(C12), SRF-19.

Vinayachandran, P. N., Shetye, S. R., Sengupta, D., & Gadgil, S. (1996). Forcing mechanisms of the Bay of Bengal circulation. Current Science, 753-763.

Wang, S., & Moore, J.K. (2012). Variability of primary production and air-sea CO_2 flux in the Southern Ocean, Global Biogeochemical Cycles, 26 (GB1008), doi:10.1029/2010GB003981.

Wanninkhof, R. (1992). Relationship between wind speed and gas exchange over the ocean, Journal of Geophysical Research, 97(C5), 7373-7382.

Weiss, R.F., 1974. Carbon dioxide in water and sea water: the solubility of a non-ideal gas, Marine Chemistry, vol 2, pp 203-215

Weiss, R. F., & Price, B. A. (1980). Nitrous oxide solubility in water and seawater. Marine chemistry, 8(4), 347-359.

Young, D. K., & Kindle, J. C. (1994). Physical processes affecting availability of dissolved silicate for diatom production in the Arabian Sea. Journal of Geophysical Research: Oceans, 99(C11), 22619-22632.

Zeebe, R.E. (2012). History of Seawater Carbonate Chemistry, Atmospheric CO_2, and Ocean Acidification, Annual Review of Earth and Planetary Sciences, 40, 141-165.

Zhai, W., Dai, Minhan., Cai, W., Wang, Y., & Hong, H. (2005). The partial pressure of carbon dioxide and air-sea fluxes in the northern South China Sea in spring, summer and autumn, Marine Chemistry, 96, 86-97.

Zhu, Y., Shag, S., Zhai, W., & Dai, M. (2009). Satellite-derived surface water pCO_2 and air-sea CO_2 fluxes in the northern South China Sea in Summer, Progress in Natural Science, 19, 775-779.

Zondervan, I., Zeebe, R.E., Rost, B., & Riebesell, U. (2001). Decreasing marine biogenic calcification: A negative feedback on rising atmospheric pCO_2, Global Biogeochemical Cycles, 15(2), 507-516

Zui, T., Bangyong, B., Ziwei1, L., & Xiaofeng,Y. (2012). Satellite observations of the partial pressure of carbon dioxide in the surface water of the Huanghai Sea and the Bohai Sea, Acta Oceanologica Sinica, 31(3), 67-73, doi: 10.1007/s13131-012-0207-y.
